Deliverable 7.8: HITEC – Influence of temperature on clay-based material behaviour

Work Package 7

The project leading to this application has received funding from the European Union's Horizon 2020 research and innovation programme under grant agreement No 847593.

Document information

Project Acronym	**EURAD**
Project Title	**European Joint Programme on Radioactive Waste Management**
Project Type	**European Joint Programme (EJP)**
EC grant agreement No.	**847593**
Project starting / end date	**1st June 2019 – 30 May 2024**
Work Package No.	**7**
Work Package Title	**Influence of Temperature on Clay-based Material Behaviour**
Work Package Acronym	**HITEC**
Deliverable No.	**7.8**
Deliverable Title	**HITEC technical report on Material characterisation**
Lead Beneficiary	**UKRI**
Contractual Delivery Date	**March 2023**
Actual Delivery Date	**June 2024**
Type	**Final report of WP7 Task 3.2**
Dissemination level	**Public**
Authors	**Caroline C. Graham (BGS), Katherine Daniels (BGS), Jon F. Harrington (BGS), Roy Chaaya (BRGM), Stéphane Gaboreau (BRGM), Joachim Tremosa (BRGM), María Victoria Villar (CIEMAT), Carlos Gutiérrez-Álvarez (CIEMAT), Guillermo García-Herrera (CIEMAT), Rubén J. Iglesias (CIEMAT), Natalia Gimeno (CIEMAT), Jiří Svoboda (CTU), Kateřina Černochová (CTU), Jan Najser (CU), David Mašín (CU), Janne Yliharju (JYU), Sergey Sayenko (KIPT), Veli-Matti Pulkkanen (VTT), Olli-Pekka Rauhala (VTT), Gianni Vettese (UH), Noora Pakkanen (UH), Marja Siitari-Kauppi (UH).**

To be cited as:

Graham C. C., Daniels K., Harrington J. F., Chaaya R., Gaboreau S., Tremosa J., Villar M. V., Gutiérrez-Álvarez C., García-Herrera G., Iglesias, R. J., Gimeno, N., Svoboda J., Černochová K., Najser J., Mašín D., Yliharju J., Sayenko S., Pulkkanen V., Rauhala O., Vettese G., Pakkanen N., Siitari-Kauppi M. (2023): HITEC technical report on Material characterisation. Final version as of 09.11.2023 of deliverable D7.8 of the HORIZON 2020 project EURAD. EC Grant agreement no: 847593.

Disclaimer

Acknowledgement

This document is a deliverable of the European Joint Programme on Radioactive Waste Management (EURAD). EURAD has received funding from the European Union's Horizon 2020 research and innovation programme under grant agreement No 847593.

Status of deliverable		
	By	Date
Delivered (Lead Beneficiary)	[UKRI]	09/11/2023
Verified (WP Leader)	Markus Olin [VTT]	17/02/2024
Reviewed (Reviewers)	Michael Holmboe, Jarmo Lehikoinen	15/04/2024
Approved (PMO)	Bharti Reddy	31/05/2024
Submitted to EC	Andra (Coordinator)	03/06/2024

Authors

Organisation	Authors
British Geological Survey (BGS) United Kingdon Research and Innovation (UKRI)	Caroline C. Graham, Katherine Daniels, Jon Harrington
Bureau de Recherches Géologiques et Minières (BRGM)	Roy Chaaya, Stéphane Gaboreau, Joachim Tremosa
Centro de Investigaciones Energéticas, Medioambientales y Tecnológicas (CIEMAT)	María Victoria Villar, Carlos Gutiérrez-Álvarez, Guillermo García-Herrera, Rubén J. Iglesias, Natalia Gimeno
Czech Technical University in Prague (CTU)	Jiří Svoboda, Kateřina Černochová
Charles University in Prague (CU)	Jan Najser, David Mašín
University of Jyväskylä (JYU)	Janne Yliharju
Kharkiv Institute of Physics and Technology (KIPT)	Sergey Sayenko
VTT Technical Research Centre of Finland (VTT)	Veli-Matti Pulkkanen, Olli-Pekka Rauhala
University of Helsinki (UH)	Gianni Vettese, Noora Pakkanen, Marja Siitari-Kauppi

Executive Summary

This report presents an overview of Task 3.2 progress in the HITEC work package of the European Joint Programme on Radioactive Waste Management programme. The objectives of this task are focussed around evaluating the behaviour of clay buffer materials at high temperature. The findings are expected to inform the feasibility of designing geological disposal facilities to operate at elevated temperature conditions. The objectives of this work are described, followed by an overview of progress on this task from each project partner. An emphasis is given on materials used, research planned, laboratory set-ups used and results available to date. Testing is focussed on a range of bentonites including: Mx80, Kunipia-G, FEBEX, BCV, Bara-Kade, PBC. Finally, general conclusions from resulting from this work are also provided, with an emphasis on the impacts for repository design, remaining uncertainties and recommendations for future work.

Despite delays resulting from the Covid-19 crisis, substantial progress has been made in the development and construction of a wide range of experimental apparatus within this task. Progress has been made in the development of imaging methodologies and preliminary observations indicate that the uptake of water is sensitive to elevated temperatures. Relationships delineated within Task 3.2 include: (i) the observation of swelling pressure and permeability as a function of temperature for various dry densities, swelling strains, chemical states and conditions and (ii) water retention curves, as function of temperature. For the materials and conditions tested, an influence of elevated temperature on water retention capacity has been observed. Multiple test programmes, in both Ca- and Na-bentonite have also found evidence that, whilst changes to hydraulic permeability are perhaps less significant, swelling pressure can be substantially impacted by elevated temperatures. Further work to consider the mechanisms and consequences of this behaviour for repository design are recommended as a result.

The extensive datasets generated by this Task 3.2 will enable the parameterisation, modification and validation of numerical simulations to more accurately represent the thermo-hydro-mechanical behaviour of bentonite at elevated temperatures.

Table of content

List of figures

List of Tables

Glossary

Abbreviation	Full Term
HLW	High-Level Waste
SF	Spent Fuel
WP	Work Package

1 Introduction

Task 3.2 is focussed on evaluating the feasibility and safety of elevated temperatures in a geological disposal facility, in relation to the hydromechanical behaviour of engineered barrier materials. This involves the application of pre-existing knowledge, as well as additional information generated within this task to examine the response of clay buffer materials at high temperatures.

To address this, several effects of relevance must be considered. The clay may be directly impacted by the high temperatures, which have the potential to impact the mineralogy mechanical state and physio-chemical behaviour of the clay. In addition, higher temperatures may result in strong evaporation near the heater and vapour movement towards the external part of the buffer. Consequently, part or all of the barrier, depending on the disposal concept, will remain unsaturated and whilst experiencing elevated thermal loading for long periods of time. Moreover, steep pore pressure and temperature gradients have the potential to impact the water phase, which may result in boiling and potentially adverse impacts on barrier performance. In collaboration with other subtasks in T3, the primary objectives of Task 3.2 subtask were defined as:

- Determination of bentonite hydro-mechanical properties for temperatures greater than 100°C, which will provide parameters for the modelling work.

This document provides an overview of the progress made addressing these objectives throughout the duration of Task 3.2. The following sections describe the work carried out by each project partner, giving detail on the materials, research plan, procedures and results achieved so far. Finally, a conclusion section synthesises findings from across the project partners, provides specific statements relating to the impacts for repository design and provides recommendations for future work.

2 BGS

2.1 Introduction

Overall objective

Recent experiments (Zihms and Harrington, 2015; Daniels et al., 2017) have demonstrated the importance of temperature in defining the hydraulic properties of bentonite engineered barriers. Permeability decreases on heating, so long as water remains liquid (as defined by its phase envelope). This reduction in permeability is thought to be linked to thermally-induced consolidation of the clay, which is likely to occur during the operational and early post-closure phases of a repository. The role of saturation and dry density, their impact on thermal conductivity and its subsequent effect on the hydraulic and mechanical properties remain unclear. This raises several important questions that have yet to be addressed regarding the long-term stability and integrity of the buffer, including the effect of thermal loading and thermal gradient on the material permeability and hydromechanical behaviour.

To address this, BGS has conducted a suite of laboratory experiments using bespoke apparatuses specifically designed for low permeability studies at high temperatures (from 100 to 200°C). Two experimental suites have been carried out, examining bentonite behaviour at elevated temperatures, with emphasis on the evolution of: (i) swelling pressure and (ii) permeability. The first suite of tests involved examination of bentonite samples, either (i) constrained to a fixed volume or (ii) allowed to swell into an engineering void. In both cases, the role of density was examined as well as the impact of varying temperature. The second suite of tests is focussed on the evolution and hysteresis of permeability and swelling pressure, as a function of temperature and initial dry density, the latter reflecting the heterogeneous conditions observed within engineered clay buffers as they hydrate. Geotechnical and mineralogical characterisation of samples before and after testing to determine changes in physical properties has also either been carried out or is underway and additional findings will published in future. In the open literature, no data could be found viewing these processes as a single system response (i.e. coupling processes such as permeability, swelling pressure and stress at high temperature). Combining thermal loading with the simultaneous measurement of permeability or

swelling pressures provides important insight into the true system behaviour under such conditions. Together, these tests provide process understanding and data for parameterisation of numerical simulations, which feed into the assessment of barrier performance under elevated temperatures.

2.1.1 Material

Engineered clays selected for testing comprise MX-80 Bentonite (VolClay) and a calcium-activated Bulgarian bentonite. The VolClay (Svensson et al. 2017) bentonite samples are compacted at the BGS from powder supplied by the American Colloid Company (now Mineral Technologies Inc.) through Sibelco Nordic, who crushed and dried the material. Ca-bentonite samples are compacted from powder supplied by Imerys through Svensk Kärnbränslehantering (SKB). Detailed information about the composition of the two different bentonite test materials can be found in Table 2.1 below.

Name	**MX-80 VolClay**	**Imerys Ca-Bentonite**
Origin/Producer	American Colloid Company (now Mineral Technologies Inc.) through Sibelco Nordic.	Ca-bentonite from Bulgaria supplied by Imerys and provided by SKB Sweden.
Description	Granular Na-bentonite, crushed and dried. Average particle size ranges from 16 to 200 micron. This material is composed of predominantly montmorillonite (>90%), with small amounts of feldspar, biotite, selenite etc. At a 5% solids dispersion in distilled water the pH of the mixture ranges between 8.5 and 10.5.	Granular Ca-activated bentonite from Bulgaria, industrially homogenised and milled to a granular powder. The material contents are predominantly montmorillonite (>80%), with calcite, quartz, mica and trace gypsum.

Table 2.1 – Origin and composition of the bentonite powders utilised or available as the test materials for the experimental program in Task 3.2.

Due to delays in the test programme resulting from the Covid-19 pandemic, experiments to date have only been conducted using MX-80 bentonite, though Ca-activated bentonite is also available for testing, should the new timeframe allow. Granular MX-80 is mixed with deionised water and compacted at 80MPa for 24 hours to produce the test sample. The sample is then lathed to precisely fit the pressure vessel interiors used during testing.

2.1.2 Research plan

Two experimental test programmes have been operating within the UKRI (BGS) contribution to this task. To date, these have been conducted in two different apparatuses and are focussed on the examination of:

(i) Swelling pressure development in bentonites at elevated temperatures, under a constant volume configuration
(ii) Permeability evolution in bentonite at elevated temperatures

The research plan for each of these test programmes is described separately below.

Swelling pressure development

The primary objective for this test programme was to assess the impact of dry density and thermal loading on swelling pressure development in bentonite.

The initial intention was to conduct the first tests on samples that, at the start of testing, already fully occupy the interior volume of the pressure vessel, thereby resulting in the immediate generation of substantial stresses as the clay is hydrated. However, production of these longer samples required the

development of a new sample press, the delivery of which was substantially impacted by lack of onsite access for workshop staff and supply chain disruption for necessary components during the Covid-19 crisis. As such, the test programme was continued by rearranging the planned test order and beginning with shorter samples, which are then allowed to swell axially into a void within the pressure vessel interior. By using samples of varying lengths, the influence of voidage on swelling pressure in the presence of elevated temperatures can be examined as a function of axial strain. Testing then proceeded to consider bentonite behaviour under fully constrained (constant volume) conditions.

A brief summary of the experimental materials and procedure is given in Table 2.2. Each individual test was carried out at a fixed temperature, for a duration of up to 100 days. Tests were planned to cover a range of elevated temperatures: 100, 150 and 200°C. However, early in the project concerns around degradation of the apparatus seals at the highest temperatures led to a decision to run the highest temperature at 17°C instead. Swelling behaviour of the bentonite was, however, still investigated in the permeability tests described in the next section. The test programme follows the test matrix given in Table 2.3. Tests 1 to 11 have now been completed and Test 12 will be completed before the end of the project.

The planned test programme was substantially impacted by the Covid-19 global pandemic, with multiple factors setting the test programme back more than 6 months. However, substantial progress was made in bringing testing back on track and the objectives of this experimental programme have been achieved despite this, by careful planning.

2.1.2.1 Material (BoM item): MX-80 to date, Ca-activated bentonite may still be tested before the end of the project, if time allows.
2.1.2.2 Temperature (to which material was/will be exposed to) and exposure time Granular MX-80 is mixed with deionised water and compacted at 80MPa for 24 hours to produce the test sample. The sample is then turned down in a machine lathe to fit precisely the constant volume (CVRF) apparatus.
2.1.2.3 Material treatment (sample preparation for test and loading procedure): Tests to be carried out at a range of temperatures: 100, 150 and 175°C. Each individual test is carried out at a fixed temperature and for a duration of up to 100 days
2.1.2.4 Temperature (to which material was/will be exposed to) and exposure time Tests to be carried out at a range of temperatures: 100, 150 and 175°C. Each individual test is carried out at a fixed temperature and for a duration of up to 100 days.
2.1.2.5 Tests carried out (name, description, sample preparation, procedure, results): Initial testing was carried out using shorter samples, which were then allowed to swell axially into a void within the pressure vessel interior. By using samples of varying lengths, the influence of voidage on swelling pressure in the presence of elevated temperatures could be examined as a function of axial strain. The same procedure is applied for each test, as follows: • The sample is installed in the base of the constant volume pressure vessel. This vessel has been manufactured from a type of steel with a low thermal expansion coefficient (INVAR). The vessel is sited in the vertical orientation (sample vertical along its length). • If a void is to be present, this is filled with the same water as the clay sample. Deionised water is used as the external pressurising fluid in all of the tests performed. • The apparatus is heated to the testing temperature (100, 150 or 175°C) in a large oven and left to equilibrate overnight. • A constant water pressure is applied to both ends of the sample. • The sample is allowed to hydrate and swell. Swelling pressure development is measured at multiple locations (both axial and radial) on the sample surface. • In axial swelling tests, samples were 95mm in length and were allowed to swell axially into a remaining void of 25 mm. In constant volume tests, samples were 120 mm in length: the full length of the pressure vessel interior.

Table 2.2 – BGS – Swelling pressure development in constant volume configuration.

Test	Geometry	Temperature (^{o}C)	Initial length	Dry Density (kg/m^{3})	Duration (days)
1 (FPR-20-008)	Axial swelling, radially constrained	100	95 mm	1.7	100
2 (FPR-20-024)	Axial swelling, radially constrained	100	95 mm	1.5	100
3 (FPR-21-010)	Axial swelling, radially constrained	150	95 mm	1.7	100
4 (FPR-21-030)	Axial swelling, radially constrained	150	95 mm	1.5	100
5 (FPR-22-023)	Axial swelling, radially constrained	175	95 mm	1.7	100
6 (FPR-22-048)	Constant volume	100	Full length	1.7	50
7 (FPR-22-092)	Constant volume	175	Full length	1.7	50
8 (FPR-22-051)	Constant volume	150	Full length	1.7	50
9 (FPR-22-118)	Constant volume	100	Full length	1.3	50
10 (FPR-23-011)	Constant volume	175	Full length	1.3	<50
11 (FPR-23-060)	Constant volume	150	Full length	1.3	<50
12 (FPR-23-xxx)	Constant volume	175	Full length	1.5	<50

Table 2.3 – Test matrix *for experiments allowing axial swelling of samples. All tests have been completed except Test 12, which will be completed by the end of the project.*

Permeability evolution

The primary objective for this test programme was to assess the evolution and potential hysteresis of permeability and swelling pressure in bentonite, as a function of temperature and initial dry density.

A brief summary of the experimental materials and procedure is given in Table 2.4. Two permeability tests have been conducted on bentonite samples with a dry density of 1.56 g/cm^3 and 1.7 g/cm^3. A third test is currently operating and will be completed by the end of the project, with a sample of dry density = 1.3 g/cm^3. The first permeability experiment suffered some delays due to a leak in the backpressure system and lasted a period of approximately 250 days. It was subjected to two thermal loading cycles with temperatures ranging from 100 to 200°C. At each thermal step the temperature was held constant and swelling pressures and flows were allowed to equilibrate before the next step was applied. The same approach was also applied for the second test. The test matrix is outlined in Table 2.5. The inclusion of thermal loading cycles means that the duration of these tests is much longer than for the swelling pressure development tests, but the result is a continuous dataset showing the long-term response of the bentonite to high thermal loads.

2.1.2.6 Material (BoM item): MX-80
2.1.2.7 Material treatment (sample preparation for test and loading procedure): Granular MX-80 is mixed with deionised water and compacted at 80 MPa for 24 hours to produce the test sample. The sample is then turned down in a machine lathe to fit precisely the constant volume (CVRF) apparatus.
2.1.2.8 Temperature (to which material was/will be exposed to) and exposure time All three experiments include several temperature steps across the range: 100-200 °C. The temperature is held constant at each step to allow steady-state to be approached and measurements to be made before the next step. Each test duration is of the order of several months.
2.1.2.9 Tests carried out (name, description, sample preparation, procedure, results): Each test is carried out according to the following procedure: • The sample is installed in the constant volume pressure vessel. • The apparatus is heated to the first testing temperature (100°C) in a large oven. • Deionised water is used to apply a constant pressure to both ends of the sample. • The sample is allowed to hydrate and swell. • A hydraulic pressure gradient is applied across the sample, inducing a small flow and allowing the hydraulic permeability to be determined. • The temperature is then increased and (once swelling and flows have stabilised) the permeability is determined again. This procedure is repeated for multiple temperature steps (100, 150 and 200°C), to assess the impact of thermal loading and unloading. Two permeability tests have been conducted on bentonite samples with a dry density of 1.56 g/cm^3 and 1.7 g/cm^3. A third test is currently operating and will be completed by the end of the project, with a sample of dry density = 1.3 g/cm^3.

Table 2.4 – BGS – Permeability evolution in constant volume configuration.

Test	Apparatus	Temperature stages (°C)	Dry Density (g/cm³)	Duration
A (FPR-20-026)	INVAR CVRF	100, 150, 200, 150, 200, 150, 100	1.56	6 months
B (FPR-22-043)	INVAR CVRF	100, 150, 200, 150, 200, 150, 100	1.7	6 months
C (FPR-22-094)	INVAR CVRF	100, 150, 200 °C	1.3	~3 months

Table 2.5 – Test matrix for permeability testing of bentonite. Tests A-B have been completed. Test C is running and will be completed by the project end.

The planned test programme was substantially impacted by the Covid-19 global pandemic, with multiple factors setting the test programme back more than 6 months. In particular, Test C was substantially delayed due to excessive lead times in the delivery of high temperature seals during this time. Test C will have a shorter duration than Tests A-B but will still provide its planned outputs. The objectives of this subtask have, therefore, all still been achieved.

2.2 Procedures

2.2.1 Laboratory set-ups, procedures and protocols

Two apparatuses were constructed for the test programmes being conducted in Task 3.2 (Figure 2.1; Figure 2.4). Both of these can constrain a sample under a constant volume boundary condition (both radially and axial). Alternatively, a shorter sample than the interior of the vessel can be used, such that swelling is permitted in an axial direction until the pressure vessel interior volume is filled by the clay. Both of these geometries have been tested in this project. In the permeability experiments, full length volume samples have been used, meaning that both axial and radial volume change of the sample is minimal. The test apparatuses used for the two test programmes are described below.

Swelling pressure development

This is a bespoke apparatus that was designed and built at the BGS, and consists of (1) a thick-walled, dual-closure pressure vessel; (2) an injection pressure system; (3) a backpressure system; (4) 12 bespoke pressure transducers measuring radial and axial total stress; and (5) a microcomputer-based high-speed data acquisition system (Figure 2.1). The pressure vessel is comprised of a dual-closure tubular vessel manufactured from Invar Alloy 36 steel, pressure-rated to 70 MPa, with the internal surfaces hard-chromed to prevent damage. Samples can be hydrated and/or a backpressure can be applied through two porous filters mounted on the end-closures. Samples are constrained radially, by the rigid stainless-steel cell, resulting in the development of a swelling pressure on hydration.

The pressure sensors used in this vessel are XP1147-200BS temperature-compensated custom sensors supplied by StrainSense Ltd. A detailed description of this second apparatus is given by (Daniels et al., 2017). The pressure measurements made in these experiments can be considered accurate to ±15 kPa. Large axial sintered filters were also inserted into the end closures to ensure an even distribution of fluid entering the vessel at each of its ends. The test fluid (deionised water) was supplied to the sample using high precision syringe pumps (Teledyne ISCO D-Series 260D). The entire

apparatus is contained within a BINDER GmbH oven (Series FED 400), to allow heating, whilst the syringe pumps operate outside the oven.

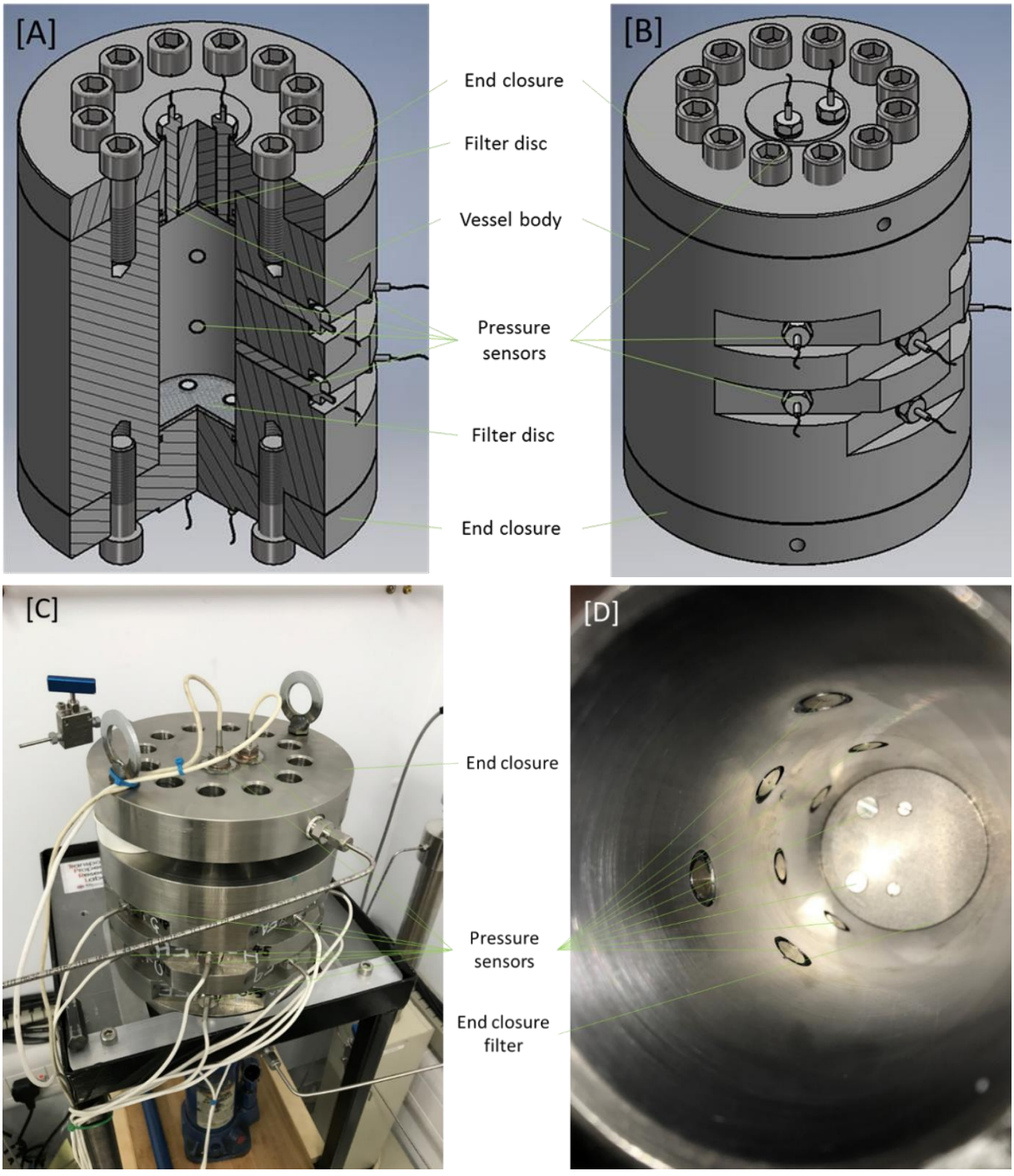

Figure 2.1 – [A] cut-away diagram and [B] schematic of the apparatus for the swelling pressure development tests showing the positioning of the pressure sensors and axial filter discs; [C] photo of the experimental set up including vessel, end closures and pressure sensors. This part of the assembly is now situated in a large oven; [D] internal view showing the eight radial and two axial pressure sensors. The axial sensors are embedded in the end closure filter (from Harrington and Daniels, 2018). [BGS © UKRI]

Permeability evolution

The constant volume apparatus used to conduct permeability testing in this Task is shown in Figure 2.4. As with the apparatus for the swelling pressure tests, this is a bespoke set-up that has been designed and built at the BGS, and consists of (1) a thick-walled, dual-closure pressure vessel; (2) an injection pressure system; (3) a backpressure system; (4) 5 bespoke pressure transducers measuring radial and axial total stress; (5) 3 port-arrays with transducers for porewater pressure measurement; and (6) a microcomputer-based high-speed data acquisition system. The pressure vessel is comprised of a dual-closure tubular vessel manufactured from 316-stainless steel, pressure-rated to 70 MPa, with the internal surfaces hard-chromed to prevent damage.

The pressure sensors used to measure swelling pressure in this vessel are XP1147-200BS temperature-compensated custom sensors, supplied by StrainSense Ltd. A detailed description of this second apparatus is given by (Daniesl et al., 2017). The pressure measurements made in these experiments can be considered accurate to ±15 kPa. Large axial sintered filters were also inserted into the end closures to ensure an even distribution of fluid enring the vessel at each of its ends. The test fluid (deionised water) was supplied to the sample using high precision syringe pumps (Teledyne ISCO D-Series 260D). The entire apparatus is contained within a BINDER GmbH oven (Series FED 400), to allow heating, whilst the syringe pumps operate outside the oven.

Calibration procedure

Extensive efforts have been made on calibration of pumps and sensors during this test programme. Whilst customised sensors have been utilised, which have been specifically designed to compensate for changes in temperature. It was considered important to assess sensor performance as a function of temperature. The following calibration procedures were therefore used:

- The pressure vessel was filled with water and the injection and backpressure pumps were set to zero at atmospheric pressure.
- A pressure calibrator (periodically recalibrated to a certified standard) was connected to the injection pump.
- The oven was switched on and set to the temperature planned for testing. The vessel was then allowed to equilibrate (as assessed by thermocouple data)
- The injection pump was then cycled from low to high pressure in a series of steps of the same duration and then lowered again. Output from the pressure calibrator was also logged for each step (*Figure 2.2Figure 2.2 – Example Calibration test data, showing temperature steps (left) and sensor responses on pressure cycling (right).*).
- The injection pump was next set to run on an equivalent programmed pressure cycle over a minimum period of 24 hrs, whilst all sensor responses were logged.
- A least squares regression was used to find a linear fit to the injection pump and calibrator data, providing coefficients for correcting injection pump pressure outputs and calculating test set-points.
- This calibration was next applied to the injection pump data over the programmed pressure cycle, which was then used to allow further linear regression of each individual sensor and again provide correction coefficients (*Figure 2.3*).

In the case of permeability testing, this calibration procedure was conducted for each of the temperature steps planned during testing to assess any potential hysteresis.

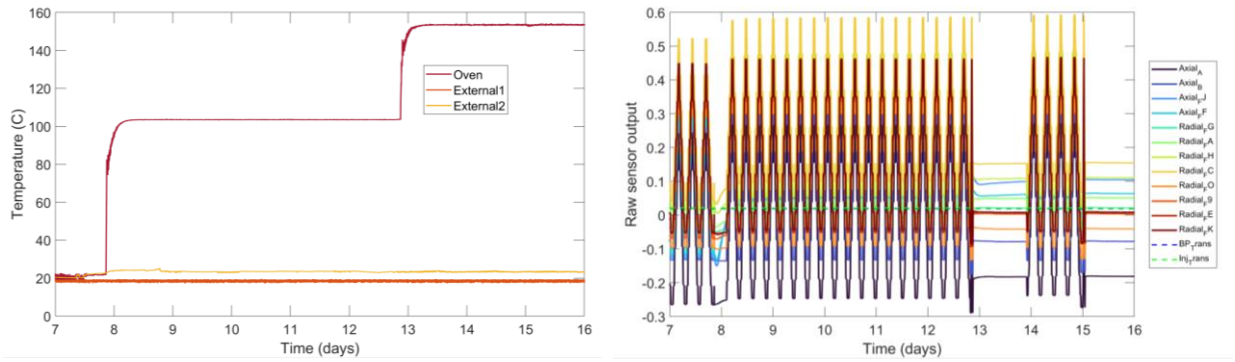

Figure 2.2 – Example Calibration test data, showing temperature steps (left) and sensor responses on pressure cycling (right).

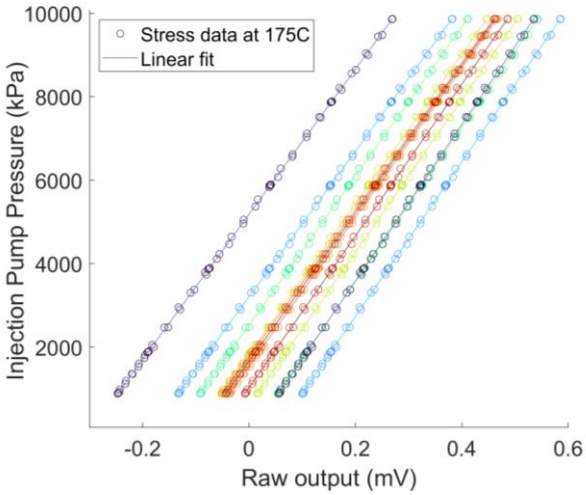

Figure 2.3 – Example showing sensor responses to calibrated pump pressure and least squares regression fits, for a given temperature (175°C). [BGS © UKRI]

Test procedure for the swelling pressure experiments

The whole pressure vessel assembly (excluding the syringe pumps) was stationed inside an oven (BINDER GmbH, Tuttlingen, Germany, Series FED 400) that has a temperature range of 5°C above room temperature to 300°C. At the start of the testing programme, the apparatus was calibrated. The calibration was carried out by placing a steel bung in the bore of the test vessel and filling the apparatus with the test fluid (distilled water). All of the tubework was carefully flushed with the test fluid through each available port to ensure no residual air remained. The apparatus was then heated to the testing temperature before the commencement of the first test. The sample was pushed to the base of the void inside the apparatus. For shorter samples intended to swell axially, the remaining void space above the sample was filled with distilled water; the sample was not heated in advance of insertion because this would have affected the pre-test saturation.

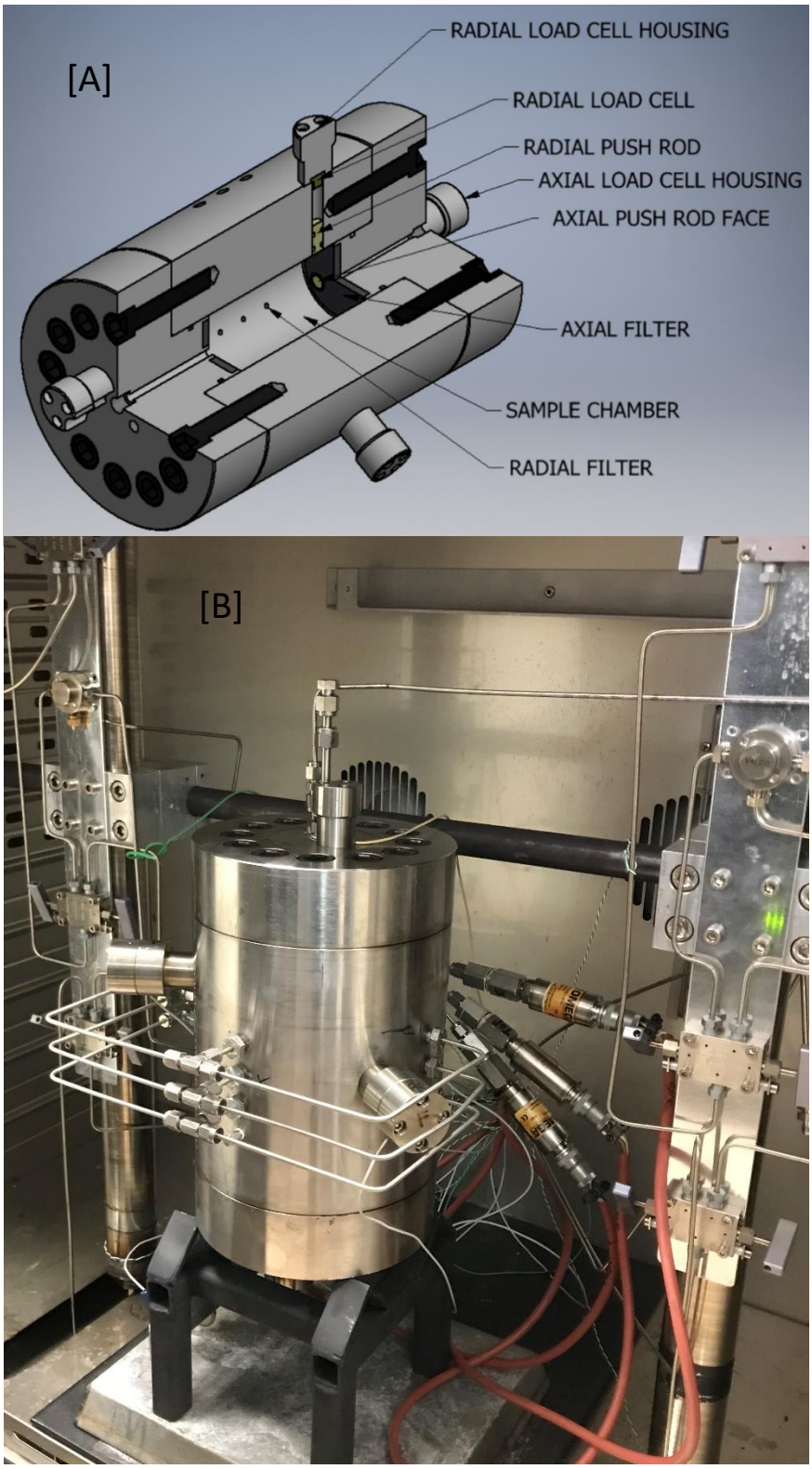

Figure 2.4 – [A] Cut-away diagram of the apparatus for the permeability evolution tests showing positioning of the total stress sensor locations and load cell housings, and the locations of the porewater pressure filters; [B] Photograph of the apparatus inside the large experimental oven. Five total stress sensors are located around the periphery of the sample, two axial and three radial. Three radial flow arrays record the porewater pressure in the sample at three points along its length. Each radial flow array comprises four filters set at 90° to each other (from Harrington and Daniels, 2018). [BGS © UKRI]

Where a sample smaller than the pressure vessel interior was used, pore pressure was carefully applied alternately to each end of the sample in steps to the target value of 4.5 MPa, starting at the end of the apparatus that was originally void space. This kept the sample fixed against the other end of the apparatus interior and prevented it from sliding along the bore of the vessel before the sample swelling began. The pore pressure reference value was chosen for comparability with Swedish plans for a disposal facility, as outlined by SKB. This also ensured water would remain in the liquid phase during testing. The flow rate into and/or out of the sample was then controlled and monitored using the syringe pumps and a single digital control unit. Each pump was operated in a constant pressure mode and thus the flow rate and direction were not prescribed. Inflow or outflow could, therefore, occur at either end of the test vessel. Once the pore pressure had been applied to the sample, no external hydraulic gradient was then applied to the clay at any further point in the test. FieldPoint™ and cRIO logging hardware and the LabVIEW™ data acquisition software (National Instruments Corporation, Austin, TX, USA) were used to log the flow rate, stresses and pore pressure at 2 min intervals, providing a detailed time series dataset. Over the duration of each test, the sample was able to swell in the axial direction, into the remaining interior void space.

Each test was operated for a fixed duration of 100 days, allowing comparison between the tests. At the end of each test, the pressure was incrementally reduced at both ends of the vessel at the same time to ensure that there was no hydraulic gradient applied across the sample. The oven was also switched off, but remained closed for a minimum of 16 h whilst the temperature reduced to ambient. The sample was extruded out of the vessel in increments and sliced into approximately 10 mm thick pieces using a sharp blade. The slices were weighed immediately after their extrusion, whilst the remainder of the sample still in the vessel was covered with cling-film to minimise moisture loss.

The weighed slices were placed in an oven at 105°C and dried to determine the moisture content. The post-test dry density was calculated from the moisture content for each sample, using a specific gravity of 2.77 and assuming a saturation of 1. This is a reasonable assumption because the start saturation of the samples was close to unity and the void was filled with water (Daniels et al. 2021).

Test procedure for the permeability experiments

The initial test procedure for the permeability experiments is outlined in Table 2.4 and followed that of the swelling pressure test programme described above, with the exception that the initial water pressure applied to the samples was lower, at 2 MPa. The sample was left to hydrate until swelling pressures had reached a plateau. At this stage, the test programmes diverge and the injection pressure was increased to a value of 4 MPa to initiate hydraulic testing. This resulted in a 2 MPa pressure gradient across the sample, which induced a small flow, allowing the hydraulic permeability to be determined. Once swelling and flows had stabilised, the oven temperature was then increased and the permeability could be determined again. This procedure was then repeated for multiple temperature steps (100, 150, 200, 150, 200, 150, 100°C), to assess the impact of thermal cycling on the clay. Decommissioning of the experiment was conducted in the same fashion as for the swelling pressure tests.

2.2.2 Data and other results available

Swelling pressure development

The parameters/properties measured/determined by these experiments include:

- the swelling pressure as a function of time at various temperatures and dry densities
- the fluid volume into and out of the sample, providing the net fluid volume change with time
- post-test geotechnical information
- XRD analysis of test samples after heating is currently underway

Permeability evolution

The parameters/properties measured/determined by these experiments include:

- the fluid volume change with time as the sample hydrates
- the swelling pressure as a function of time and temperature at a range of temperatures from 100-200°C
- the fluid flow rates across the sample during hydraulic testing under a constant pressure gradient
- the hydraulic permeability as a function of temperature
- the porewater pressure development in the sample at multiple locations, as function of time
- post-test geotechnical information
- XRD analysis of test samples after heating is currently underway

2.3 Results

2.3.1 Investigation performed

The tests planned for this study are summarised in Table 2.3 and Table 2.5. All of these tests have been completed except Swelling Test 12, which is due to start and Permeability Test C, which has yet to finish. Both will be completed by the end of the project. The objectives of this study have, therefore, been achieved.

2.3.2 Results from investigation

Swelling pressure development – axial swelling permitted

This section details the findings from swelling pressure experiments where axial swelling into a void was allowed (samples were smaller than the interior of the pressure vessel). The samples were subjected to an applied water pressure of 4.5 MPa, whilst being subjected to an elevated temperature of either 100 or 150°C for a period of 100 days. Swelling pressures were calculated by subtracting the average applied water pressure (at the up- and down-stream pumps) from the recorded axial and radial stresses.

As would be expected, the initially-generated swelling pressures were seen to vary substantially at different measurement locations (Figure 2.5) for all tests. The lowest pressures were recorded at the void end of the vessel and the highest pressures were detected at the end where the clay sample was initially present. Over the duration of testing, axial and radial stresses were observed to converge, as the clay swelled into the void end of the pressure vessel. Nevertheless, a significant heterogeneity in the observed stress distribution was found to persist even after 100 days (Figure 2.5). As would be expected, substantially greater swelling pressures were generated for the higher density samples (Figure 2.5). For the same dry density, similar peak swelling pressures were observed at 150°C, as compared to 100°C. However, at the higher temperature, swelling pressures had yet to reach a plateau by day 100 and were continuing to decline at the end of testing (Figure 2.5). This experiment also showed a wider residual range of differential pressures at the end of testing, indicating that homogenisation was inhibited. This observation was in contrast to previous findings from the EC BEACON project that indicate a higher uniformity at temperatures of 90°C, as compared to ambient temperature conditions. It may be that this effect may only become significant at the higher temperatures used in this test programme. Additional geochemical (XRD) analysis may provide further insight.

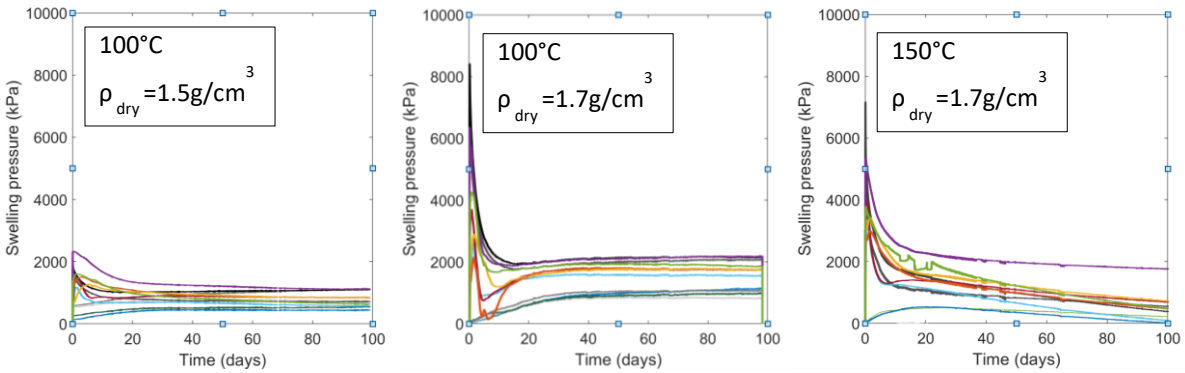

Figure 2.5 – From left to right, Swelling pressure evolution of tests: FPR-20-24 (100°C, 1.5g/cm3), FPR-20-008 (100°C, 1.7g/cm3), and FPR-21-010 (150°C, 1.7g/cm3). [BGS © UKRI]

This dataset completes the existing data generated from the EC BEACON research project by Daniels et al. (2021) and the findings from both test programmes are compiled here to provide a deeper insight into the observations to-date. To compare the evolution of swelling pressures at a range of temperature conditions and in the presence of a void, an average swelling pressure was found over an interval of 30 data points at day 100 of each experiment. Given the ongoing differential pressures seen at this stage of testing, an average value was found for those sensors closest to the initial void location and those closest to the compacted clay end of the pressure vessel interior. These values are shown in Figure 2.6, as a function of temperature. A substantial difference is apparent in the swelling pressures determined above and below 100°C.

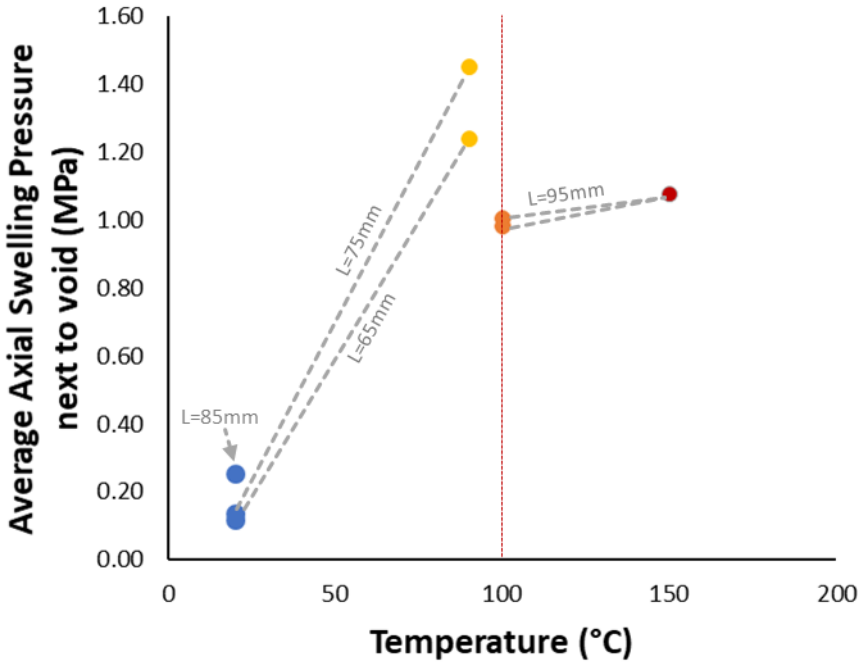

Figure 2.6 – Swelling pressure as a function of temperature at the low density (initially void) end of the sample. [BGS © UKRI]

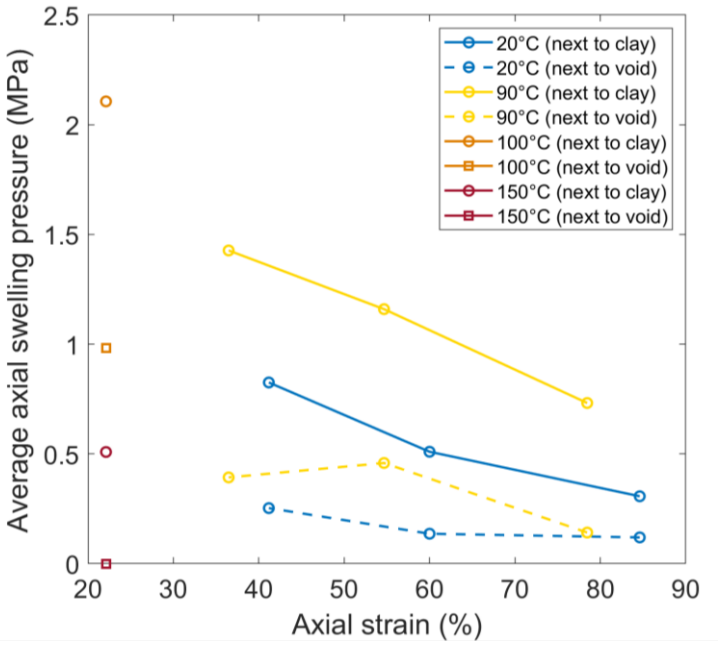

Figure 2.7 – Average swelling pressure after 100 days, as a function of axial strain resulting from swelling into remaining void. [BGS © UKRI]

Figure 2.7 shows the estimated average swelling pressures as a function of axial strain resulting from swelling into the remaining void, for all test samples with a dry density of 1.7 g/cm^3. Measured swelling pressures are comparatively lower for those experiments conducted at or above 100°C, although since less swelling was allowed in these samples it is not yet clear what fraction of this observation is the result of the elevated temperatures, as opposed to the differences in axial strain between tests. Nevertheless, a similar finding was also apparent at this higher dry density in the constant volume experiments (see below). Measured swelling pressures at the low (initially void) and high density (initially clay) ends of the same test samples appear to be much closer in value for those experiments at or above 100°C.

At the time of writing, the moisture content data was available for 2 out of 3 of the swelling pressure tests that have been completed; both were run at 100°C. Variation in moisture content along the sample length is shown in Figure 2.8. Values were observed to be highest at the top of the vessel, which is intuitive, given that this was initially occupied solely by water and was expected to contain the lowest density part of the sample at decommissioning. Data are also shown from two comparable experiments conducted on Mx80 bentonite (dry density=1.7 g/cm^3) at 20 and 90°C Daniels et al. (2021).

Comparison of the results indicates an increase in uniformity of the moisture content distribution as a result of increasing test temperature. However, it should be noted that the tests shown at 20 and 90°C were conducted on slightly shorter samples, which has also been shown to decrease the degree of uniformity. Nevertheless, a larger increase in uniformity is observed between 90 and 100°C than between 20 and 90°C and it seems likely that the elevated temperatures have also played a role. Comparison between the moisture content profiles for the two tests conducted at 100°C also demonstrates a much greater degree of variation along the sample for the lower density (1.5 g/cm^3) sample, suggesting that heterogeneity is more likely to persist over the same timeframe at lower densities. The additional test data from the remaining planned experiments have yet to be compiled, but should provide deeper insight into these observations.

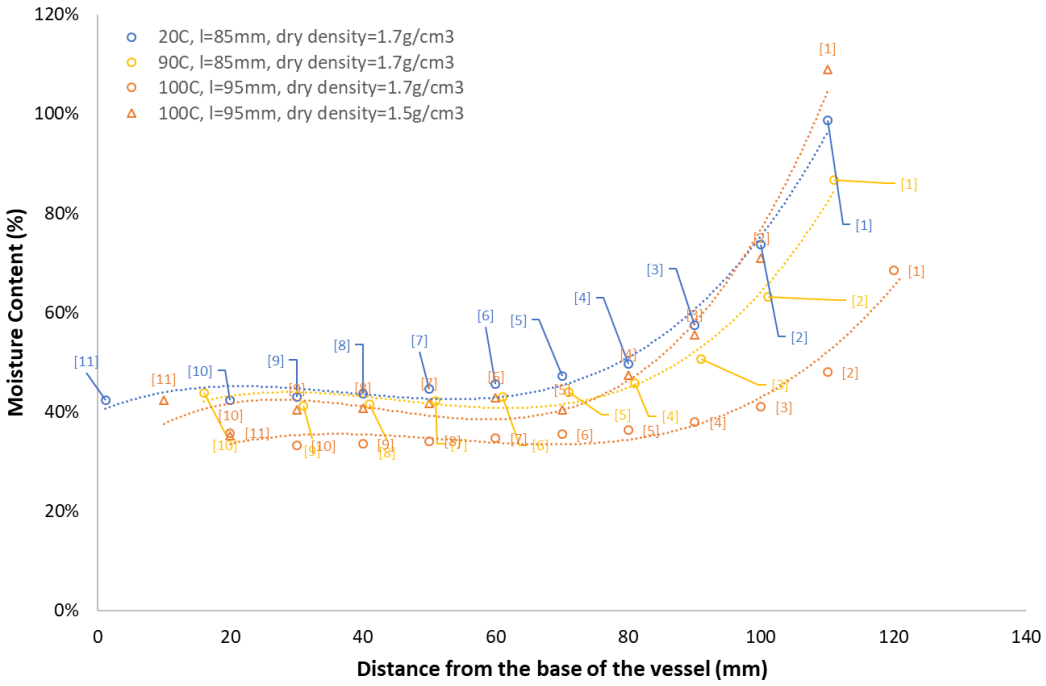

Figure 2.8 – Moisture content distributions along samples post-testing, for various temperatures and dry densities. [BGS © UKRI]

Swelling pressure development – constant volume

This section details the findings from swelling pressure experiments run under a constant volume boundary condition (samples had the same length as the interior of the pressure vessel). The samples were subjected to an applied water pressure of 4.5 MPa, whilst also being subjected to an elevated temperature of either 100, 150 or 175°C for a period of approximately 50 days. Swelling pressures were calculated by subtracting the applied water pressure from the recorded axial and radial stresses.

The resulting swelling pressure evolution for samples with dry densities of 1.3 and 1.7 g/cm^3 are shown in

Figure 2.9 – Swelling pressure evolution for swelling tests on bentonite samples with a dry density of (top row) 1.3 g/cm^3 (Swelling Tests 9, 11, 10, from left to right) and (bottom row) 1.7 g/cm^3 (Swelling Tests 6.8.7, from left to right). [BGS © UKRI]Figure 2.9. Two findings are immediately apparent. Firstly, tests run at equivalent temperatures show a substantially higher swelling pressure for the higher dry density samples. This is in line with many previous studies and provides confidence in the test approach. Secondly, in the case of the higher dry density samples (1.7 g/cm^3), a clear reduction in the observed swelling pressure is apparent with increasing temperature. In contrast, the lower dry density samples (1.3 g/cm^3) show relatively minimal response to increasing temperature. This relative insensitivity/sensitivity to temperature is further demonstrated in Figure 2.10, which shows the average swelling pressure calculated for an interval of the last 100 data points in each test. Comparison with pre-existing room temperature data in future should delineate these trends further.

It is also interesting to note some differences in the form of the swelling pressure curves between tests. In particular, the lower dry density samples show a relatively rapid response to boundary conditions, whilst at higher dry densities a more gradual evolution is apparent and pressures had not yet reached an asymptote before testing had concluded. More particularly, the measured swelling pressure shows a gradual degradation with time in these tests, which appears most pronounced at higher temperatures.

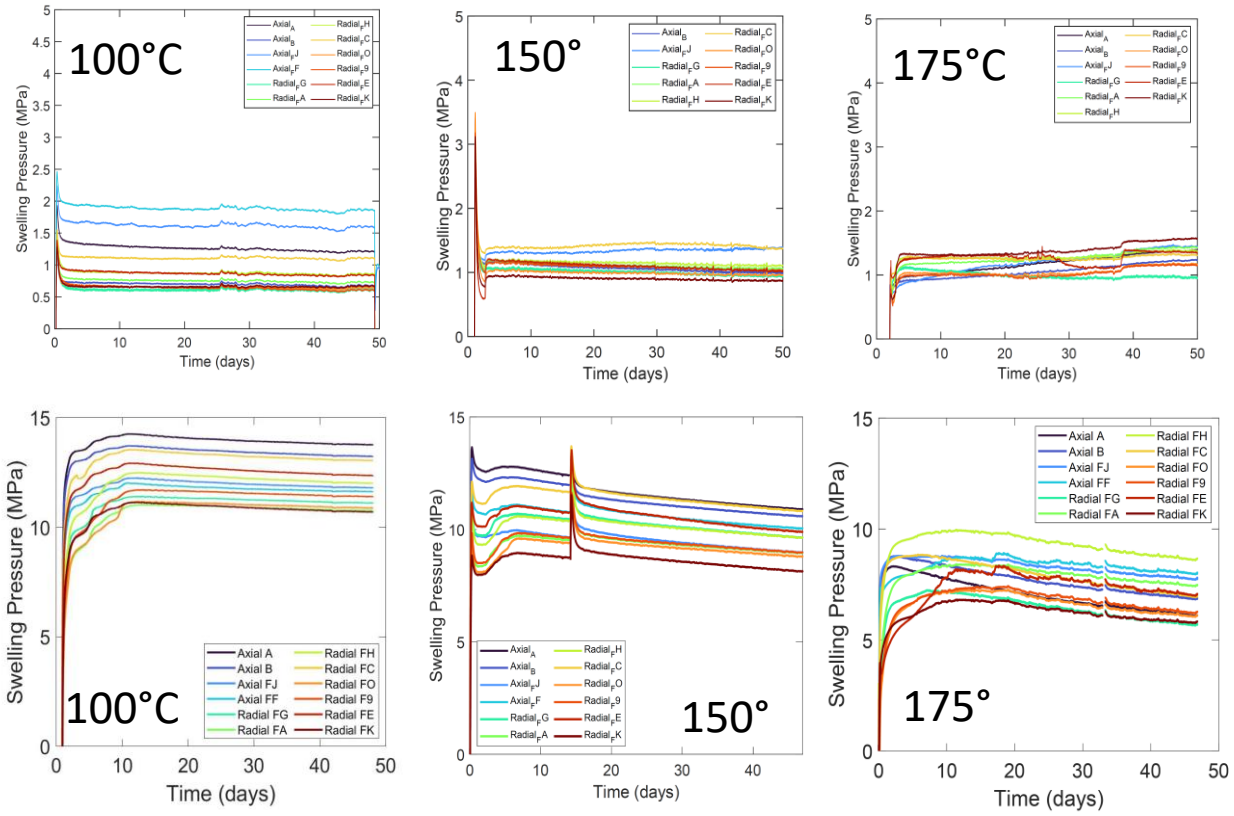

Figure 2.9 – Swelling pressure evolution for swelling tests on bentonite samples with a dry density of (top row) 1.3 g/cm³ (Swelling Tests 9, 11, 10, from left to right) and (bottom row) 1.7 g/cm³ (Swelling Tests 6.8.7, from left to right). [BGS © UKRI]

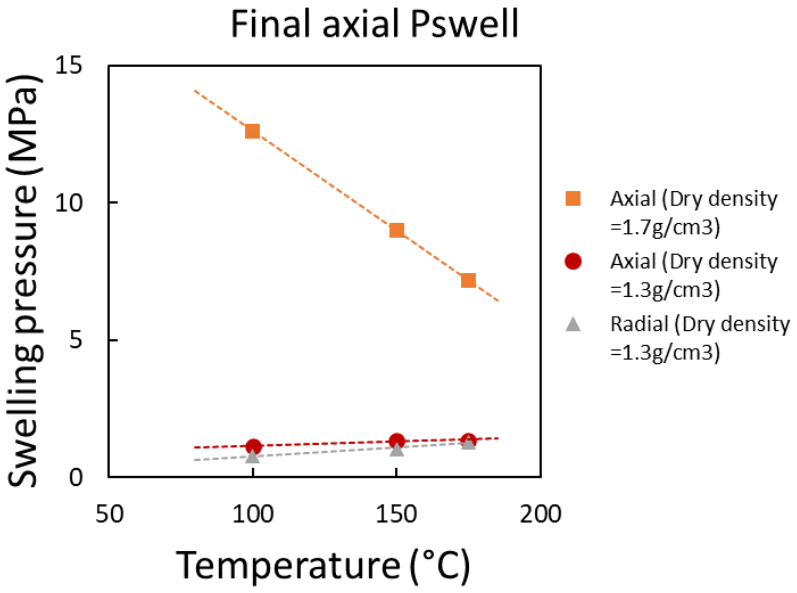

Figure 2.10 – Average swelling pressure, calculated for an interval of the last 100 data points in each test, against temperature. [BGS © UKRI]

Permeability evolution

These tests consist of an initial hydration phase, followed by hydraulic testing whilst the sample is subjected to thermal cycling. Figure 2.11 shows the test history for Permeability Test A (dry density=1.56 g/cm^3). The sample was hydrated from both ends at a constant pressure of 2 MPa and changes in the local stress field were monitored. Figure 2.12 shows the resulting evolution of swelling pressure during this time. Swelling pressures were calculated by subtracting the average applied water pressure (at the up- and down-stream pumps) from the recorded axial and radial stresses.

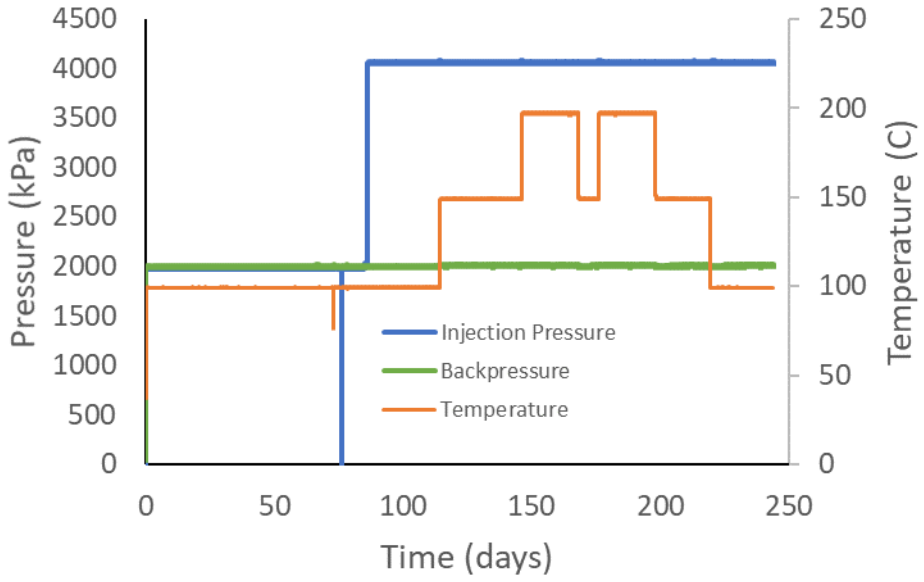

Figure 2.11 – Test history for Permeability Test A, including initial hydration and swelling phase, followed by constant pressure hydraulic testing and two thermal loading cycles. [BGS © UKRI]

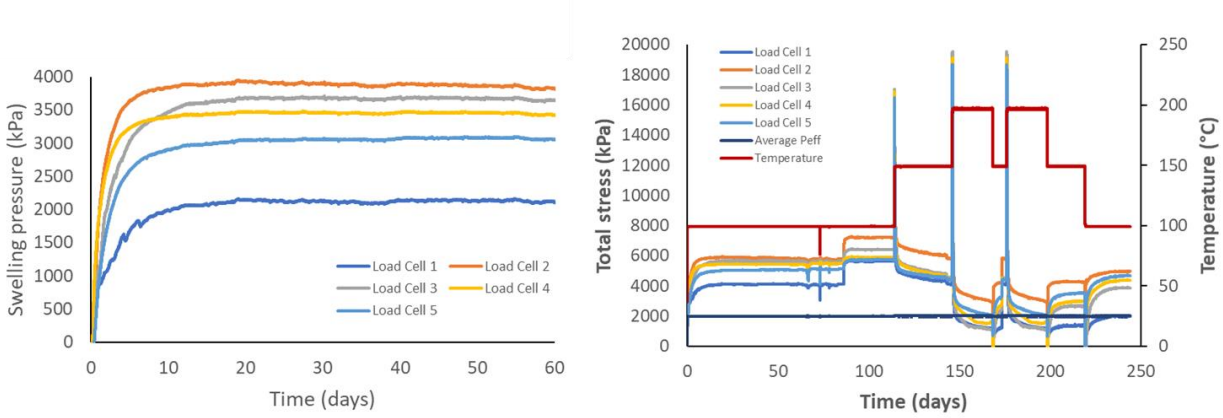

Figure 2.12 – Permeability Test A (Left): Swelling pressure evolution during the initial hydration phase. (Right): Changes in measured stresses during initial hydration (days 0-86), application of a hydraulic gradient (days 86-114) and thermal loading (days 114-250). The brief decline in temperature and associated changes in swelling pressure at around day 75 is the result of efforts to reduce a leak in the downstream system. [BGS © UKRI]

During this hydration phase it became apparent that there was a leak in the backpressure system and efforts were made to improve leakage rates, but only a small reduction could be achieved. Given the relatively small leakage rate, at day 86.2, the applied water at the injection filter was increased to 4 MPa, applying a 2 MPa pressure gradient across the sample and resulting in hydraulic flow across the sample. The associated cumulative volume changes at the injection and backpressure pumps are shown in Figure 2.13. The injection pump showed an inflow of fluid, as expected, but the downstream pump

recorded a greater change in volume than expected, which is attributed to the ongoing leak previously detected during hydration. Further efforts were made to reduce the leak at this stage, but it was thought to have arisen from a pressure connector that could not be accessed without reducing to ambient temperature and disassembling the apparatus. Instead, an attempt was made to correct for this by removing an assumed linear leakage rate from the backpressure data (Figure 2.13, yellow). The results were not fully satisfactory, however, and it was decided to rely only on the upstream data provided by the injection pump for the remainder of testing and to calculate hydraulic permeability.

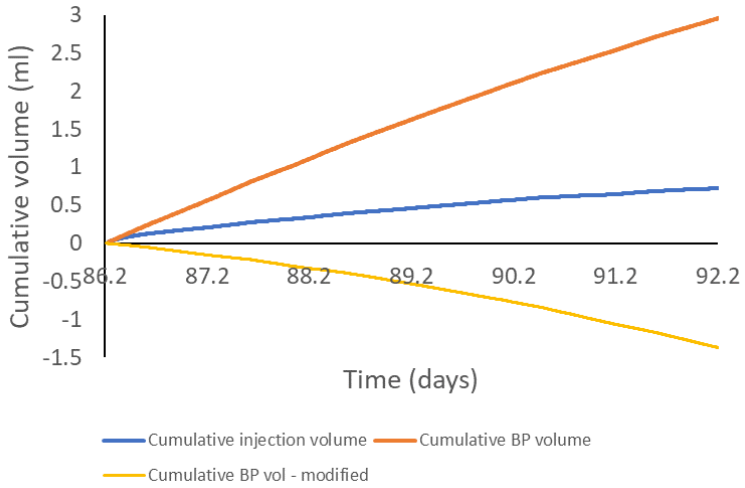

Figure 2.13 – Cumulative fluid flow volumes during the first step of hydraulic testing (Permeability Test A). [BGS © UKRI]

Swelling pressures were estimated for each thermal step of the experiment and the results indicate a substantial decline as a result of thermal loading (Figure 2.14, left). At 200°C (Step 3), negative values are reported representing the incapacity of the apparatus to measure swelling pressures which were essentially non-existent at this stage. Initial estimates of swelling pressure were calculated using the average pore-water pressure across the sample length, but it should be noted that this is a crude approximation, since a 2 MPa pressure gradient was applied to induce hydraulic flow. Future interpretation will include further examination of the approaches to estimating swelling pressure, including using pore water pressure values recorded at the closest location to the swelling pressure measurement. Nevertheless, over the course of the test programme a similar trend is observed across all sensors. The overall form of the swelling pressure curve is similar to that observed for mechanical consolidation of clays and suggests that non-recoverable yield of the clay occurred. As with the experiments conducted in the swelling pressure test programme, at 100°C, swelling pressures were observed to equilibrate after a change in temperature. However, as temperature was stepped up higher, pressures were seen to continue to decline, rather than reach a plateau, and testing was moved onto the next temperature step. It is interesting to note that a similar temporal degradation was observed in the swelling pressure tests conducted at a slightly higher dry density (1.7 g/cm^3; see Figure 2.9).

The rate of hydraulic inflow was also observed to increase in response to thermal loading. Given the previously described leak in the downstream system, hydraulic permeabilities were calculated using upstream values measured by the injection pump and calculated using values for viscosity and density of water at the pressure and temperature at which they were obtained. After correction for these changes the resulting calculated permeabilities were still found to increase during thermal loading and ranged between 5.4x10^{-21} and 7.9x10^{-21} m^2 (Figure 2.14, right). However, the observed increase was relatively minimal, despite persisting throughout the duration of the experiment, even after temperatures were returned to the initial baseline of 100°C. This hysteresis in permeability is coincident with the permanent reduction in swelling pressure observed during testing and could be explained by a contraction in sample volume resulting from thermal consolidation at elevated temperatures.

Additional XRD analysis is underway and may help to exclude or provide another, geochemical, cause for this behaviour. This work, combined with numerical modelling of the test dataset, may provide additional insight into this observed behaviour on thermal loading.

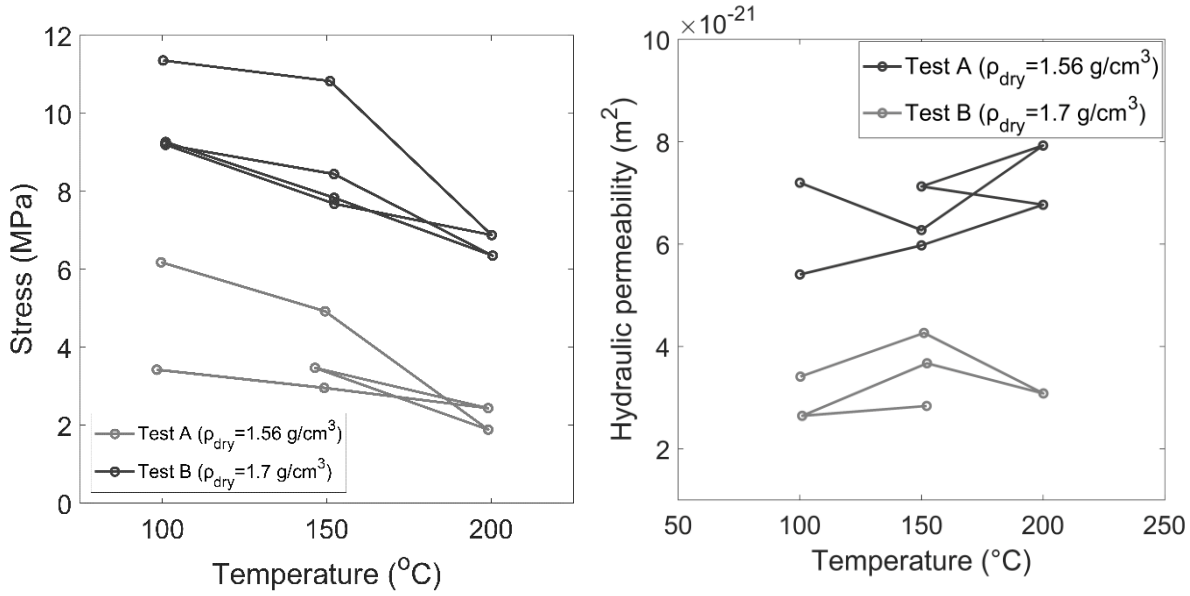

Figure 2.14 – Measured average stress (left) and hydraulic permeability (right), as a function of temperature, for each test stage at selected intervals throughout the test programme. [BGS © UKRI]

Permeability Test B followed a similar test history to Test A (Figure 2.15) on a sample with a dry density of 1.7 g/cm^3. As expected, higher stresses were recorded than those in Test A, which can be explained by the higher dry density. Similarly, measured hydraulic permeability values were lower than in the previous test, which can be explained by the difference in dry density. A reduction in swelling pressure was apparent with increasing temperature and displayed a similar form (Figure 2.16). As before, this reduction was not recovered in full on returning to the original temperature (Figure 2.14). A continual temporal degradation in swelling pressure was again apparent when temperatures of 150°C and above were applied, although this degradation was no longer significant during the second thermal loading cycle. It is interesting to note that this sample was fully unloaded to 100°C, before being reloaded. Comparison with thermal loading in Permeability Test C (dry density=1.3 g/cm^3), will provide additional insight into these findings shortly.

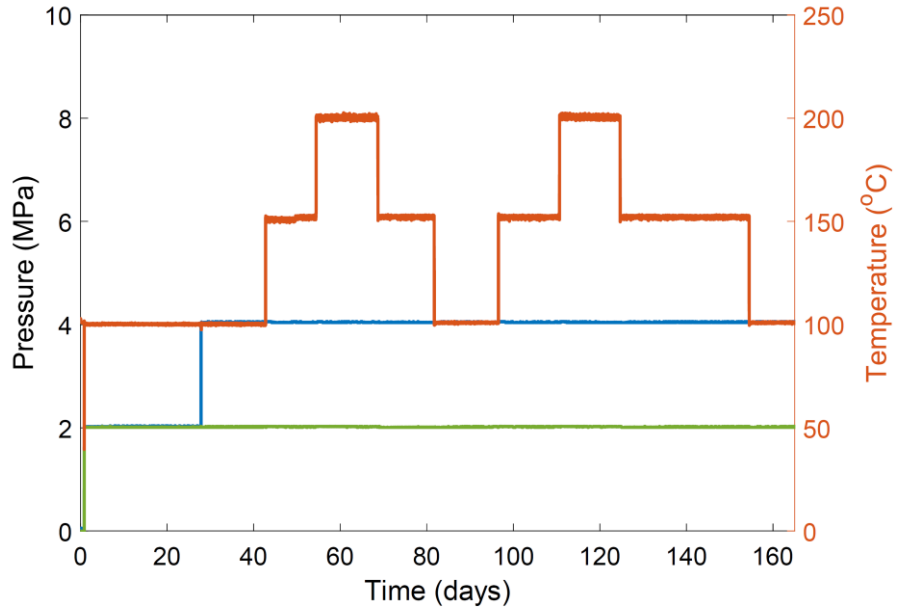

Figure 2.15 –Test history for Permeability Test B, including initial hydration and swelling phase, followed by constant pressure hydraulic testing and two thermal loading cycles. [BGS © UKRI]

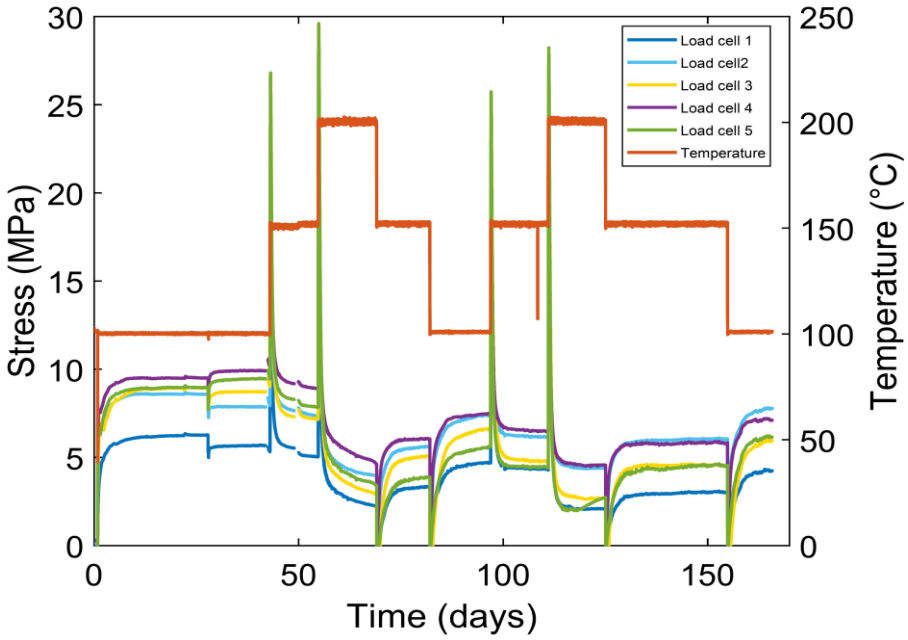

Figure 2.16 – Permeability Test B, showing changes in measured stresses during initial hydration (days 0-28), application of a hydraulic gradient (days 28-42) and thermal loading (days 42-165). [BGS © UKRI]

2.4 Conclusion

A series of experiments have been conducted to examine the hydromechanical response of bentonite at high temperatures and the following objectives have been achieved:

- The influence of elevated temperatures on swelling pressure has been examined, for several dry densities and axial strains.

- The evolution of permeability (and associated swelling pressures) has been delineated, as a function of temperature, for two different dry densities (with a third ongoing).

Testing has included two experimental programmes, which focussed on examining the impact of high temperatures on: (i) swelling pressure development and (ii) permeability evolution. More specifically, the influence of elevated temperatures on swelling pressure has been examined for several test samples and the form of this relationship has been examined for a range of dry densities and axial strains. The evolution of permeability (and associated swelling pressures) has been delineated, as a function of temperature, for one of three dry densities under consideration.

Key findings were as follows:

- Significant heterogeneity remains in most of the observed swelling pressure distributions, even after 50 days. This heterogeneity is substantially greater in those samples allowed to swelling axially over the course of 100 days.
- As expected, in all cases, significantly higher swelling pressures were generated for higher dry density samples.
- Measured swelling pressure was found to reduce with increasing temperature (100-175°C) for dry densities of 1.6 g/cm^3 (Permeability Test A) and 1.7 g/cm^3 (Swelling Tests 6-8, Permeability Test B). This was also the case in tests where axial swelling was permitted (Swelling Tests 1-5; dry densities of 1.5 g/cm^3 and 1.7 g/cm^3).
- Measured swelling pressure was found to be comparably insensitive to temperature for a lower dry density of 1.3 g/cm^3 (Swelling Tests 9-11).
- Where swelling pressure is seen to reduce, a notable temporal degradation is apparent in swelling pressure (Swelling Tests 6-8, Permeability Test B), which is not observed for lower dry density tests (Swelling Tests 9-11).
- Thermal cycling indicates that this reduction in swelling pressure is hysteretic and not recovered on unloading (Permeability Test A, Permeability Test B).
- Minimal change in hydraulic permeability was found to occur with increasing temperature (100-200°C), despite measured impacts on swelling pressure (Permeability Test A, Permeability Test B).

One possible explanation for the observed reduction in swelling pressure at higher dry densities is thermally-induced yield of the sample, between temperatures of 100-200°C. Contraction of the bentonite, as a result, would result in a drop in stresses under a constant volume condition and is consistent with only a minimal increase in hydraulic permeability that can be explained by flow of water along the sides of the sample. Further work is required to fully assess this hypothesis. In particular, XRD analysis is currently underway to assess the possibility of a geochemical mechanism. Inclusion of pre-existing room temperature swelling pressure measurements and additional testing at intermediate dry densities will be particularly helpful to examine this behaviour. Further work examining the rate and controls on the observed time-dependent degradation in swelling pressure at higher dry densities will also be crucial to understand the causes and consequences of this behaviour. These findings clearly demonstrate the importance of examining THM behaviour of bentonite when considering the scenario of a geological disposal facility operating at temperatures >100°C.

3 BRGM (ANDRA)

3.1 Introduction

The optimization of the swelling behaviour of bentonites in a nuclear waste disposal as a function of the physical and chemical conditions and the imposed temperature requires a good description of the mechanisms driving the swelling of the bentonite during the infiltration of a given solution. Indeed, the swelling of bentonite has its origin at the crystal layer scale. The two main mechanisms driving the swelling of smectite-rich materials are the crystalline swelling and the osmotic swelling. Several experiments have been undertaken to understand the effect of temperature on these mechanisms of crystalline and osmotic swelling.

In task 3.2 the goal of the BRGM is characterizing the effect of temperature on the total swelling pressure. With this aim, a miniature oedometer cell has been developed to combine swelling pressure measurement and imaging of the bentonite microstructure evolution during its hydration. The objective is the acquisition of swelling pressures at different temperatures (25, 60, 80, 100 and 150°C), densities (1.4, 1.5 and 1.6 g·cm^{-3}) and chemical conditions (Na or Ca Kunipia bentonite, salinities). The Kunipia-G bentonite was used in these tests.

3.1.1 Material

For a detailed material description, please refer to deliverable D7.7 on Task 3.1.

3.1.2 Research plan

3.1.2.1 Material (BoM item): Kunipia-G. Powder as delivered by producer
3.1.2.2 Material treatment (sample preparation for test): Na or Ca homoionization of the bentonite. Uniaxial compaction to reach densities of 1.4; 1.5; 1.6 g.cm^{-3}.
3.1.2.3 Temperature (at which measurement/test is carried out): 25°C to test the oedometer cell suitable for X-ray tomography acquisition and to have a reference behaviour, then at several temperatures 60°C, 80°C, 100°C and 150°C.
3.1.2.4 Tests carried out (name, description, sample preparation, procedure, results): Measurements of the swelling pressure during the hydration of the bentonite with solutions of different compositions (cations and ionic strength), at different temperatures (25°C, 60°C, 80°C, 100°C and 150°C), using Na-Kunipia or Ca-Kunipia compacted at different densities (1.4, 1.5, 1.6 g/cm^3). The microstructure evolution along the hydration experiment will be followed, visualizing it directly in the oedometer cell. The goal is to be able to explain the swelling behaviour of the bentonite because the pore scale electrostatic properties and the microstructure rearrangement during hydration.
3.1.2.5 Schedule and expected date(s) of results delivery: September 2022

Table 3.1 – BRGM – Synthesis of research plan in Task 3.2

3.2 Procedures

3.2.1 Laboratory set-ups, procedures and protocols

The swelling pressure generated by the hydration of Kunipia-G at constant volume is measured using a miniaturized device specifically designed for the EURAD/HITEC project (Figure 3.1). The smectite is compacted at the chosen density in a 9 mm high and diameter cylindrical peek cell. The volume of the sample is blocked by an upper and lower piston. A load sensor flush with the face of the upper piston is screwed against a press cylinder fixing the system (sensor, cell). An LVDT sensor also measures the minimum allowed displacement of the upper piston. A saline solution of a well-defined concentration is then injected into the cell through the lower piston. Two methods were considered to increase the temperature: either the whole device is placed inside an oven (Figure 3.2), or the cell body is exclusively heated with heating pads. The swelling force and the displacement are recorded in a database during the test.

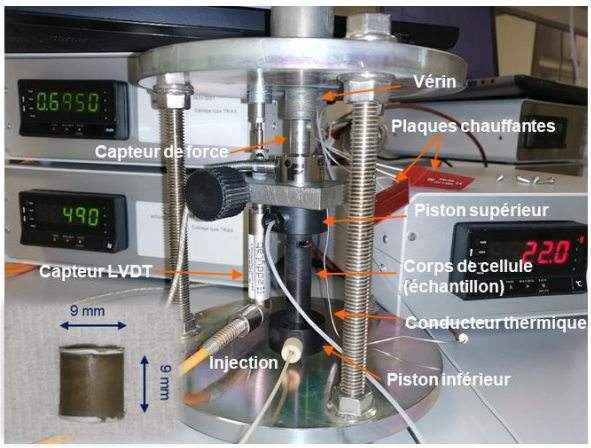

Figure 3.1 – Swelling pressure measurement device

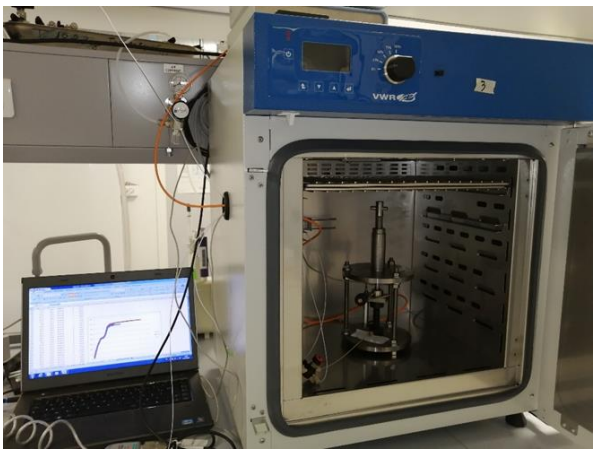

Figure 3.2 – Swelling pressure test inside an oven

Swelling experiment conditions

Several swelling tests are conducted in different physico-chemical conditions allowing to evaluate their impact on the swelling pressures. The conditions that are changing between the different experiments are the density, the nature of the interlayer cations, the ionic strength of the hydrating solutions and the temperature. The swelling forces and pressures, the final height of the hydrated sample and the water content are then determined. Swelling tests are performed on a sodium and calcium Kunipia bentonite compacted at densities of 1.4, 1.5 and 1.6 g/cm^3, hydrated by saline solutions of ionic strength of 10^{-4} M, 10^{-1} M and 1 M and at temperatures ranging from 25°C to 150°C.

3.3 Results

3.3.1 Investigation performed

The swelling tests already performed considered a sodium and calcium Kunipia compacted at densities of 1.4, 1.5 and 1.6 g/cm^3, hydrated by saline solutions of ionic strength 10^{-4} M, 10^{-1} M and 1 M, at temperatures of 25°C, 60°C and 80°C. In the following months, it is planned to conduct these same tests at temperatures of 100°C and 150°C.

3.3.2 Results from investigation

Effect of compaction

Swelling tests realized on compacted sodium and calcium bentonites at different densities showed that the swelling pressure at equilibrium increases by densifying the material (Figure 3.3). It is also interesting to note that the double peak shape observed for the swelling pressure curves becomes less pronounced with increasing density. This double peak shape is associated with macropores collapse during hydration at constant volume when the swelling pressure exceeds the aggregate shear strength. Hence, by densifying the material the macropores are considerably reduced and the rearrangement of the aggregates is more restrained.

A comparison of our results is made in Figure 3.4 with the normalized swelling pressures of a dozen clayey materials from the literature as a function of the dry density. We notice that the swelling pressures of Na-Kunipia follow the typical exponential evolution of all available data but rather in its upper envelope since it is a pure material. The spreading of the points can also be related to different hypotheses, such as the method of sample preparation. Our results are in line with those of (Massat, Cuisinier et al. 2016) who worked on the same material. As for the swelling pressures of Ca-Kunipia, they follow a slightly higher tendency because divalent montmorillonites generate higher pressures.

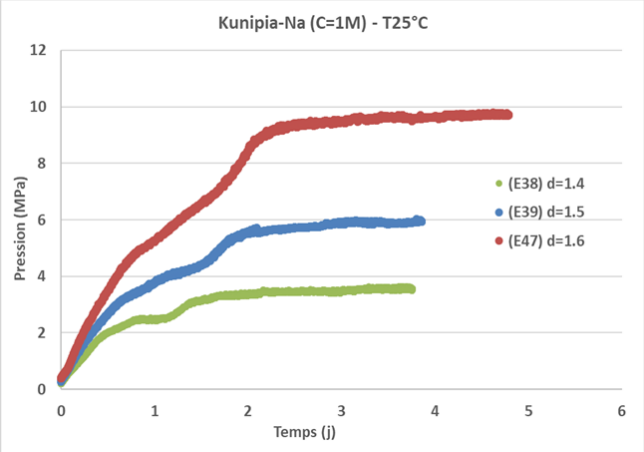

Figure 3.3 – Swelling pressure curves of Kunipia-Na compacted at d=1.4; 1.5 and 1.6 g·cm^{-3}.

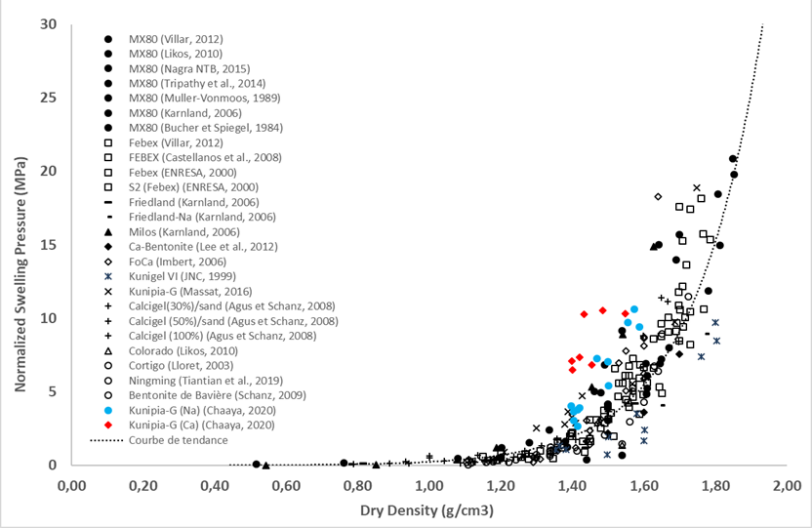

Figure 3.4 – Summary of swelling pressure tests

Effect of chemistry

Another result of interest is that the pressure at the equilibrium state is more important when the ionic strength is low. More precisely, a decrease of the ionic strength generates an increase of the diffuse double layer thickness, thus generating an increase of the repulsive forces (osmotic pressure) and thus of the swelling pressure.

The results of the swelling tests conducted at room temperature are shown in Figure 3.5 as a function of ionic strength at different densities to evaluate the effect of salinity on the swelling. The effect of the interlayer cations on the swelling pressure has also been evaluated.

First of all, we notice that the swelling pressures of Ca-Kunipia are more significant than those of Na-Kunipia. We also notice that by densifying the sodium or calcium Kunipia, the osmotic effect (generating a difference in total pressure at equilibrium as a function of the ionic strength) becomes less important (as the inter-particle spaces where the double layers develop are reduced). The crystalline pressure becomes the main component of the swelling pressure and therefore the ionic strength has a less significant effect on the equilibrium swelling pressures. This mechanism remains relatively more pronounced in monovalent bentonites, as compared to divalent bentonites, which is in agreement with the bibliographic results.

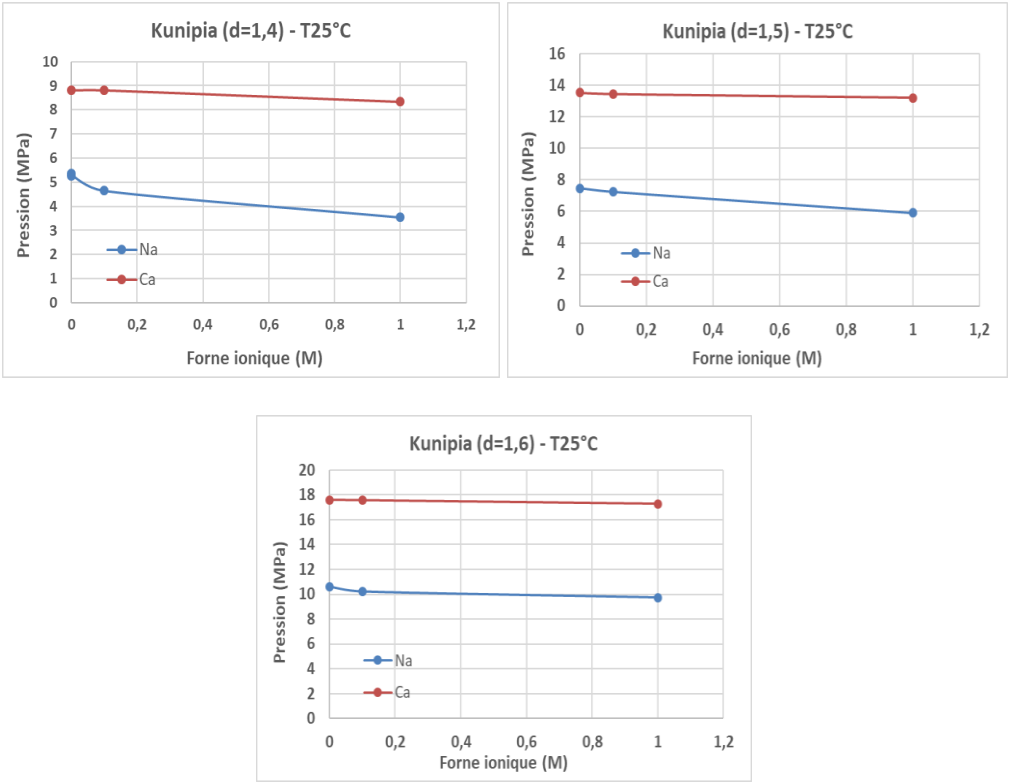

Figure 3.5 – Swelling pressure measured on Na and Ca Kunipia bentonite as a function of the solution ionic strength at compaction densities of 1.4, 1.5 and 1.6 g/cm³,. Measurements made at 25°C.

Effect of temperature

The preliminary results show that the swelling pressure measured on Na-Kunipia decreases with increasing temperature (Figure 3.6). The steady state is also reached more rapidly. We also notice that the temperature effect becomes less significant by increasing the density and the ionic strength of the hydrating solution. In particular, at 80°C we can no longer visualize any concentration effect on the swelling pressures of Na-Kunipia. For Ca-Kunipia, the effect of temperature on the swelling pressures is significantly reduced (Figure 3.7). Indeed, the swelling pressure remains almost constant regardless of the temperature.

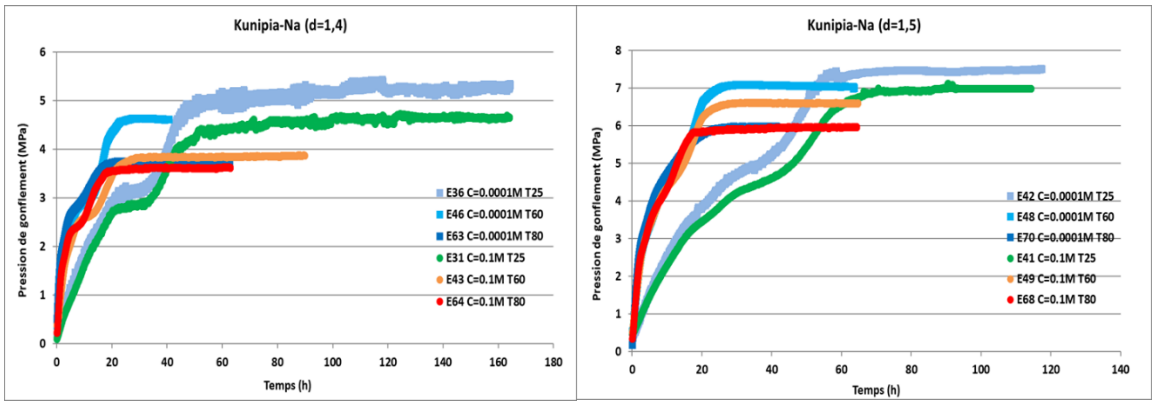

Figure 3.6 – Effect of temperature (25, 60, 80°C) on the swelling pressure of Na-Kunipia compacted at densities of 1.4 and 1.5 and using saturation solutions of ionic strengths of 0.0001 M and 1 M.

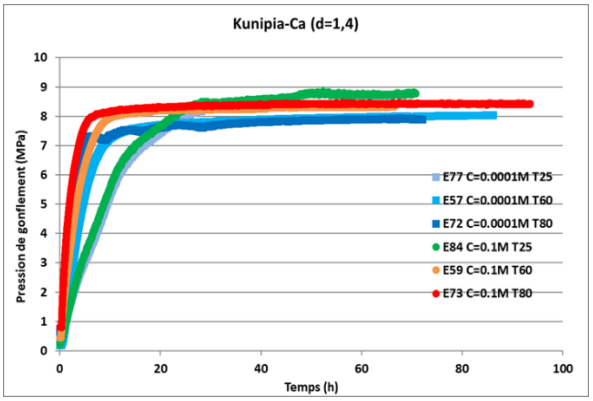

Figure 3.7 – Effect of temperature (25, 60, 80°C) on the swelling pressure of Ca-Kunipia compacted at a density of 1.4 and using saturation solutions of ionic strengths of 0.0001 M and 1 M.

3.4 Conclusion

In this task 3.2, the effect of temperature on the total swelling pressure is investigated. A miniature oedometer cell has been developed to combine swelling pressure measurement and imaging of the bentonite microstructure evolution during its hydration. For the moment, swelling pressures have been measured at different temperatures (25°C, 60°C and 80°C), densities (1.4, 1.5 and 1.6 g·cm^3) and chemical conditions (Na or Ca Kunipia bentonite, ionic strengths of 10^{-4}, 10^{-1} and 1 M). A conceptual interpretation of these respective effects on the swelling behaviour of the bentonite has been initiated.

In the remainder of the EURAD/HITEC project, swelling pressure measurements will be performed at higher temperatures (100°C and 150°C). The microstructure evolution will be followed in-situ during several tests of bentonite hydration in the miniature oedometer. An in-depth interpretation of the swelling pressure measurements will be performed, using numerical models capable of identifying the respective contribution of crystalline and osmotic swelling.

4 CIEMAT

4.1 Introduction

The water retention curve of two different bentonites has been determined at temperatures of up to 100°C with focus on the low suction range. The measurements in this suction range, which is very relevant for the final stages of barrier saturation, are more complicated and the available curves are usually not well defined in this range.

The methodology selected did not allow to reach temperatures as high as initially foreseen (140°C). To make up for this deviation with respect to the initial plan, a methodology was fine-tuned to determine the swelling pressure of compacted bentonite at high temperature using swelling tests performed in oedometers under different vertical loads.

4.1.1 Material

FEBEX bentonite

It is a 900-t batch prepared in 1996 coming from the Cortijo de Archidona quarry (Cabo de Gata area, SE Spain). On-site it was homogenised, air-dried and volcanic pebbles were manually removed. At the factory the processing consisted of crumbling, drying in a rotary oven at temperatures between 50 and 60°C and sieving through a 5-mm mesh.

More than 90% is a montmorillonite-illite mixed layer (with 10-15% of illite layers), with variable quantities of quartz (2±1%), plagioclase (3±1%), K-felspar (traces), calcite (1±1%), and cristobalite-trydimite (2±1%). Ca^{2+} (33±2 meq/100 g), Mg^{2+} (33±3 meq/100 g) and Na^{+} (28±1 meq/100 g) are the main exchangeable cations. The main soluble ions are sodium and chloride (ENRESA 2006). Other THM properties can be found in (Villar and Gómez-Espina 2009).

MX-80 bentonite

From Wyoming (USA), produced by American Colloid Co. It is a bentonite of volcanic origin, powdered and Na-homogenised. The powder used was received from Posiva (supplier Sibelco Nordic AB).

The content of montmorillonite is between 65 and 90% (~77% for the batch used), with quartz, plagioclase and K-feldspars (contents between 4 and 15%), and minor quantities of cristobalite, trydimite, calcite, gypsum, pyrite, illite. Na^{+} is the main exchangeable cation (50-74 meq/100 g), with also Ca^{2+} (10-30 meq/100 g) and Mg^{2+} (3-8 meq/100g) (Villar 2005, Villar, Gómez-Espina et al. 2006, Kiviranta and Kumpulainen 2011, Kiviranta, Kumpulainen et al. 2018).

4.1.2 Research plan

4.1.2.1 Material (BoM item): MX-80 powder and FEBEX granulate as-received
4.1.2.2 Material treatment (sample preparation for test): Samples compacted directly into constant volume, hermetic cells at high density (1.5 and 1.6 g/cm^3) with different water contents
4.1.2.3 Temperature (at which measurement/test is carried out) 20-100°C (initial aim was 140°C but it was not achievable)
4.1.2.4 Tests carried out (name, description, sample preparation, procedure, results): Global heating with no vapour lost and simultaneous measurement of relative humidity
4.1.2.5 Schedule and expected date(s) of results delivery: 2019-2021

Table 4.1 – CIEMAT - Water retention curve at high temperature

4.1.2.6 Material (BoM item): MX-80 powder and FEBEX granulate as-received
4.1.2.7 Material treatment (sample preparation for test): Samples compacted directly into the oedometer ring at density 1.5 and 1.6 g/cm^3 with initial hygroscopic water content
4.1.2.8 Temperature (at which measurement/test is carried out) 80°C (initial aim was to get to 120°C but not time enough because these tests started late)
4.1.2.9 Tests carried out (name, description, sample preparation, procedure, results): Swelling tests using deionised water under different vertical loads. Extrapolation from them of swelling pressure
4.1.2.10 Schedule and expected date(s) of results delivery: 2023-2024

Table 4.2 – CIEMAT – Swelling capacity and swelling pressure at high temperature

4.2 Procedures

4.2.1 Water retetention curves

The tests consisted in determining the suction of bentonite samples compacted at nominal dry densities of 1.5 and 1.6 g/cm^3 with different water contents. The relative humidity and temperature of the

compacted samples were measured with psychrometers (Caged-screen Spanner-type thermocouple psychrometers Wecor Elitech PST-55-30-SF, precision ~30 kPa) or capacitive sensors (Sensirion SHT75 or Vaisala HMP233) and these values were converted into suction through Equation 1:

$$s = \frac{\rho_w \times R \times T}{M_w} \ln\left(\frac{\mathrm{RH}}{100}\right) \quad (1)$$

where R is the universal constant of gases (8.3143 J/mol·K), T the absolute temperature, ρ_w the density of water (998 kg/m^3 at 293 K) and M_w, the molecular weight of water (0.018 kg/mol).

The bentonite was mixed with different quantities of deionised water. These mixtures were preserved in hermetic plastic bags for several days to ensure a good homogenization. Afterwards, the wet bentonite was compacted inside stainless-steel cells at dry densities of 1.5 and 1.6 g/cm^3 applying uniaxial pressures between 6 and 69 MPa, higher for FEBEX and as the water content was higher. The samples had diameters of 70 mm and heights of 100 mm. A drill was made in the centre of the top of the cylinders to insert the sensors inside. In some cases two different sensors (capacitive and thermocouple psychrometers) were inserted at a time in the same sample. In these cases holes were drilled through top and bottom and each sensor was inserted through a different side. For the capacitive sensors the hole had a diameter of 14 mm and for the psychrometers of 8 mm. Afterwards the lid of the cell was tightened and the hole through which the cable passed through the lid was sealed with thermoresistant silicone. The cell was covered laterally with a silicone heater mat and external insulation was wrapped around (Figure 4.1).

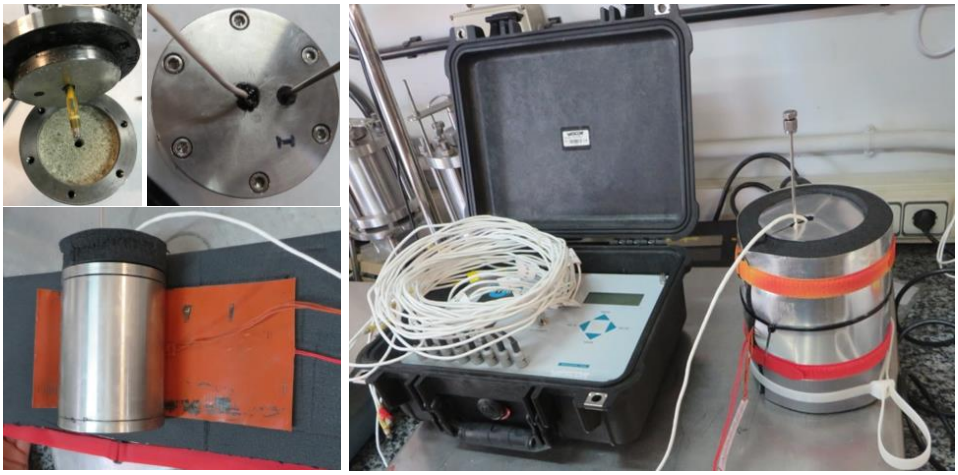

Figure 4.1 – Cell assemblage: hole drilled on the bentonite surface to insert the sensor, sealing of the cable inlet with thermoresistant silicone, wrapping with heating mat and insulating material (left); cell in operation with a psychrometer inserted

The tests started at room temperature and the temperature was increased from 40°C to 100°C at intervals of 20°C. The time interval for a stable measurement was >60 min. The initial characteristics of the samples tested are shown in Table 4.3, including dry density (ρ_d) and water content (w). Since there is no accurate knowledge of the values that the average density of water can take (which would depend on the bentonite density and water content), the customary value of 1 g/cm^3 was used to compute the degree of saturation (S_r) values shown in the Table. This would partially explain the degrees of saturation higher than 100% found in some samples (Lloret and Villar 2007, Jacinto, Villar et al. 2012).

Reference	**Initial *w* (%)**	**Initial ρ_d (g/cm^3)**	**Initial S_r (%)**	**Reference**	**Initial *w* (%)**	**Initial ρ_d (g/cm^3)**	**Initial S_r (%)**
Febex 1.6 Sr90% r[a]	22.9	1.50	77	MX80 1.5 Sr70	22.2	1.48	69
Febex 1.5 Sr85%	25.0	1.48	82	MX80 1.5 Sr77	24.0	1.48	75

Reference	Initial *w* (%)	Initial ρ_d (g/cm^3)	Initial S_r (%)	Reference	Initial *w* (%)	Initial ρ_d (g/cm^3)	Initial S_r (%)
Febex 1.5 Sr90%	26.9	1.50	90	MX80 1.5 Sr90	28.0	1.49	88
Febex 1.5 Sr94%	29.2	1.47	94	MX80 1.5 Sr95	29.9	1.49	94
Febex 1.5 Sr95%	30.1	1.45	95	Mx80 1.6 Sr80	21.9	1.57	78
Febex 1.6 Sr82%	22.3	1.56	83	Mx80 1.6 Sr90	24.4	1.59	88
Febex 1.6 Sr87% r	23.4	1.56	87	Mx80 1.6 Sr95	26.1	1.58	94
Febex 1.6 Sr90%	22.9	1.58	87	Mx80 1.6 Sr100	27.2	1.58	98
Febex 1.6 Sr95%	24.5	1.57	92				
Febex 1.6 Sr95% r	23.8	1.62	97				
Febex 1.6 Sr100%	25.4	1.61	102				
Febex 1.6 Sr105%	28.9	1.57	108				
Febex 1.6 Sr105% r	28.0	1.56	104				

[a] density below the target value

Table 4.3 – Characteristics of the samples used for the determination of the water retention curve

4.2.1 Swelling tests

The granulated clay with its hygroscopic water content was compacted uniaxially and statically at room temperature in the oedometer ring, which had an inner diameter of 5 cm approximately, the length of the resulting specimen being 1.2 cm. Nominal dry densities of 1.50 and 1.60 g/cm^3 were used. The ring-specimen assemblage thus obtained was placed in the oedometer cell where the sample was confined between porous ceramic sinters (Figure 4.2). The oedometer assemblage was placed inside a thermostatic bath, a small setting load of around 0.01 MPa was applied to the sample though the loading ram and the linear transducer was adjusted. The bath was slowly filled with silicone oil and the heating device was switched on. Once the target temperature was reached in the silicone oil (80°C for all the tests performed so far), the axial strain was written down and the vertical load was applied. Vertical loads of between 2 and 5 MPa were applied. After a period of 10 minutes to stabilise the deformation of the sample caused by loading, hydration started through the bottom of the sample with deionised water injected through a peristaltic pump. During the test the vertical load remained constant and the vertical strain was continuously measured with a linear transducer. The test was considered finished when the vertical strain did not change in the same sense for more than two days. Then heating and hydration were stopped and, after some cooling (~1 h), the cell was extracted from the bath and dismounted. The sample height was measured indirectly and directly at different moments during the disassembling process, the sample was weighed and dried in the oven at 110°C for 48 h to determine its water content and check the final state of saturation.

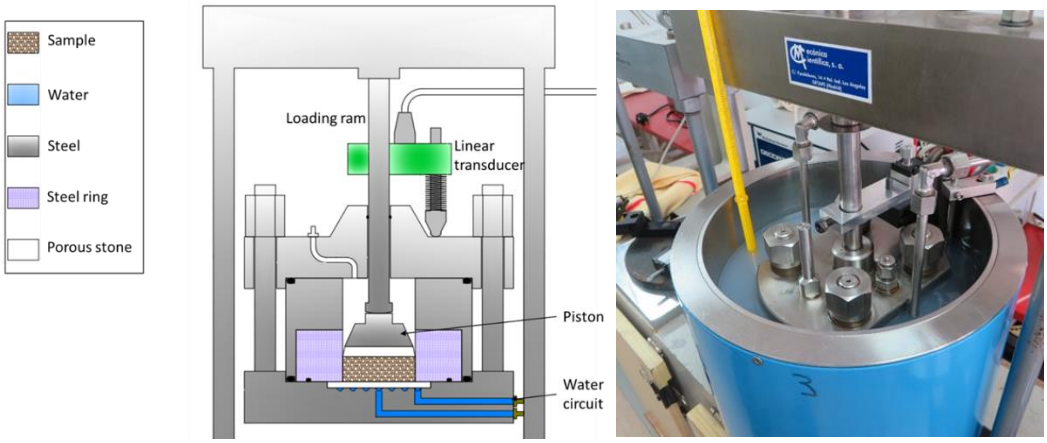

Figure 4.2 – Cartoon of the oedometer cell used (left) and oedometer cell immersed in the silicone bath (right)

Hence, for each dry density saturation took place under different vertical loads using different specimens. In some cases the sample swelled and in others it consolidated. By plotting the final strain as a function of the vertical load, and interpolation the load necessary for zero strain, a swelling pressure value was inferred.

4.3 Results

4.3.1 Water retention curve

CIEMAT fine-tuned a method to determine the water retention curve of bentonites at high temperature, focusing on high degrees of saturation. New tests were performed with FEBEX and MX-80 bentonite compacted at dry densities of 1.5 and 1.6 g/cm^3. A contribution with the first results and lessons learned was presented at the 4th European Conference on Unsaturated Soils, held online in October 19th-21st 2020.

Figure 4.3 shows the change of suction as temperature increased for FEBEX samples of different degree of saturation and Figure 4.4 shows the same kind of results for MX-80. Some of the samples were measured with both sensors. The error bars of the measurements are also indicated, although for the psychrometer measurements they are too small to be seen. The measurements performed showed the usual decrease of suction as temperature increased. The accuracy of the measurement worsened as the temperature increased, as a result of the higher uncertainty in the relative humidity measurement for the higher values (Villar, Gutiérrez-Álvarez et al. 2020). The measurements performed for the lower values of RH with the psychrometers were not valid for temperatures below 60°C. In this low range of RH, and for higher temperatures, the psychrometers started to give values that were inside the error interval of the capacitive sensors measurements, but around the limit of the psychrometers' upper range (6 MPa). Maybe for this reason some values obtained with the psychrometers for the lower degrees of saturation did not show any clear trend with temperature (e.g. FEBEX ρ_d=1.5 g/cm^3 S_r=80%, FEBEX ρ_d=1.6 g/cm^3 S_r=90%, FEBEX ρ_d=1.6 g/cm^3 S_r=95%, MX-80 ρ_d=1.5 g/cm^3 S_r=70%). For the samples with higher degrees of saturation, which could be properly measured with psychrometers, suction decreased with the increase of temperature until reaching 0 MPa at lower temperatures as the degree of saturation was higher. The increase in temperature triggers the transfer of water from the microstructure to the macrostructure, where it behaves as free water, making RH to reach 100% for lower temperatures as the bentonite degree of saturation is higher (Lloret and Villar 2007). The comparison of the measurements with the capacitive sensors and the psychrometers on the same samples, suggests that the suctions measured with the capacitive sensors tended to be overestimated.

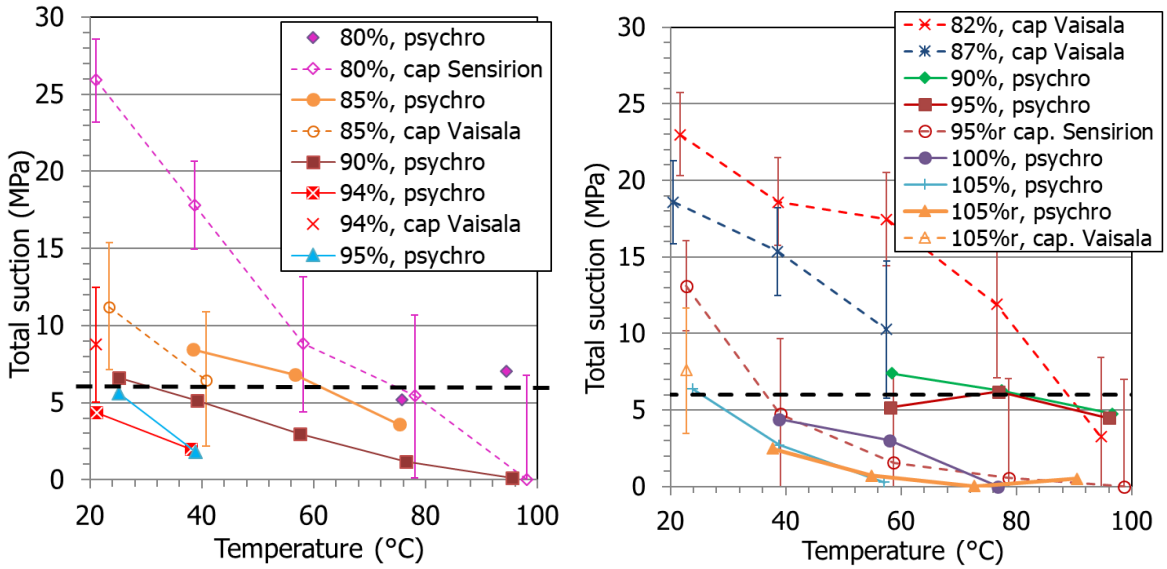

Figure 4.3 – Change of suction with temperature for FEBEX samples compacted at dry density 1.5 g/cm³ (left) and 1.6 g/cm³ (right) with different water contents (the S_r is given in the legend). The dotted horizontal line indicates the upper limit of the measuring range for psychrometers at room temperature.

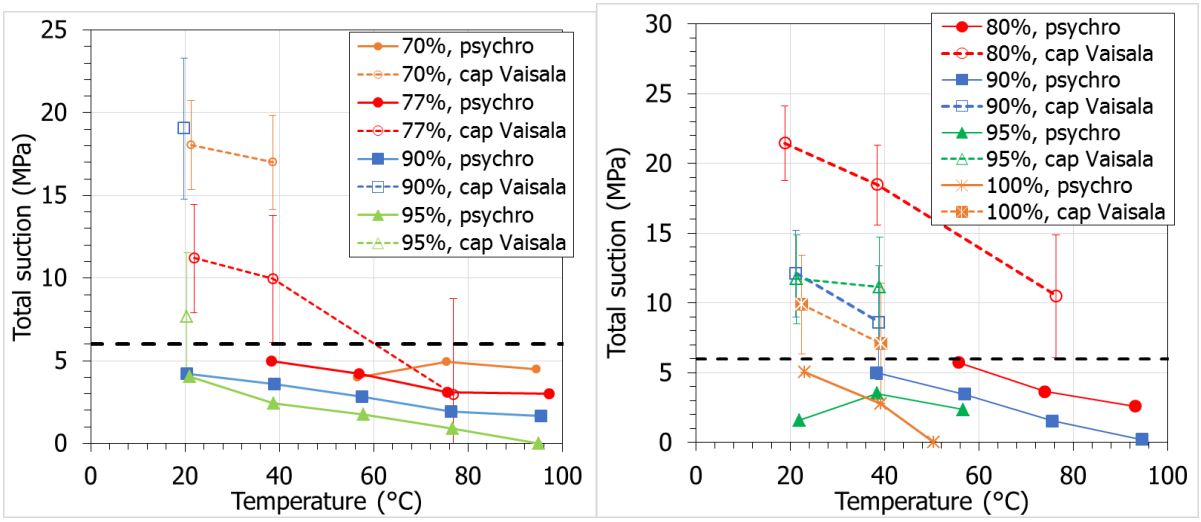

Figure 4.4 – Change of suction with temperature for MX-80 samples compacted at dry density 1.5 g/cm³ (left) and 1.6 g/cm³ (right) with different water contents (the Sr is given in the legend). The dotted horizontal line indicates the upper limit of the measuring range for psychrometers at room temperature.

Figure 4.5 and Figure 4.6 show the results expressed as water retention curves for different temperatures for FEBEX and for MX-80, respectively. The lines included are only illustrative of the general trends. The shape of the WRC in the low suction range clearly changes with temperature, the decrease of suction with water content being steeper as the temperature is higher. The results obtained are consistent with those obtained in previous projects using capacitive sensors for water contents below 20% (Villar and Gómez-Espina 2009)(Figure 4.7, Figure 4.8).

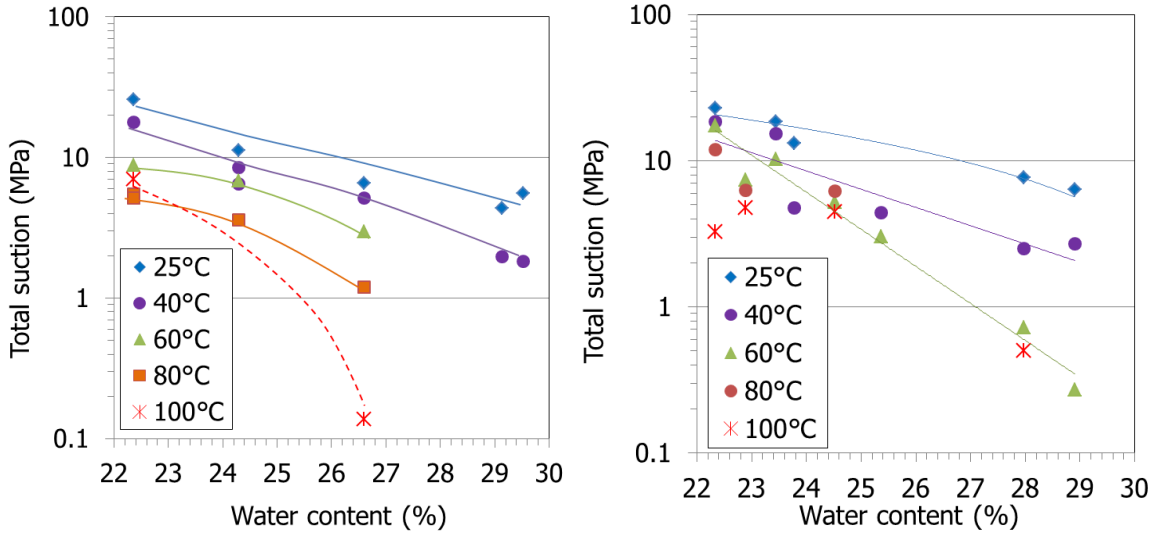

Figure 4.5 – Water retention curves at different temperatures for FEBEX bentonite compacted at dry density 1.5 g/cm³ (left) and 1.6 g/cm³ (right).

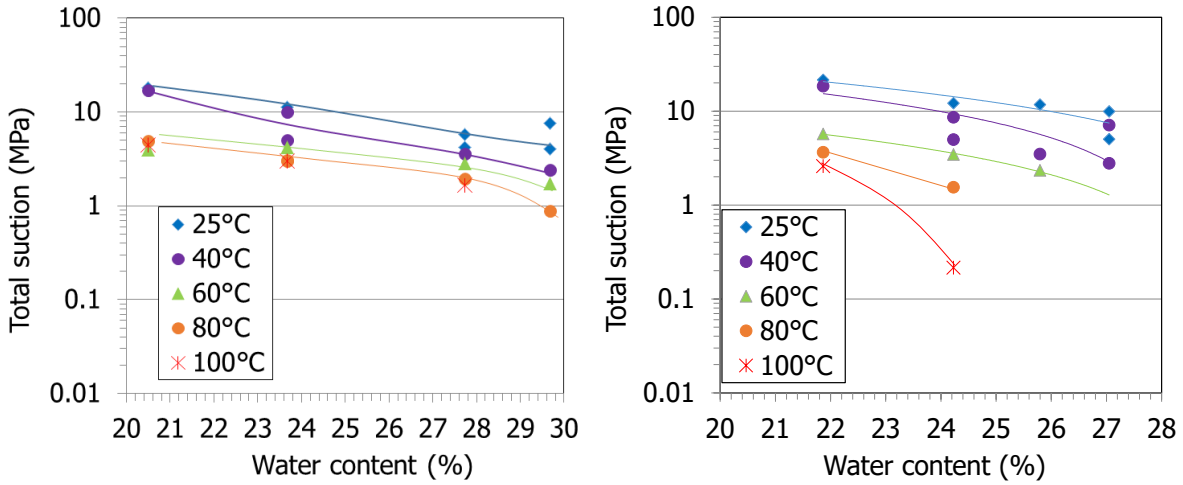

Figure 4.6 – Water retention curves at different temperatures for MX-80 bentonite compacted at dry density 1.5 g/cm³ (left) and 1.6 g/cm³ (right).

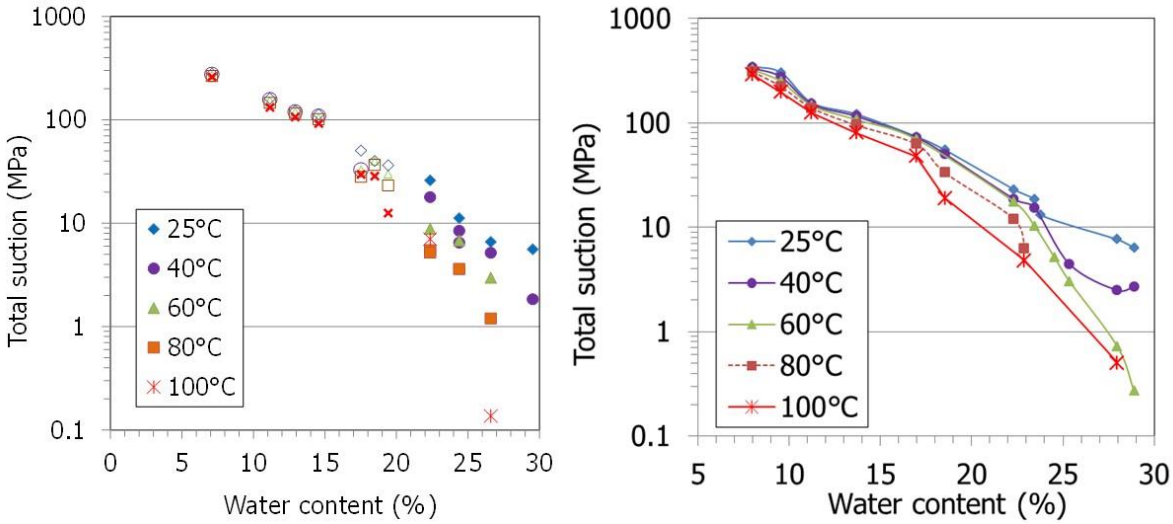

Figure 4.7 – Water retention curves at different temperatures for FEBEX bentonite compacted at dry density 1.5 g/cm³ (left) and 1.6 g/cm³ (right), obtained during HITEC and in previous projects (w<20%).

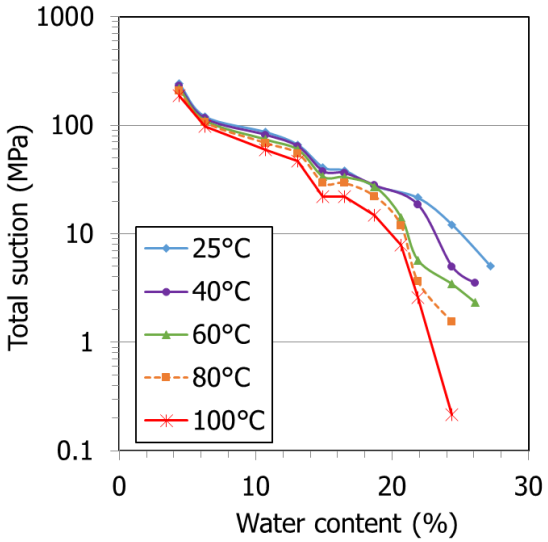

Figure 4.8 – Water retention curves at different temperatures for MX-80 bentonite compacted at dry density 1.6 g/cm³.

The comparison between the two bentonites shows that below 40°C the water retention curves of both are similar. Above this temperature, the suction for a given water content is higher for the FEBEX bentonite, particularly for the high density.

4.3.2 Swelling tests

Six swelling tests have been performed so far for each bentonite, FEBEX and MX-80, compacted at dry densities of 1.6 and 1.5 g/cm³, using vertical loads between 2 and 5 MPa. The tests lasted between 4 and 26 days and full saturation was checked at the end of the tests in all cases. Figure 4.9 shows an example of the evolution of axial strain over time during saturation obtained for samples of MX-80. The axial deformation during the three phases of the tests can be identified in the Figure:

- Initial heating, which involved a small swelling;
- Loading to the target vertical stress, which involved some compression of the sample. The deformation of the equipment upon heating and loading has been taken into account in the results plotted in the Figure;

- Hydration with deionised water, which involved swelling for the two lower vertical stress and consolidation for the other one.

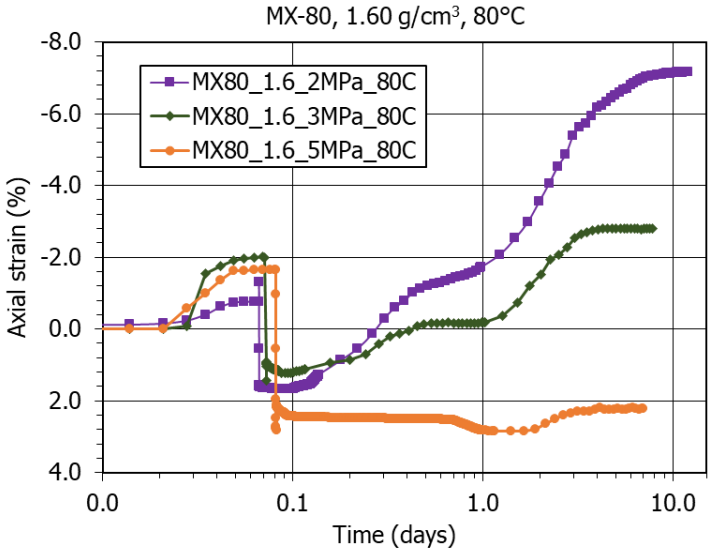

Figure 4.9 – Evolution of axial strain during heating, loading and saturation of samples of MX-80 bentonite of dry density 1.6 g/cm³ saturated with deionised water at 80°C

The final stresses measured in the tests performed so far are plotted in Figure 4.10 for the two bentonites and dry densities tested. From the linear fittings between axial strain and load, a swelling pressure value can be interpolated. These interpolated values, although preliminary, especially for the FEBEX bentonite, are plotted in Figure 4.11 along with the exponential fittings between swelling pressure and dry density for 20°C determined at CIEMAT in previous researches (Villar and Lloret 2008, Villar 2013). The experimental fittings shown in the Figure for 20°C were obtained from measurements in samples kept under constant volume during saturation, hence, with a different methodology. Although generally the constant volume test (tests at 20°C) is considered to yield higher swelling pressure values than the swell under load test (tests at 80°C), in the case of the FEBEX bentonite it was checked that for dry densities below 1.65 g/cm³ the difference between the two methods was very small (Villar and Lloret 2008). In any case, it seems clear that the temperature reduced the swelling pressure in the case of the two bentonites, swelling pressure being clearly higher for the MX-80 when the dry density was lower. The decrease of swelling pressure and swelling capacity with temperature had already being observed for FEBEX bentonite (Villar and Lloret 2004), (Villar, Gómez-Espina et al. 2010). Temperature-induced transfers between intra-aggregate adsorbed water—of density higher than that of free water—and inter-aggregate free water were invoked to explain the changes observed.

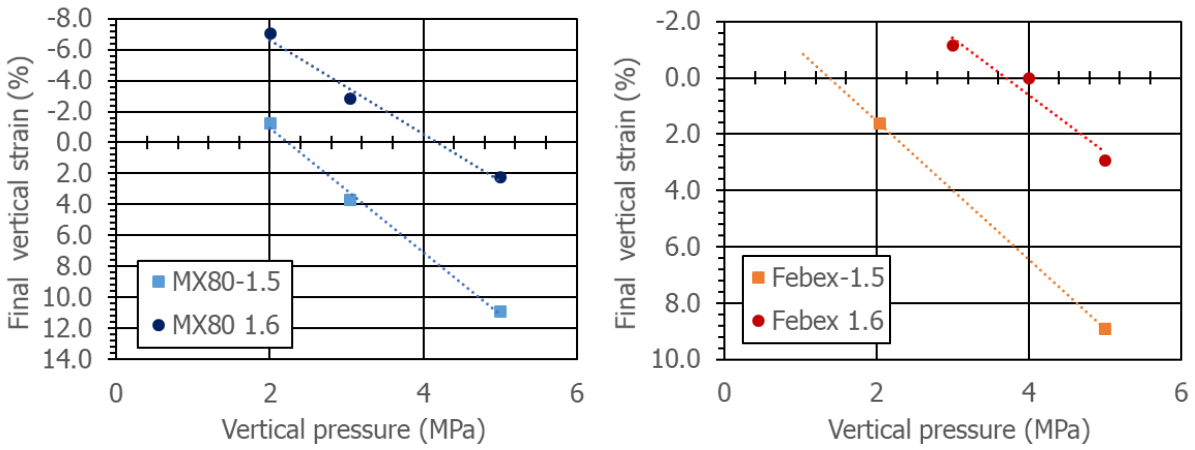

Figure 4.10 – Final strains measured in the swelling tests performed with MX-80 and FEBEX bentonite at 80°C. The swelling pressure values inferred from these results correspond to the interpolation of the linear fitting for strain=0. The dry densities are indicated in the legends in g/cm³

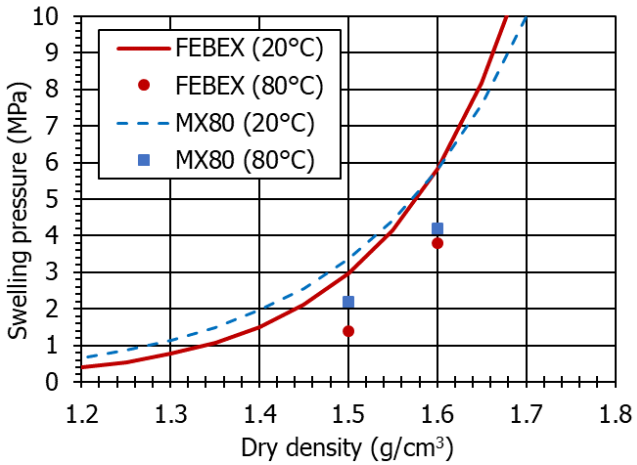

Figure 4.11 – Swelling pressure values of MX-80 bentonite at 20 and 80°C

4.4 Conclusion

The water retention curves obtained at temperatures between 20 and 100°C showed a sharper decrease of suction with water content as the temperature was higher, particularly above 60°C. The comparison with results obtained in previous investigations for water contents <20% confirms the same trends. Unfortunately, the psychrometers did not reach the equilibrium necessary for the measurement for temperatures higher than 60°C, which did not allow to define the curves in the low suction range as much as it would have been desirable. For temperatures above 40°C and in the range of water contents analysed, the water retention capacity of the FEBEX bentonite tends to be higher than that of MX-80.

The swelling pressure at a temperature of 80°C was lower than at 20°C for the two bentonites. For dry densities lower than 1.6 g/cm³ the swelling pressure of MX-80 (predominantly sodic) for a given dry density is higher than that of FEBEX (predominantly divalent).

5 CTU (SÚRAO)

5.1 Introduction

Bentonite intended for use as a buffer around the waste canister will be exposed to elevated temperatures and will also come into contact with groundwater. It is anticipated that the bentonite may be exposed to elevated temperatures under adverse conditions and at the same time saturated, which could potentially affect the hydromechanical processes occurring in the bentonite.

The aim of the research under Task 3.2 is to monitor the evolution of these properties under thermal and hydraulic loading in real time. Measurements and heating were carried out simultaneously. It was therefore possible to determine the response of the system to different temperatures and to simultaneously measure the hydraulic properties.

5.1.1 Material

Czech origin bentonites are under consideration as buffer and backfill material in the Czech deep geological repository. Thus, the research in HITEC project has been focused on Czech bentonite of calcium/magnesium (Ca/Mg) type extracted from the Černý Vrch deposit. The material had been extracted and processed (dried and milled) by the manufacturer and the texture of the final material ready for testing is a very fine powder. The material was first subjected to testing in 2017 and its designation is BCV_2017. The basic characteristics of tested bentonite have been summarized in (Hausmannová, Hanusová et al. 2018). The data concerning the original material are acquired from another projects (Červinka, Večerník et al. 2018, Svoboda and al. 2019) . The same bentonite was used in HITEC T3.1 and T3.3.

5.1.2 Research plan

The project aimed to determine hydraulic and mechanical properties of saturated Ca/Mg bentonite during the temperature exposure. The hydraulic conductivity and total/swelling pressure at room temperature, 40°C, 60°C, 90°C, 130 °C were monitored. Three tests focused on behaviour of bentonite during heating were done. **Erreur ! Source du renvoi introuvable.** shows a summary of material used, the laboratory plan and procedures.

5.1.2.1 Material (BoM item): BCV bentonite (Ca-Mg type), powder as delivered by producer
5.1.2.2 Material treatment (sample preparation for test and loading procedure): Bentonite sample compacted directly into constant volume cell
5.1.2.3 Temperature (to which material was/will be exposed to) and exposure time 40°C, 60°C, 90°C, 130°C. Each temperature step takes 1-3 months of exposure
5.1.2.4 Tests carried out (name, description, sample preparation, procedure, results): Permeability and swelling pressure were measured in constant volume cells at various temperatures up to 130 °C. At first hydraulic conductivity and total pressure had been measured followed by swelling pressure determination. Hydraulic conductivity and total pressure were measured continuously during the whole test. Water flow through the sample was ensured by saturation pressure 1MPa, the boiling was avoid due to application of back pressure of 0,5 MPa. 5.1.2.4.1 Hydraulic conductivity - K [m/s] Hydraulic conductivity was measured using a constant pressure gradient permeameter. Samples had been compacted directly into constant volume cells, then a water gradient was applied, and water inflow and total pressure development were measured at laboratory temperature, once the sample had been saturated the temperature was raised and was gradually increased up to 130 °C. Once stable flow and total pressure had been obtained, permeability was calculated. The pressure gradient was then released, and swelling pressure measurements began. Hydraulic conductivity after heating was measured at the end of experiment. 5.1.2.4.2 Swelling pressure - σ_{sw} [MPa] Swelling pressure was determined on fully saturated sample from permeability test. The pressure gradient was released (the pore pressure = 0). The swelling pressure was determined after the total pressure and hydraulic conductivity had stabilized.

Table 5.1 – CTU - Permeability and swelling pressure in constant volume cell

5.2 Procedures

The initial water content of the sample was determined prior to the start of the experimental procedure. The experimental procedure itself consisted of two consecutive parts. The first part involved saturating the sample and determining the hydraulic conductivity and swelling pressure of the thermally untreated sample, measurements were taken at laboratory temperature. Once the sample had been saturated, the second part began, which involved thermal loading. The temperature was gradually increased up to a final temperature of 130 °C. At the end of each temperature step, the hydraulic conductivity and swelling pressure were determined (changes in permeability/water flow and total pressure were continuously monitored). After dismantling, the exact dry density and degree of saturation were determined.

5.2.1 Laboratory set-ups

For measurement of hydro-mechanical response of saturated bentonite to thermal loading, a special heated permeameter cell was designed. It is a constant volume permeameter cell modified to fulfil the requirement of thermal heating of the sample. No boiling should be permitted in the sample however the temperatures reach above the boiling point at atmospheric pressure. To meet this condition back pressure of 0.55 MPa is applied, thus increasing the boiling point. With forced saturation at 1 MPa

pressure is applied from the bottom, the back pressure is used on the top of the sample. The measurement is based on Darcy's law using a constant hydraulic gradient.

Laboratory set-up for hydraulic conductivity and swelling pressure measurement during the heating

The permeameter cell consists of a cylindrical steel chamber (ring) for the housing of the sample (diameter: 30 mm, height: 20 mm). The top and bottom of the sample have been fitted with sintered steel permeable plates to prevent the leaching (“mobilisation”) of the material. The sample is constrained in vertical direction by two pistons which are positioned on each side of the sample. The position of the piston is always between the flange (with the space for the sensor) and the surface of the steel plate. The thermal loading of the sample was provided by a heating sleeve strung situated on the chamber with the sample. The temperature of the heater was controlled by the PID controller depending on the temperature measured inside the heater.

Two load cells were used in the experiment, one on the top, the other on the bottom to monitor total pressure evolution. Miniature load cells Honeywell model 53 with temperature compensation up to 70°C were used. The miniature load cells provided measurement of the force induced by swelling of the bentonite and pore pressure after start of the saturation. The load cells were placed between the piston and the flange. The load cells are connected to the central data logger and the signal is stored on the server in required interval (5 minutes)

The temperature of the cell itself was monitored by 7 thermometers placed on the surface of the pistons and the chamber. Special emphasis was put on monitoring of the temperature near the load cells as safety measure. The pore pressure was monitored by an electronic pressure transmitter connected to the data logger. The hydraulic gradient was provided by a pressure vessel filled by gas (argon) which exerts pressure within the other vessel with distilled water, which was used for the saturation. Distilled water entered to the sample from the bottom with the pressure of 1 MPa and on the top of the sample back pressure of 0,6 kPa exerted by the same system was applied. The hydraulic gradient corresponds to the difference between the water pressure at the inflow and the pressure at the outflow. A schematic of the system of saturation and back pressure and the permeameter cell itself is shown in Figure 5.1. In Figure 5.2 an image of the cell is shown. On the picture Figure 5.3 is thermal image of the permeameter cell during heating.

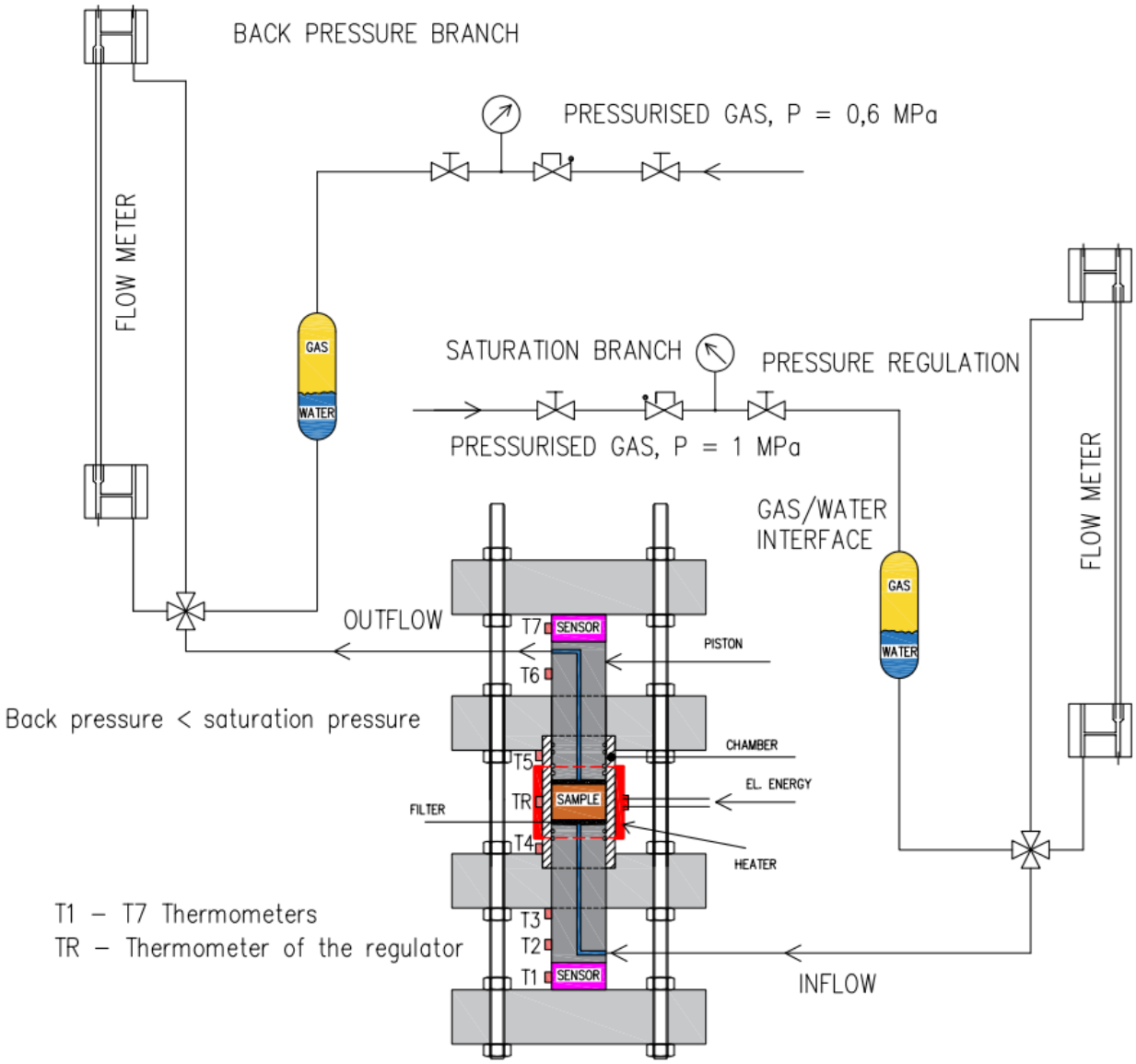

Figure 5.1 – Schematic illustration of the heated permeameter cell.

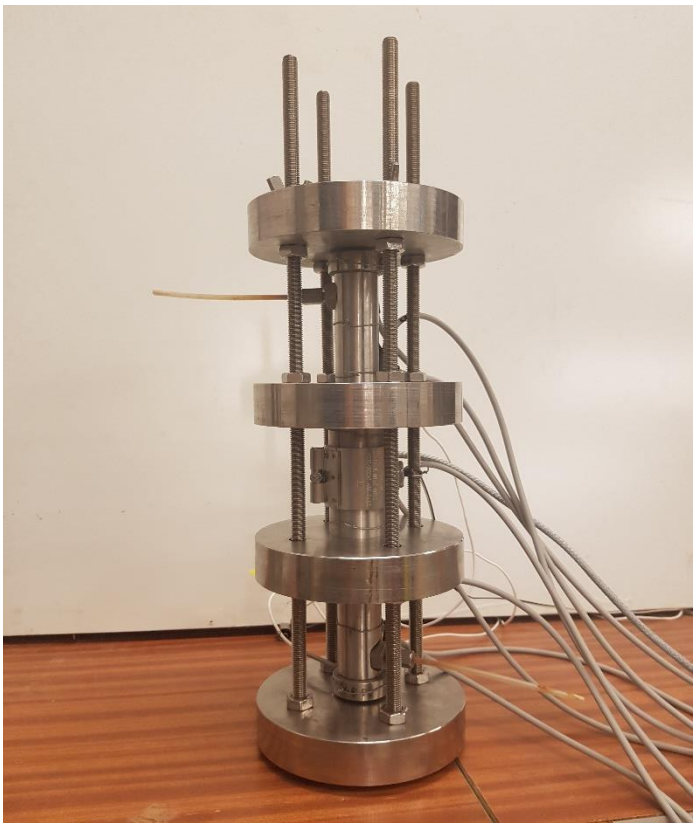

Figure 5.2 – Heating permeameter cell.

Figure 5.3 – Thermal image of the permeameter cell at 60°C.

5.2.2 Test procedures

Sample preparation for the testing in the heated permeameter cell

The sample comprises powdered BCV bentonite with an initial water content of approximately 10%. The material was uniaxially compacted directly in the chamber using a piston up to desired dry density, which was 1450 kg.m^{-3}. Exact dry density is always measured after dismantling of the experiment. The diameter of the samples was 30mm and the height was 20 mm. After the bentonite is compacted into the chamber, a heating element is placed on the chamber, and the cell is assembled and equipped with load cells. Once the permeameter is assembled, the thermometers are placed on top of it.

Procedure of the measurement in the heated permeameter cell

First the sample was fully saturated at laboratory temperature. Once the water flow through the sample was steady the hydraulic conductivity of the untreated material at laboratory temperature was determined. Then the water pressure was switched off and the pore pressure in the sample released to swelling pressure measurement. The release of the pore pressure was ensured by disconnecting the saturation pressure and back pressure, thus ensuring the application of atmospheric pressure at both ends of the sample and elimination of the hydraulic gradient.

After determining the hydromechanical properties, the water flow was switched on. After the observed properties had stabilized, the temperature was raised to the next temperature of interest, and measurements were taken after the properties had stabilized.

The properties were determined at room temperature, 40°C, 60°C, 90°C and the final temperature of 130°C.

5.3 Results

The investigation was focused on determination of hydraulic-mechanical properties of BCV bentonite during thermal loading. The results from three completed tests are available.

5.3.1 Investigation performed

A total of three tests were carried out to measure hydraulic conductivity and swelling pressure during heating at 130°C. The tests were focused on determination of hydraulic conductivity and direct measurement of swelling pressure at 40°C, 60°C and 90°C and then on hydraulic conductivity and total pressure at 130°C. In order to avoid boiling and drying of the sample, swelling pressure at 130°C had not been measured directly but was recalculated from total pressure.

As part of the testing of the second sample (sample 2), cyclic temperature loading was performed, i.e. the sample was cooled to room temperature and then heated again to 130°C. In this case, total pressure measurements were performed without the presence of a hydraulic gradient. A pressure of 1 MPa was applied to both ends of the sample to prevent boiling in the sample at high temperatures.

5.3.2 Results from investigation

Sample 1

Erreur ! Source du renvoi introuvable. contains results of the measurement of hydraulic conductivity at room temperature, 40°C, 60°C, 90°C and 130°C and swelling pressure at room temperature, 90°C, calculated swelling pressure at 130°C and swelling pressure at room temperature after heating. **Erreur ! Source du renvoi introuvable.** contains results from the first experiment provided on sample 1. Figure 5.5 shows the progress of hydraulic conductivity and total pressure as response to temperature increase applied to sample 1. Hydraulic conductivity is there expressed as measured values without any converting (light pink squares) and converted values to temperature 10°C (red squares). Dry density of the sample is 1392 kg·m^{-3}. The dependence of hydraulic conductivity and swelling pressure on temperature is shown in Figure 5.4.

Temperature	Hydraulic conductivity (m/s)	Hydraulic conductivity (m/s) (converted to 10 °C)	Swelling Pressure (MPa)	Swelling Pressure (%)
T = 20°C	8.09E-13	6.24E-13	1.49	100%
T = 40°C	1.12E-12	5.64E-13	-	-
T = 60°C	1.98E-12	7.06E-13	-	-
T = 90°C	4.92E-12	1.15E-12	1.39	93%
T = 130°C	2.11E-11	3.15E-12	0.8	54%
T = 20°C	-	-	1.03	69%

Table 5.2 – Results of hydraulic conductivity and swelling pressure of sample 1 during the thermal loading

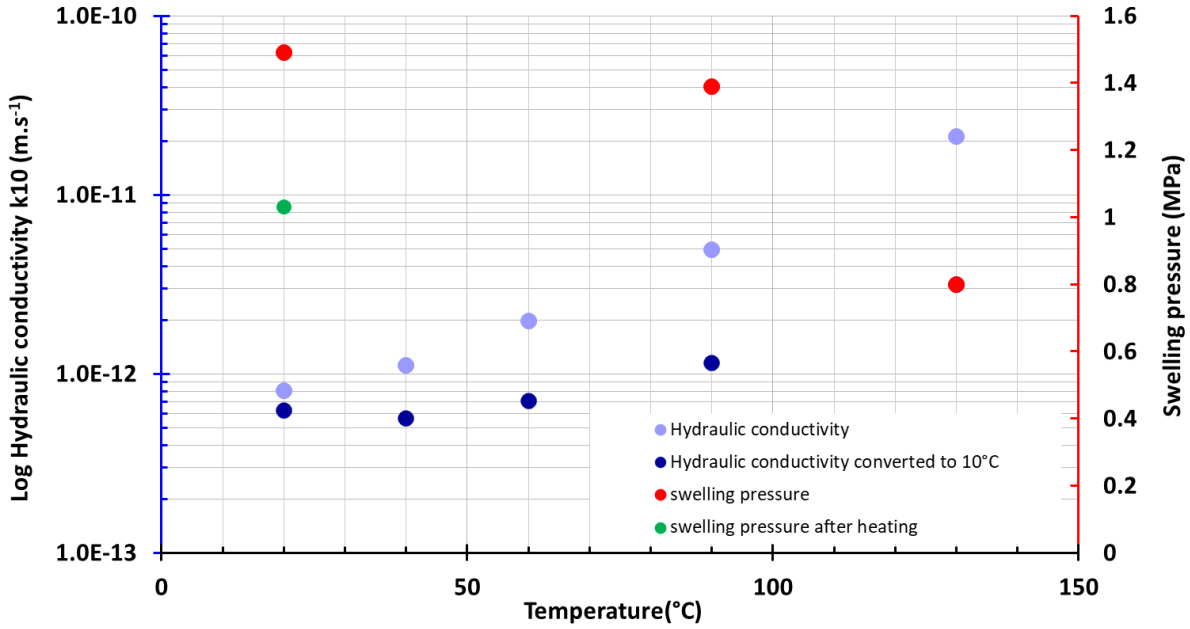

Figure 5.4 – Hydraulic conductivity and swelling pressure of sample 1 at different temperatures and swelling pressure after heating

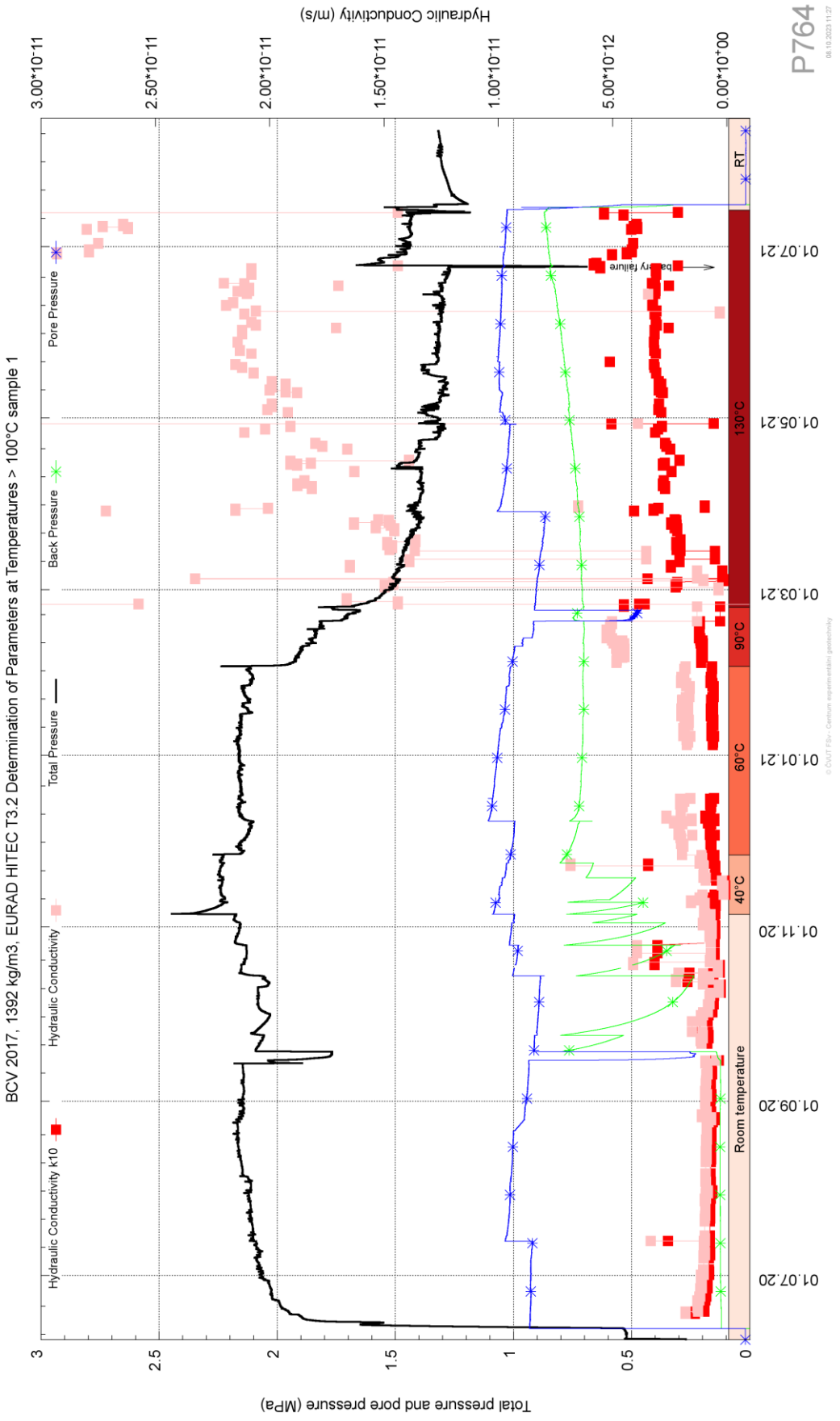

Figure 5.5 – The development of total pressure, hydraulic conductivity, and temperature in time during the heating of the sample 1

In Figure 5.5 a continuous drop in total pressure could be seen, although the hydraulic gradient does not change. The declining trend depends on temperature. A steeper decline is observed at higher temperatures (especially at temperatures >90°C). Hydraulic conductivity increases with temperature, but this increase is due to the changing viscosity of water as a function of temperature and is not a change in the behaviour of bentonite. In order to investigate the effect of temperature on bentonite, the hydraulic conductivity was reduced by the effect of changing viscosity by converting it to hydraulic conductivity at 10°C. The converted hydraulic conductivity increases with increase of temperature. The increase is apparent, but it is not fatal. Based on the tests performed, it can be said that the increase in hydraulic conductivity is more significant for the dry density of bentonite lower than 1450 kg·m^{-3}.

The same phenomena as in the next two tests can be observed on sample 1, i.e., a continuous decrease in total pressure and a decrease in swelling pressure which does not reach the original value. Swelling pressure was measured at the end of the experiment at room temperature. After cooling to room temperature, a slight increase in swelling pressure was observed, but after a few days this began to level off until only very small increments were observed, and the swelling pressure stabilized. The final swelling pressure after heating was 72 % of original swelling pressure of untreated bentonite.

Sample 2

Dry density of sample 2 is 1450 kg.m^{-3}. Erreur ! Source du renvoi introuvable. shows the results of hydraulic conductivity and swelling pressure measurements. These data are visualized in Figure 5.6. Hydraulic conductivity was measured at room temperature, at 20°C, 40°C, 60°C and 90°C. Swelling pressure was measured at 20°C, 40°C, 60°C, 90°C and calculated from total pressure at 130°C. Development of hydraulic conductivity and total pressure depending on the temperature in time is shown in Figure 5.7. This test included measurements during warm-up cycles.

Sample 2, ρd = 1450 kg/m^3	**Hydraulic conductivity (m/s)**	**Hydraulic conductivity (m/s) (converted to 10 °C)**	**Swelling Pressure (MPa)**	**Swelling Pressure (%)**
T = 20°C	4.99E-13	3.85E-13	1.8	100%
T = 40°C	1.06E-12	5.31E-13	1.8	100%
T = 60°C	1.64E-12	5.83E-13	1.6	89%
T = 90°C	3.64E-12	8.50E-13	0.8	44%
T = 130°C	-	-	0.67	37%
T = 20°C	1.03E-12	8.0E-13	1.22	68%

Table 5.3 – Results of hydraulic conductivity and swelling pressure of sample 2 during the thermal loading

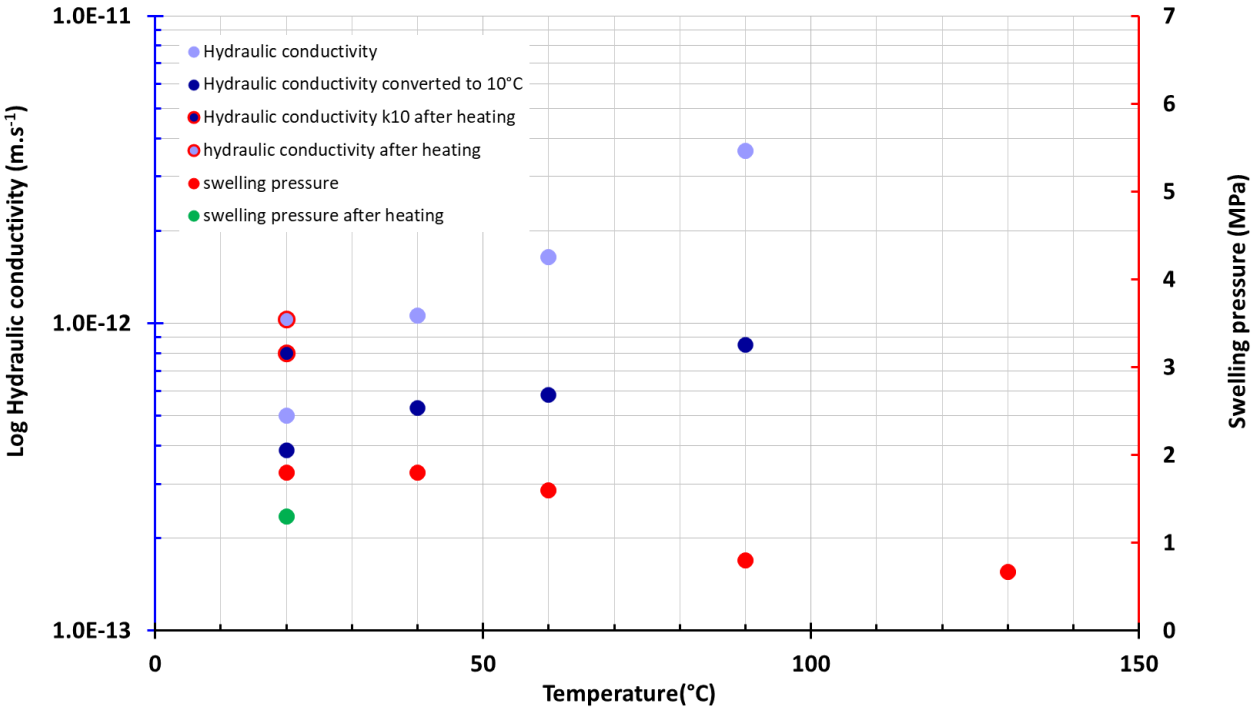

Figure 5.6 – Hydraulic conductivity and swelling pressure of sample 2 at different temperatures and after heating

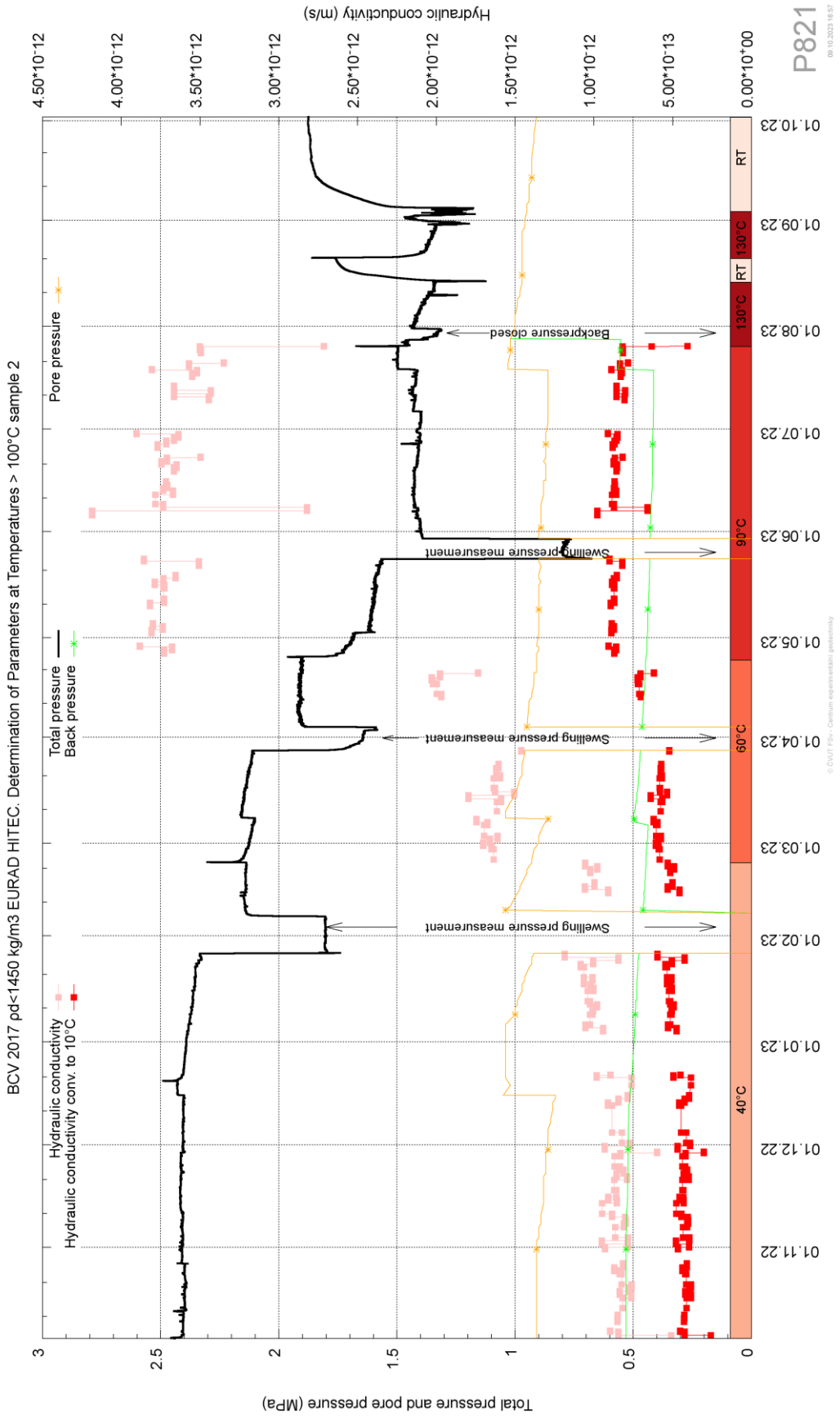

Figure 5.7 – Progress of total pressure, hydraulic conductivity and hydraulic conductivity converted to 10°C with respect to temperature raise with swelling pressure measurement marks, sample #2

In test 2, two cycles of heating were performed, where the sample was cooled from 130°C to room temperature (20°C) and then heated directly to 130°C. In neither cooling case did the swelling pressure return to the original value before heating. In Figure 5.8 is shown in detail the evolution of the total pressure during the cycle at the end of the experiment. Measurements show that the swelling pressure is only 72% of the value measured prior to the heating process.

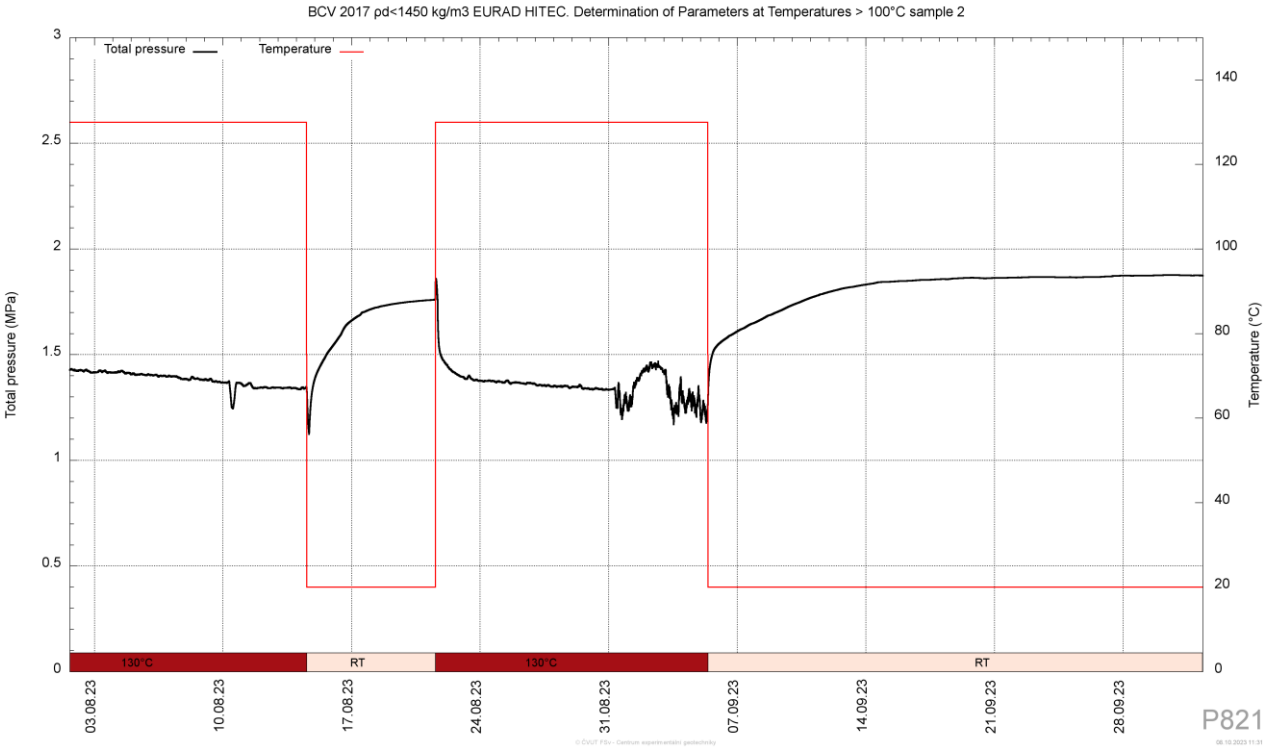

Figure 5.8 – Detail A of the total pressure trend after cycle of cooling and heating at the end of the experiment - sample 2

Sample 3

Dry density of sample 2 is 1540 kg.m^{-3}. The **Erreur ! Source du renvoi introuvable.** shows the results of hydraulic conductivity and swelling pressure measurements. These data are visualized in Figure 5.9. Hydraulic conductivity was measured at room temperature, at 20°C, 40°C, 60°C, 90°C and 130°C. Swelling pressure was measured at 20°C, 40°C, 60°C, 90°C and calculated from total pressure at 130°C. Development of hydraulic conductivity and total pressure depending on the temperature in time is shown in Figure 5.10.

Sample 3, ρd = 1540 kg/m^3	**Hydraulic conductivity (m/s)**	**Hydraulic conductivity (m/s) (converted to 10 °C)**	**Swelling Pressure (MPa)**	**Swelling Pressure (%)**
T = 20°C	2.33E-13	1.80E-13	4.6	100%
T = 40°C	5.15E-13	2.59E-13	4.4	96%
T = 60°C	7.57E-13	2.70E-13	4.17	91%
T = 90°C	1.34E-12	3.12E-13	3.7	80%

T = 130°C	2.34E-12	3.50E-13	3.1	68%
T = 20°C	-	-	3.7	80%
T=130°C	-	-	2.61	57%

Table 5.4 - Results of hydraulic conductivity and swelling pressure of sample 3 during the thermal loading

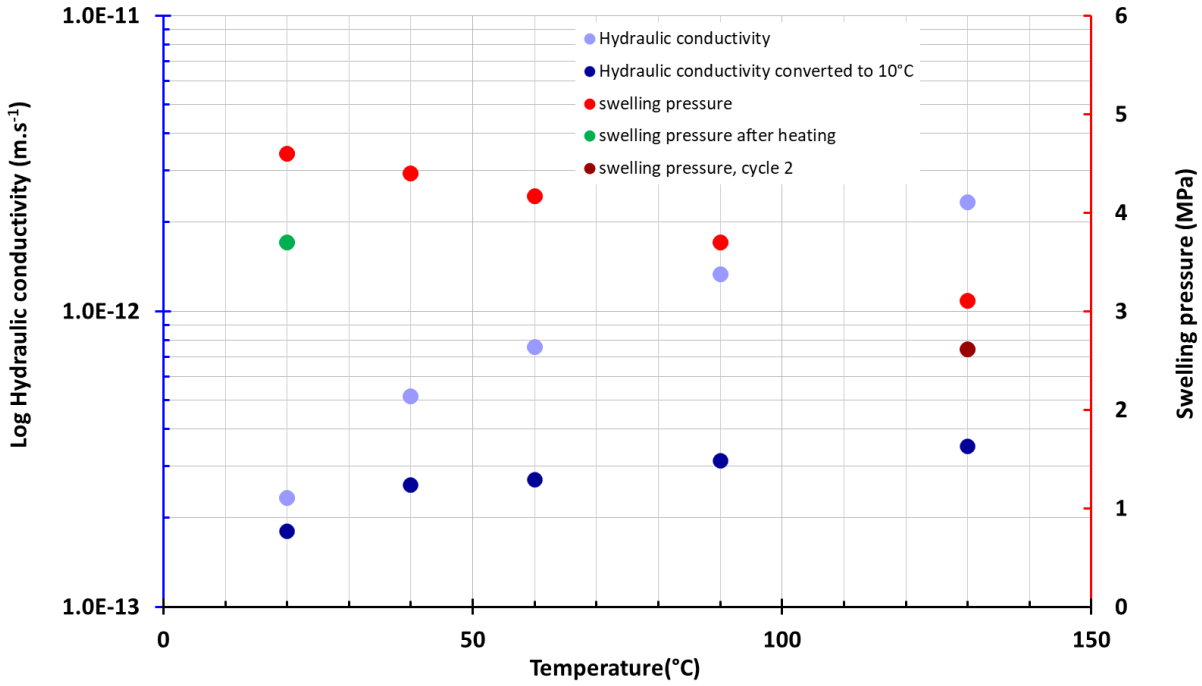

Figure 5.9 – Hydraulic conductivity and swelling pressure of sample 3 at different temperatures and swelling pressure after heating

As in the case of the previous two tests, there is a steady decrease in total stress in the test performed on sample 3. However, the curve of the decrease is not as steep as in the case of the two previous samples, which had a lower dry density. The rate of decrease is constant up to 130°C, where there is a steeper decrease. After the heating the swelling pressure was measured at room temperature and, as in the previous two tests, the value did not reach the value before the heating process. Due to the development of the experiment, a warm-up and cool down cycle was added. After measuring the swelling pressure at room temperature, the temperature was again raised to 130°C and the swelling pressure was measured at this temperature. The swelling pressure in the second heating cycle was lower than in the first cycle.

The higher dry density also affects the hydraulic conductivity converted to a 10°C hydraulic conductivity, which hardly changes with increasing temperature.

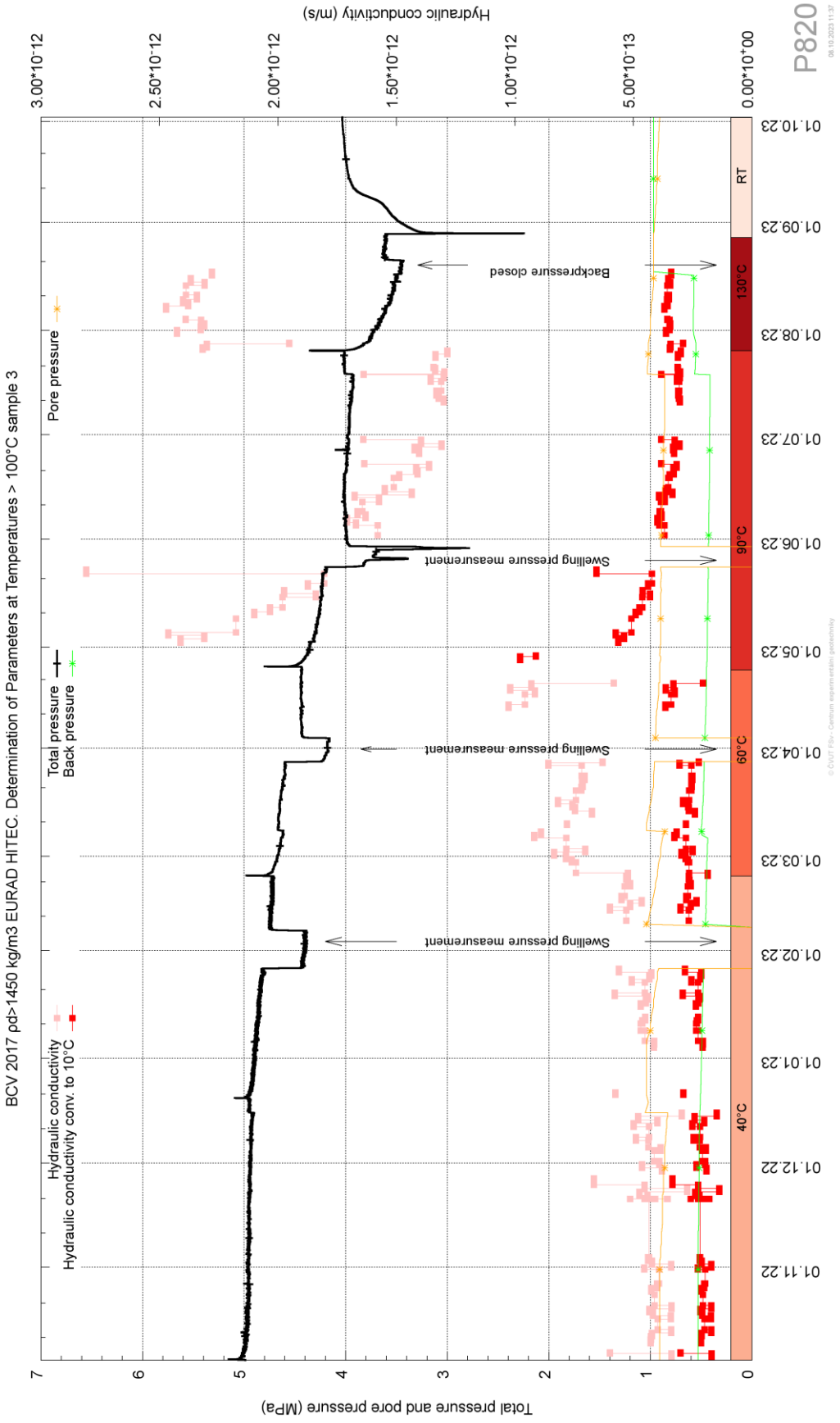

Figure 5.10 – Progress of total pressure, hydraulic conductivity and hydraulic conductivity converted to 10°C with respect to temperature raise with swelling pressure measurement marks, sample #3.

Figure 5.11 shows the results of the swelling pressure measurement as a percentage of the original swelling pressure before heating. The graph shows the effect of dry density. The higher the dry density, the smaller the change in swelling pressure after heating.

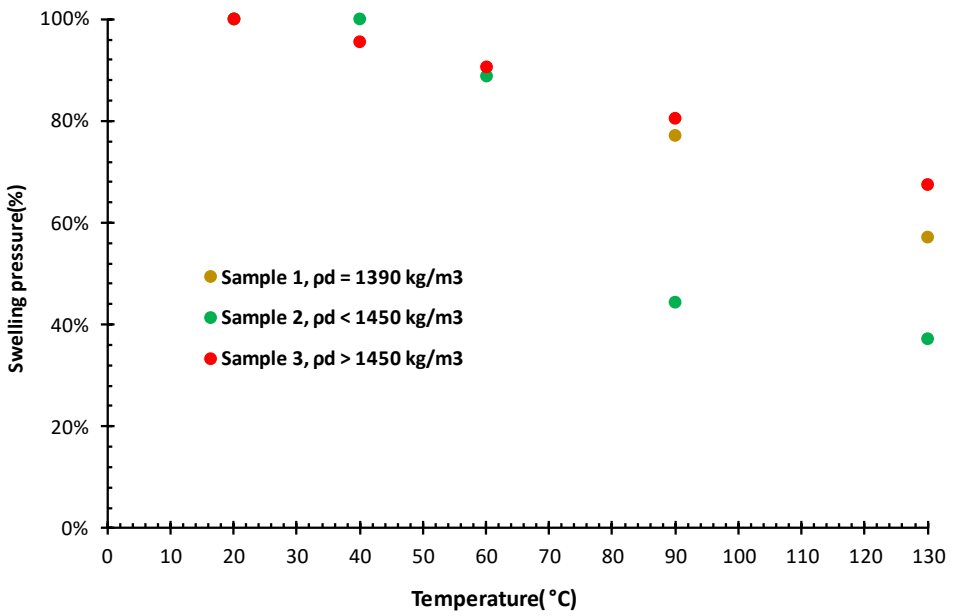

Figure 5.11 – Swelling pressure of three heated samples at different temperatures. The swelling pressure is expressed as a percentage of the swelling pressure determined at the laboratory temperature.

5.4 Conclusion

Based on the three tests performed, it was found that there is a steady decrease in total pressure with increasing temperature, although the hydraulic gradient does not change. The total pressure curve guidelines vary with temperature and dry density. At higher temperatures, a steeper decrease in total pressure is observed. The temperature at which the slope of the total pressure curve changes depends on the dry density. The higher the dry density, the higher the temperature at which the sharp decrease occurs.

A common phenomenon observed in all three cases was a steady decrease in swelling pressure after the heating cycles. After reaching and measuring all possible parameters at 130°C, the temperature was reduced to room temperature and the swelling pressure did not reach the value measured on the same sample before the heating process even after long-term measurements. The resulting swelling pressure after the experiment was 60 -70% of the value measured before the experiment for lower dry densities and 80% for dry density > 1450 kg·m^{-3}. The magnitude of the resulting temperature effect on the swelling pressure of bentonite sample is dependent on the dry density of the sample.

The magnitude of the effect of temperature on the hydraulic conductivity is also dependent on the dry density of the sample. For samples with a dry density > 1450 kg·m^{-3} the effect of temperature on the hydraulic conductivity, converted to a hydraulic conductivity equivalent to 10°C, is less than for lower dry densities.

Main conclusions from this test programme are:

- As temperature increases, total pressure decreases continuously (at constant hydraulic gradient)

- After cooling the swelling pressure has not reached the original swelling pressure
- Swelling pressure is reduced by up to 60% of the original swelling pressure prior to heating for samples with low dry density.
- The resulting effect of thermal loading on swelling pressure and hydraulic conductivity depends on the dry density. The higher the dry density the less pronounced the resulting effect.

6 CU

6.1 Introduction

The research in Task 3.2 was focused on the direct measurement of hydromechanical properties of BCV bentonite, including oedometric compressibility, swelling pressure and swelling strain at temperatures 100-150°C. The aim of this test programme was to directly simulate the THM conditions expected in the bentonite buffer in a radioactive waste repository. Experimental testing at temperatures above 100°C brings special demands on laboratory testing equipment. A significant part of the work for this subtask involved the development of new experimental devices or significant modification of existing laboratory equipment.

6.1.1 Material

The material used in the experimental programme was Czech Ca-Mg bentonite from the Černý vrch deposit (BCV). The material is produced industrially by Keramost Ltd in the form of powder with an original water content of approximately 11%. References to research reports describing the basic characteristics of the material are given in section 5.1.1.

6.1.2 Research plan

The aim of the test programme was to analyse hydromechanical properties of the bentonite at elevated temperatures. The tests were carried out in an advanced THM oedometric apparatus modified for testing at temperatures above 100°C. In addition, new advanced constant volume cells (T-MPC cells) designed for testing in the temperature range 20-150°C were constructed and further modified to minimise deformations due to thermal expansion at high temperatures.

The tests included determination of the oedometric compressibility at elevated temperatures. Swelling pressures were measured at temperatures up to 150°C in two different arrangements of T-MPC cells with additional tests performed on samples compacted to dry densities 1.4 and 1.8 g/cm^3. The effect of cyclic temperature change on swelling pressure and swelling strain was also investigated. The swelling strain test was performed as a constant load swelling test at a minimum load applicable through the experimental setup.

As the continuous decrease in swelling pressure at high temperatures was identified, an additional set of experiments was planned to further investigate swelling pressure behaviour at high temperatures. Five samples compacted to 1.6 g/cm^3 were saturated under constant volume conditions, exposed to different temperatures in the range 50-150°C and monitored under constant conditions for 30 days. The evolution of swelling pressures due to thermal exposure was analysed.

6.1.2.1 Material (BoM item): BCV bentonite (Ca-Mg type), powder as delivered by producer.
6.1.2.2 Material treatment (sample preparation for test and loading procedure): Samples compacted directly into test cells.
6.1.2.3 Temperature (to which material was/will be exposed to) and exposure time 100°C; 125°C; 150°C; variation in the range 20-150°C; exposure time up to 48 days.
6.1.2.4 Tests carried out (name, description, sample preparation, procedure, results): Oedometric compressibility (100, 150°C), swelling pressure (100, 125, 150°C), variation of swelling strain and swelling pressure induced by temperature cycles (20-100°C and 20-150°C, respectively). 6.1.2.4.1 Oedometric compressibility The oedometric compressibility was determined using an advanced THM oedometer. Samples were compacted into the test cell to an initial dry density of 1.6 g/cm^3, vertically preloaded and saturated. After equilibration, the samples were exposed to high temperature and incrementally. 6.1.2.4.2 Swelling pressure The samples were compacted directly into T-MPC cells (initial dry density 1.6 g/cm^3) and saturated through the bottom base while keeping a constant volume. The swelling pressure acting on the opposite base of the samples was measured using a load cell. The temperature was incrementally increased to evaluate the effect of different temperatures on the same sample. 6.1.2.4.3 Effect of temperature change on swelling strain and pressure Samples were compacted to T-MPC cells to an initial dry density of 1.6 g/cm^3. Two different cell arrangements were used to allow measurement of either swelling strain or swelling pressure (constant volume test). Both samples were saturated until stable values of swelling strain / pressure were reached. When the swelling strain equalised, the sample was subjected to a temperature increase to 100°C followed by a decrease to 20°C. This cycle was repeated three times with continuous measurement of the swelling strain. The constant volume sample was subjected to three thermal loops of 20°C-150°C-20°C. 6.1.2.4.4 Long-term evolution of swelling pressure Samples were compacted to T-MPC cells to an initial dry density of 1.6 g/cm^3 and saturated through the bottom base. After full saturation, the samples were exposed to different temperatures in the range of 50-150°C and monitored under constant conditions for at least 30 days. The swelling pressure evolution at high temperature was analysed. In the final stage of the tests, heating was stopped and the change in swelling pressure due to thermal exposure was evaluated.

Table 6.1 – CU – Hydromechanical experiments in temperature range 100-150°C

6.2 Procedures

6.2.1 Experimental equipment for high temperature tests

The first part of the research programme was focused on modifications to existing test equipment (advanced thermo-hydro-mechanical oedometer) for testing at temperatures above 100°C. A new type of temperature controlled apparatus for constant volume tests (T-MPC cell) was developed to increase the capacity for high temperature testing.

THM oedometer

An advanced thermo-hydro-mechanical oedometer (*Figure 6.1*), designed for 1D compressibility testing up to high vertical stresses of 25 MPa at controlled temperature, was modified to reduce the thermal compliance of the apparatus. The stainless steel components expected to be heated at high temperatures (test cell and both upper and lower pistons) were replaced with invar components with limited thermal expansion.

The modification of the apparatus was unfortunately significantly delayed due to the COVID-19 pandemic, which resulted in delayed delivery of individual components, unavailability of commercial workshops and limited laboratory manpower. The modified apparatus was only used to determine the oedometric compressibility of fully saturated bentonite samples at high temperatures (100, 150°C). Other experiments originally planned for the THM oedometer, including constant volume tests, were eventually carried out in T-MPC cells, which allowed better control of constant volume conditions due to the smaller thermal and mechanical compliance of the apparatus.

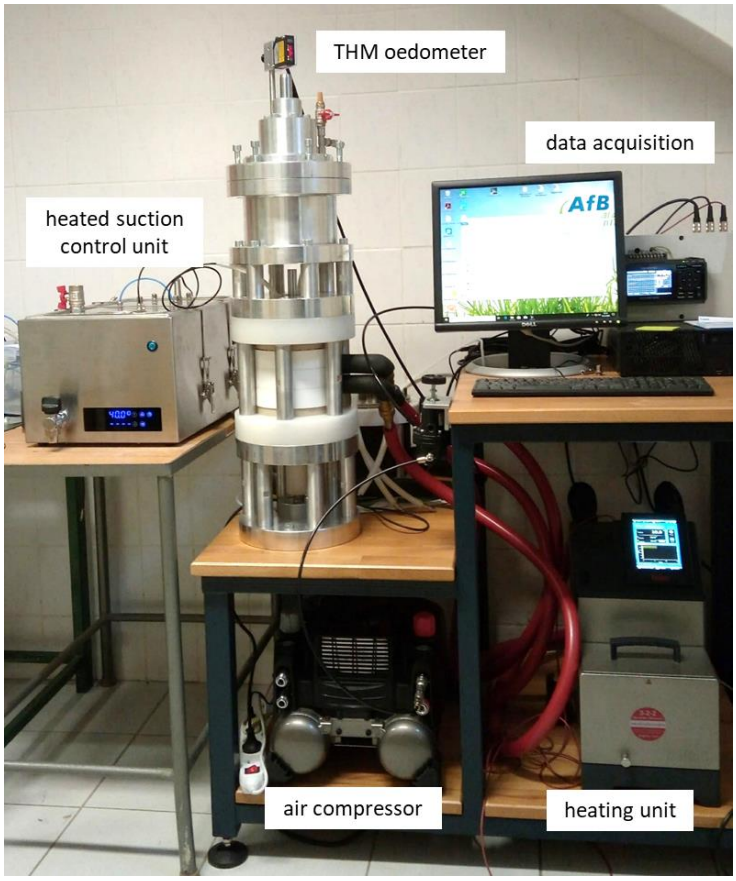

Figure 6.1 – Modified thermo-hydro-mechanical oedometer.

T-MPC cells

In order to increase the capacity for high temperature experimental testing, a new thermal constant volume apparatus (T-MPC cell) has been developed for measuring swelling pressures and swelling strains at high temperatures. The cell (**Erreur ! Source du renvoi introuvable.**) consists of a rigid confining ring, two pistons (all made of invar) and a rigid frame to hold the pistons in a fixed position. A radial heating element is located on the outside of the sample cell. A small load cell for measuring the swelling pressure is placed between the upper piston and the frame. It is separated from the heated piston by a heat buffer made of highly rigid PEEK plastic. The metal porous plates connected to drainage lines to allow saturation of the sample are integrated into both pistons. In an alternative configuration, the top frame with load cell can be removed and replaced with a dial gauge to measure vertical deformation for swelling strain determination.

Three T-MPC cells were constructed with independent heating control units (**Erreur ! Source du renvoi introuvable.**(b)). Despite the use of invar components, the first set of swelling pressure experiments showed significant deformation of the samples after heating (section 6.3.2). These deformations were caused by thermal expansion of the steel bars that formed the frame (**Erreur ! Source du renvoi introuvable.**(a)). Therefore, a modified version of the test setup with the massive external frame was developed (*Figure 6.3*). In this configuration the frame was kept at a constant temperature during the test and thermal expansion was minimised.

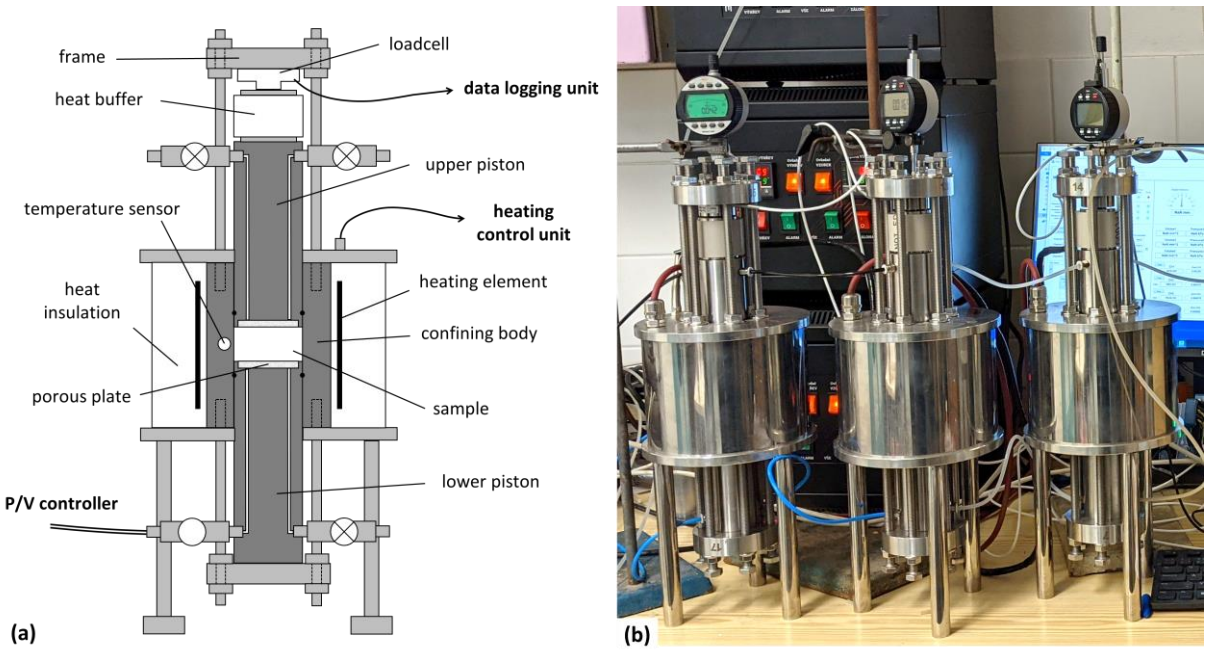

Figure 6.2 – Configuration of the initial version of T-MPC constant volume cell - (a). Invar components are shown in dark grey; set of three cells - (b).

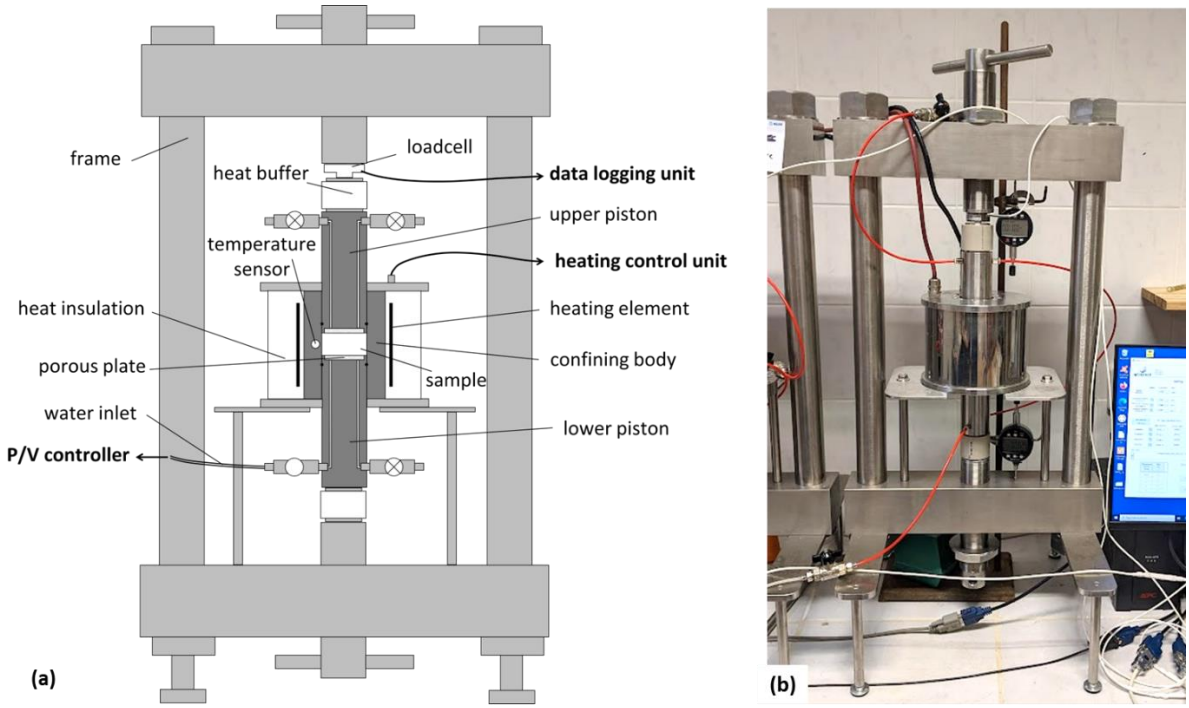

Figure 6.3 – Configuration of the modified version of T-MPC constant volume cell. Invar components are shown in dark grey.

6.2.2 Test procedures

Oedometric compressibility

Two test samples were compacted from bentonite powder of its hygroscopic water content to a target dry density 1.6 g/cm^3, preloaded vertically in the THM oedometer and saturated. After full saturation, back pressure was applied and the temperature was increased to the target value (100 and 150°C, respectively). The samples were subjected to incremental loading. The test at 100°C was successfully performed in the full range of intended vertical effective stresses (up to 20 MPa followed by an unloading path), while the test at 150°C only reached 2 MPa due to leakage in the system resulting in a reduction in back pressure.

Swelling pressure

The first set of swelling pressure experiments (Test 1), carried out in the original version of the T-MPC cells, was performed on samples compacted to target dry densities of 1.4, 1.6 and 1.8 g/cm^3. The samples were compacted directly in the test cells and saturated with distilled water through the lower piston. Only a low water pressure of 10 kPa was applied during saturation. When stable swelling pressures were reached, a back pressure of 500 kPa was applied to prevent boiling of the water. Its effect was subtracted from the measured total pressure to obtain the swelling pressure. All three samples were heated to 100°C. The sample compacted to 1.6 g/cm^3 was further heated to 125°C and 150°C to investigate the change in swelling pressure at higher temperatures.

Due to the thermal compliance of the test cells and the resulting change in sample volume during the test, it was decided to repeat the test in a modified version of the apparatus with an external frame (*Figure 6.3*). This test (Test 2) was performed on a sample compacted to 1.6 g/cm^3. The sample was prepared in the same way as the previous samples. It was subjected to a temperature of 50°C, which was subsequently increased to 100°C and 150°C. In this test, a significantly lower thermal compliance was confirmed by direct measurement.

Effect of temperature change on swelling strain and pressure

Both samples tested to evaluate the cyclic temperature change on swelling properties were prepared similarly to those used for the swelling pressure tests. The samples were compacted at 1.6 g/cm^3.

During the swelling strain experiment, the sample was saturated through the lower piston under free swelling conditions. It was loaded only by the upper piston, which generated a small constant vertical load of 11 kPa. Swelling of the sample was measured until the deformation fully stabilised. The temperature was then increased to the target of 100°C. Back pressure was not applied during this test, as it adds another level of complexity in free swelling experiments. For this reason the actual temperature was kept slightly below the boiling point at 98°C. The initial heating period of 11 days was followed by 3 days at 20°C and two further heating periods of 6 days each.

The sample for the swelling pressure test was saturated at a constant volume and then gradually heated to 150°C over 50 days. Applied thermal cycles consisted of three heating stages at 150°C (lasting 15 days, 7 days and 14 days respectively) followed by three stages at 20°C (7; 7 and 8 days respectively) to allow full equalisation of swelling pressure.

Long-term evolution of swelling pressure

The samples for evaluation of long-term development of swelling pressures were prepared following the same process as previous samples, by uniaxial compaction to a target dry density of 1.6 g/cm^3. The samples were then fully saturated under constant volume conditions in T-MPC cells. In the tests carried out at 50°C and 75°C, a pore water pressure of around 10 kPa was maintained, while in experiments performed at 100°C, 125°C, and 150°C, a back pressure of 500 kPa was applied. After full saturation, each sample was exposed to different temperature of 50°C, 75°C, 100°C, 125°C and 150°C respectively and the swelling pressure was monitored under constant conditions for at least 30 days. Following the heating stage, the swelling pressures were measured until full equilibration at laboratory temperature.

6.3 Results

6.3.1 Oedometric compressibility

The compression curves of the bentonite samples heated to 100°C and 150°C are shown in *Figure 6.4* together with compression curve of the BCV sample tested at 20°C, which is provided as a reference. Although the 150°C test was terminated at 2 MPa, the results indicate a similar slope of the normal compression lines of all three samples. The position of the compression line is shifted downwards with increasing temperature. The same effect of temperature on soil compressibility, characterised by a shifted normal compression line with a similar slope, is reported in the literature for various soil types (e.g. Uchaipchat and Khalili, 2009; Cekerevac and Laloui, 2004).

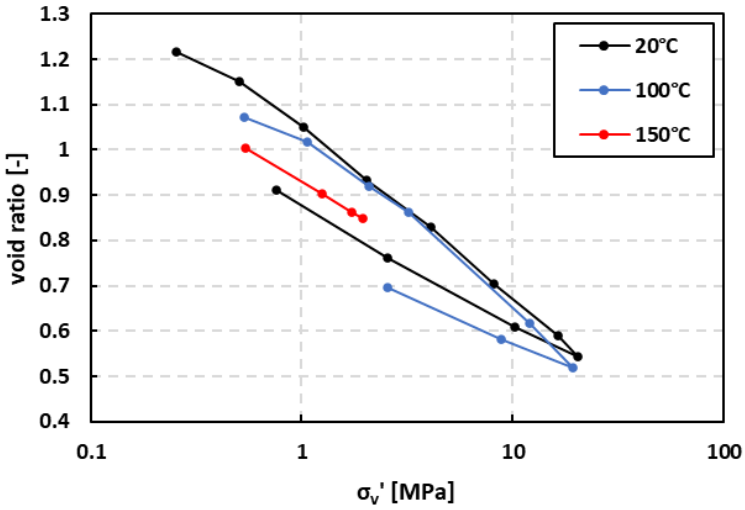

Figure 6.4 – Compression curves of BCV samples loaded at different temperatures.

6.3.2 Swelling pressure

Test 1

Figure 6.5 shows the results of the swelling pressure Test 1 carried out in the original configuration of T-MPC cells (**Erreur ! Source du renvoi introuvable.**). The swelling pressures measured at 100°C for three different dry densities show a decrease compared to the values obtained at 20°C. However, this decrease is partly due to the thermal expansion of the frame (section 6.2.2), which resulted in a decrease in dry density for all samples. All three swelling pressures are below the regression line characterising the dependence of swelling pressure on dry density at 20°C. The sample compacted to 1.6 g/cm^3 was further heated to 125°C and 150°C. This resulted in a further decrease in dry density and an even more significant reduction in swelling pressure. As the most important boundary condition for swelling pressure experiments, constant volume, was not fully achieved, the interpretation of the results is difficult. The reduction in swelling pressure could be partially attributed to wall friction and the effect of temperature cannot be quantified separately.

Test 2

Test 2 was carried out only on the sample compacted to 1.6 g/cm^3 in the modified version of the T-MPC cells (*Figure 6.3*). The results (*Figure 6.6*) show a very limited change in dry density as the thermal compliance of the apparatus was minimised. The swelling pressure measured in the applied temperature range 20-150°C increases, but the change in swelling pressure is very small.

A detailed comparison of 1.6 g/cm^3 samples examined in Tests 1 and 2 is presented in *Figure 6.7*. It shows qualitatively different trends: the decrease in swelling pressure with increasing temperature (Test 1) and the increase in swelling pressure in Test 2. This comparison demonstrates that in the complex tests relatively small modifications to the experimental equipment can lead to qualitatively different results. Due to the limited changes in sample volume, the result of Test 2 is considered more relevant. It indicates that the swelling pressure is not significantly affected by the temperatures up to 150°C.

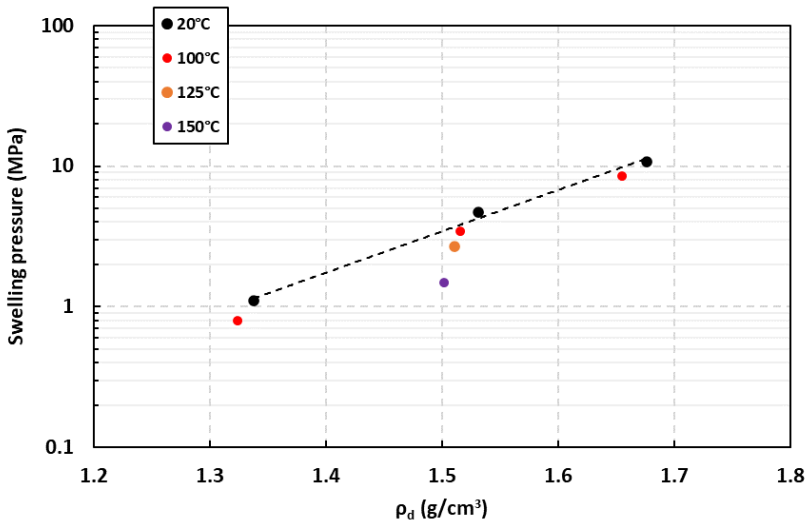

Figure 6.5 – Swelling pressures measured at elevated temperatures in Test 1.

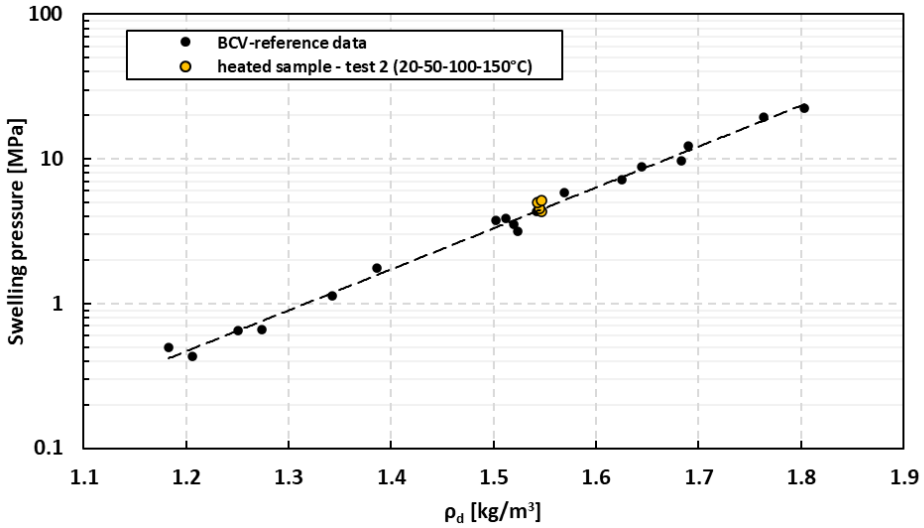

Figure 6.6 – Swelling pressures measured at elevated temperatures in Test 2.

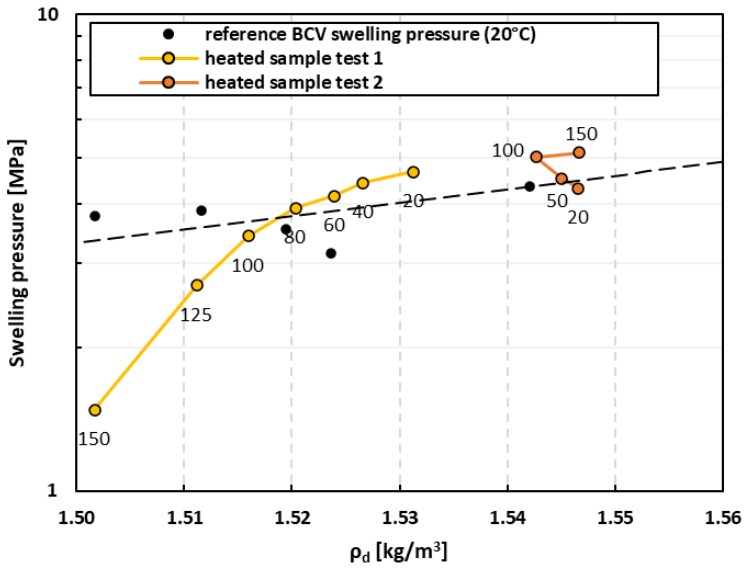

Figure 6.7 – Detailed comparison of swelling pressure development in 1.6 g/cm³ samples (Test 1 and Test 2) during heating.

6.3.3 Effect of cyclic temperature change on swelling strain and pressure

Swelling strain

The swelling strain test was carried out on the sample compacted to an initial dry density of 1.6 g/cm³. The swelling strain was fully mobilised approximately 30 days after the start of saturation (*Figure 6.8*). Rapid heating resulted in only a small increase in swelling strain of 0.9%. No reduction was measured after cooling to 20°C. The second heating cycle resulted in negligible variations in swelling strain. At the beginning of the last heating stage, the swelling strain increased from 50.0% to 51.0%. After two days the swelling strain decreased back to 50.1%, probably due to some mechanical vibrations around the apparatus. The final cooling took place after a further four days of heating and it did not cause any measurable change in sample height. In general, no major change in swelling strain was observed after heating, with only slightly higher values after the first and last heating. The swelling strain before the first heating stage reached 48.6% and the final value after three thermal cycles was 50.2%. This shows a negligible effect of the heating cycles on the swelling strain. The measured increase over time may be due to incomplete equilibration of the swelling strain before the first heating stage.

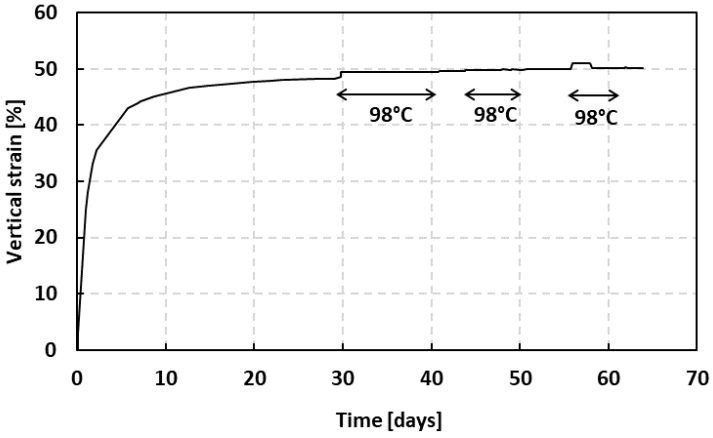

Figure 6.8 – Swelling strain of the sample exposed to three heating stages (highlighted in the graph).

Swelling pressure

The effect of cyclic temperature changes on the swelling pressure is presented in *Figure 6.9*. The sample compacted to 1.6 g/cm^3 was saturated for 12 days until a constant swelling pressure was reached. The temperature was then gradually increased. To avoid high pore water pressure gradients due to thermal expansion of water, the temperature was increased in steps to 50°C, 100°C and 150°C. Each step was applied gradually over a period of approximately one week. The times at which 50°C, 100°C and 150°C were reached are highlighted in *Figure 6.9*.

When the target temperature of 150°C was reached, the swelling pressure started to decrease gradually. This trend continued throughout the heating period of 15 days. The first heating phase was terminated by a rapid drop in temperature to 20°C. After a sharp decrease, the swelling pressure increased again and stabilised in about 7 days. The rapid decrease induced by cooling can be attributed to thermal shrinkage of the sample (both pore water and solids) and also to some thermal shrinkage of the invar pistons, which produce a small temperature dependent deformation despite limited thermal expansion. The partial recovery of swelling pressures may be caused by equilibration of pore water pressure within the sample and partial mass redistribution induced by a small change in volume. However, the swelling pressure after the first heating-cooling cycle was significantly lower than the initial swelling pressure after saturation.

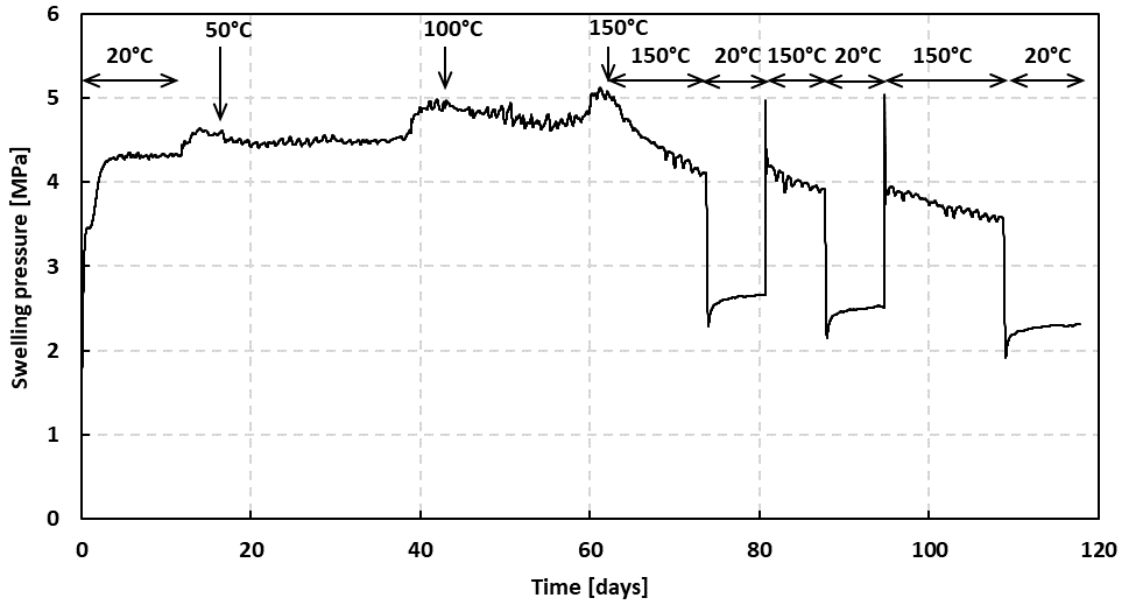

Figure 6.9 – Effect of cyclic temperature change on swelling pressure.

In the second heating cycle, the target temperature of 150°C was applied directly. A rapid increase in swelling pressure was observed followed by a partial decrease due to pore water pressure equilibration. Thereafter, the measured swelling pressure corresponded well to the value obtained at the end of the first heating stage. However, a gradual decrease similar to the first heating stage was again measured over time. A qualitatively similar response was also observed during the second cooling stage and the final heating-cooling cycle. The final swelling pressures measured in both the heating and cooling stages gradually decreased with the number of cycles (**Erreur ! Source du renvoi introuvable.**). The final value after all cycles was only 56% of the initial swelling pressure after saturation.

This test revealed a significant decrease in swelling pressure over time due to high temperature exposure. As a result of this observation, the original test plan was modified to investigate this phenomenon in detail (section 6.3.4).

Number of cycle	150°C (heating stage)	20°C (cooling stage)
0 – initial saturation		4.3 MPa
1	4.1 MPa	2.7 MPa
2	3.9 MPa	2.5 MPa
3	3.6 MPa	2.3 MPa

Table 6.2 – Summary of swelling pressures measured during the constant volume test with cyclic temperature change at the end of each stage.

6.3.4 Long term evolution of swelling pressures

The long term swelling pressure evolution at high temperatures was analysed on five samples (1.6_T50 – 1.6_T150) with similar dry densities (target density 1.6 g/cm^3). The evolution of the swelling pressures during the tests shows similar trends (Figure 6.10). A sharp increase in swelling pressure was observed immediately after heating. This was followed by a decrease, which was also extremely rapid in its initial phase, but which gradually slowed down. However, a decrease in swelling pressure was measured for most samples throughout the heating period. At the end of the heating stage, the swelling pressure dropped sharply. This was followed by a slower final recovery to a steady state value.

A comparison of the samples 1.6_T50 – 1.6_T150 shows that the decrease in swelling pressure in the high temperature stage is more significant at higher temperatures. In test 1.6_T50, the swelling pressure stabilised after approximately four days of heating, whereas all the other tests exhibited continuous decrease until the end of the heating period.

The conditions of the individual tests, the physical properties of the samples and the main results are summarised in **Erreur ! Source du renvoi introuvable.**. The final swelling pressures measured at the end of all tests ($SP_{20°C\_fin}$) are significantly lower than the swelling pressures determined before the heating stage ($SP_{20°C\_ini}$). The magnitude of this decrease also clearly reflects the temperature applied in the heating stage.

Sample	**Applied T [°C]**	**Time at high T [days]**	**Real ρ_d [g/cm^3]**	**Sample height [mm]**	**$SP_{20°C\_ini}$ [MPa]**	**SP_{T_fin} [MPa]**	**$SP_{20°C\_fin}$ [MPa]**
1.6_T50	50	30.9	1.60	10.30	4.5	4.5	4.0
1.6_T75	75	30.2	1.54	10.71	4.6	4.3	3.9
1.6_T100	100	47.9	1.56	10.57	4.1	4.0	3.1
1.6_T125	125	28.9	1.55	10.68	3.9	4.2	2.5
1.6_T150	150	33.2	1.55	10.68	3.9	3.3	1.6

Table 6.3 – Details of the long term swelling pressure tests and main results.

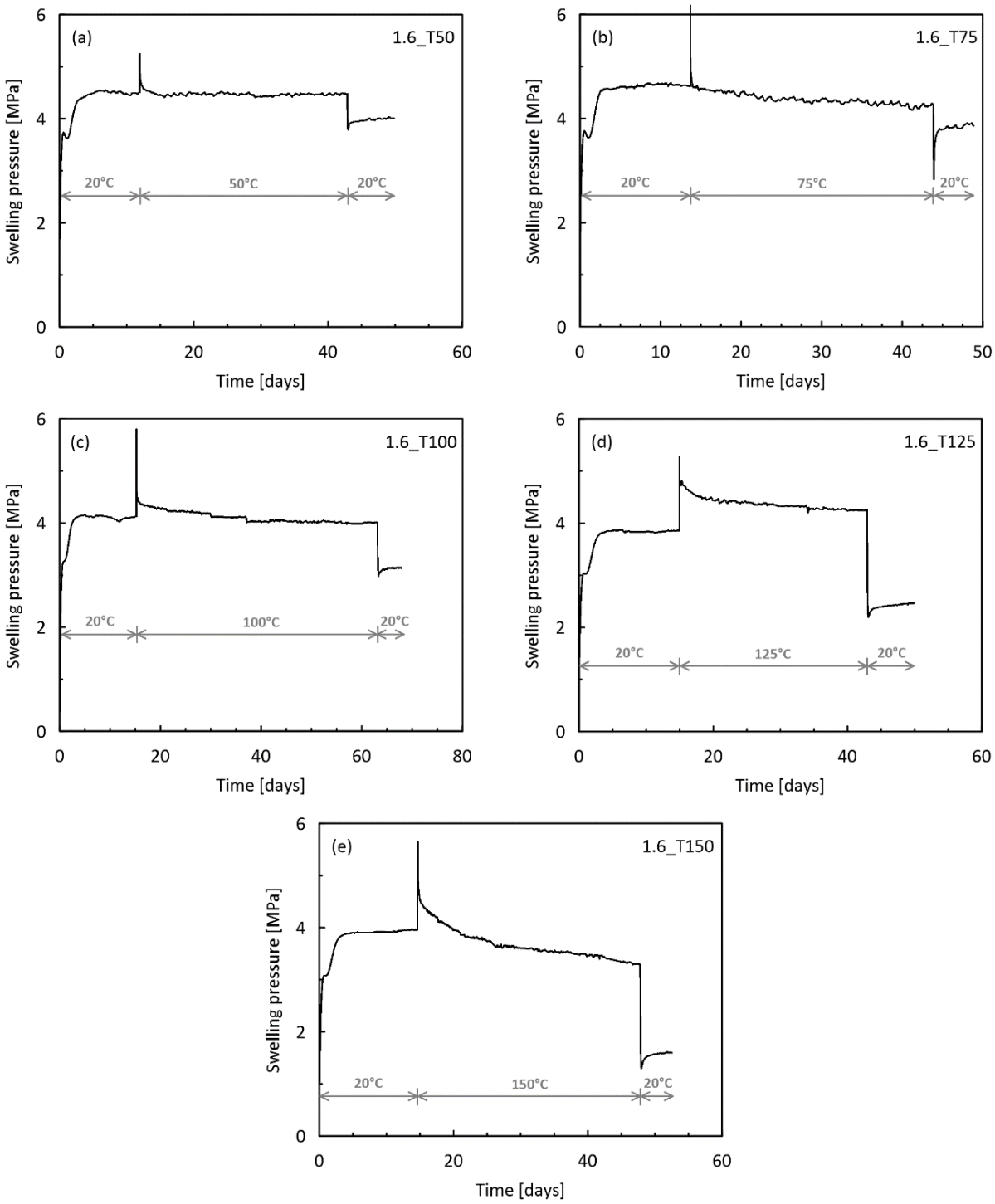

Figure 6.10 – Development of swelling pressure with time in samples compacted to 1.6 g/cm² and heated to 50°C (a) – 150°C (e).

A detailed view of the heating stage in semilogarithmic plot is shown in Figure 6.11(a). Test 1.6_T150 is presented as an example. The initial increase in swelling pressure is associated with the thermal expansion of the sample (bentonite grains and pore water). Thermal expansion of the pair of invar pistons is significantly smaller than that of the steel but due to the high temperatures applied it reaches 0.08 mm at the maximum temperature and also contributes to the measured pressure increase.

All factors contributing to the thermal expansion after heating remain constant throughout the heating stage with the exception of the pore water pressure. The excess pore water pressure generated by

heating could dissipate through the porous stones on both sides of the sample. This process can be evaluated in a similar way to consolidation. The time of full consolidation of the compacted BCV sample of the same dry density and the same sample height was independently determined by the standard Cassagrande method in a 1D compression test (t = 10.5 hours). Considering the actual dynamic viscosity of water at a given temperature, the approximate time of full dissipation of the excess pore pressure can be calculated (red cross in *Figure 6.11*).

From the moment of excess pore water pressure dissipation, the samples were kept under constant conditions (volume, temperature, pore water pressure) up to the end of the heating stage. A continuous decrease in swelling pressure was observed up to the end of the heating stage. Figure 6.11(b) demonstrates a similar decrease in all tests. For better comparison, the decrease in swelling pressure is represented here by the ratio SP_{T_p0}/SP, where SP_{T_p0} corresponds to the swelling pressure after excess pore pressure dissipation in each test (see *Figure 6.11*(a)). It shows a similar initial rate for tests 1.6_T50 – 1.6_T125. However, the swelling pressure in test 1.6_T50 stabilised after four days of heating and then remained constant. All other tests exhibited a gradual decrease up to the end of the heating period with a significantly steeper slope in test 1.6_T150.

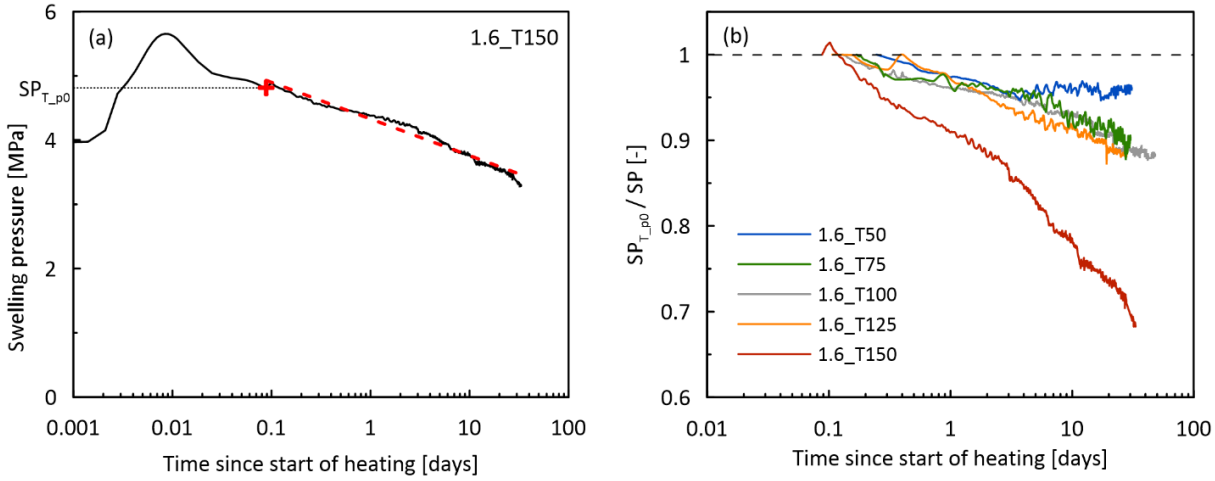

Figure 6.11 – (a) Example of swelling pressure evolution during the heating stage; 5 (b) – comparison of normalized swelling pressure development in tests 1.6_T50-1.6_T150 in the heating stage after excess pore water pressure dissipation.

The presented trends indicate that the decrease in swelling pressure can be approximately expressed by a semi-logarithmic regression as indicated in Figure 6.11(a). The slope of the regression line, referred to as the coefficient of relaxation C_{rel}, was determined in a similar way to the definition of creep in soil mechanics by the following relationship

$$C_{rel} = -\frac{\Delta SP}{\Delta \log t}$$

where ΔSP is the swelling pressure difference between the time of excess pore pressure dissipation after heating (SP_{T_p0}) and the end of the heating period.

The trend of C_{rel} change with the applied temperature for the individual tests is presented in Figure 6.12(a). It increases in the measured temperature range with a significant acceleration between 125 and 150°C. It should be noted that the C_{rel} values were determined from the whole interval between the excess pore pressure dissipation and the end of the heating stage. Sample 1.6_T50 exhibited a decrease in swelling pressure only during the first four days of heating, while the swelling pressure remained constant during the remaining 27 days of the heating stage. The value of C_{rel} determined from the initial part, where thermal relaxation took place, is 0.19, which is a similar value to that of samples

1.6_T75 and 1.6_T100. On the other hand, the value of C_{rel} of the 1.6_T150 sample increases in the last part of the heating stage. This means that the average values may depend on the duration of the heating stage especially in the case of the 1.6_T50 and 1.6_T150 samples.

The decrease in final swelling pressure measured at the end of the test compared to the swelling pressure determined after saturation is analysed in Figure 6.12(b). It demonstrates a reduction in swelling pressure due to heating, which also accelerates with the applied temperature. It also confirms that permanent changes in swelling pressure are induced by the relaxation process at elevated temperature.

Sample 1.6_T50 retained 90% of its initial value, whereas the swelling pressure of sample 1.6_T150 decreased to 41% due to heating. The presented ratio may be slightly influenced by the different duration of the heating stages of the individual samples, but due to the logarithmic trend of the swelling pressure decrease this effect is rather small. The value determined for 1.6_T50 can be considered as final, since the swelling pressure stabilised after a few days of heating and would probably not change even in the case of a longer heating stage. On the contrary the other samples exhibited a decrease in swelling pressure up to the end of the heating period and it can be expected that a longer heating period could lead to an even more significant decrease in swelling pressure.

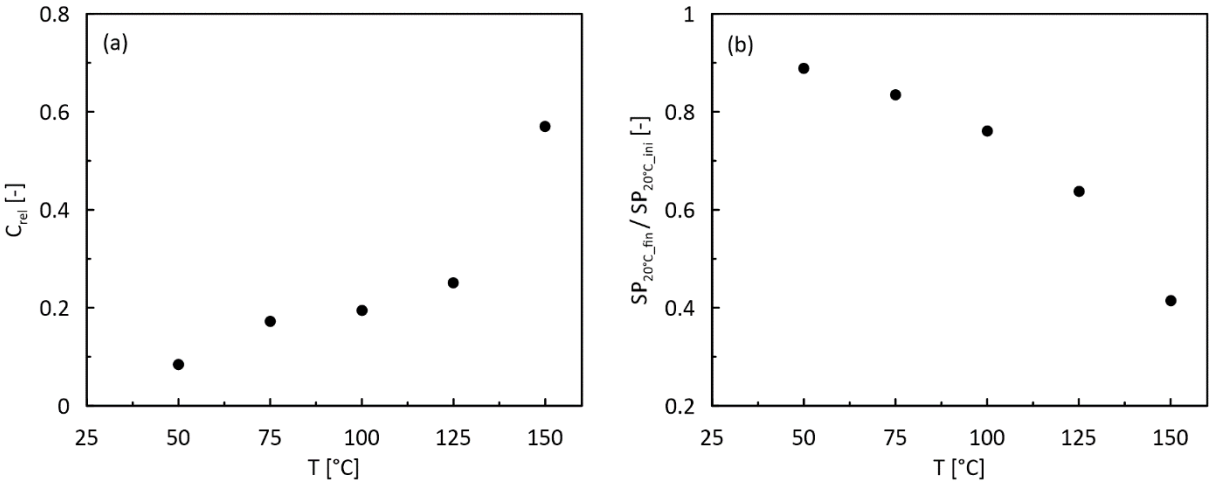

Figure 6.12 – (a) - Development of coefficient of relaxation with applied temperature in tests 1.6_T50-1.6_T150; (b) - Decrease in swelling pressure due to thermal treatment, expressed as the ratio of final swelling pressures after heating period ($SP_{20°C\_fin}$) to initial swelling pressure determined after saturation ($SP_{20°C\_ini}$).

6.4 Conclusion

The presented laboratory research focused on evaluating the hydromechanical properties of BCV bentonite at high temperatures. The results of the oedometric compression tests showed a similar slope of the normal compression line at different temperatures. The position of the compression line shifted downwards with increasing temperature.

The swelling pressure tests demonstrated a high sensitivity of the results to the experimental equipment used. Test 2, performed in a modified version of the T-MPC cell with reduced thermal expansion, showed that the swelling pressure is not significantly affected by the temperatures up to 150°C.

The cyclic change in temperature was investigated in the swelling strain and swelling pressure test. While a negligible effect of the heating cycles on the swelling strain was observed in the swelling strain test, a significant reduction in swelling pressure due to high temperature exposure was observed in the swelling pressure test.

A series of tests to evaluate the long term swelling pressure evolution at high temperatures confirmed the results of the cyclic swelling pressure test. A significant decrease in swelling pressure was observed at temperatures of 50-150°C during a 30-day heating period. This decrease accelerated with the applied temperature and, with the exception of the 50°C test, continued throughout the heating period. The effect of the decrease in swelling pressure is permanent, which was demonstrated by comparing the swelling pressure measured before and after the heating period.

7 JYU/UH (UH) + GTK/UH (UH)

7.1 Introduction

X-ray tomography and 4D (3D with time) image analysis were conducted at X-ray tomography laboratories of JYU (University of Jyväskylä) and GTK (Geological Survey of Finland) to observe water transport in compacted cylindrical Na-bentonite (Bara-Kade) samples at elevated uniform temperatures of 20, 50, 90, and 130 °C. The 3D spatial and time evolution of local partial densities of dry bentonite and water were monitored during the saturation of the sample, as well as the swelling pressure. Preliminary assessment of the chemical stability of the system was also performed at GTK using micro X-ray fluorescence (µ-XRF). The data obtained will be organized in an open database to support related modelling and model validation carried out in Task 3.3.

In addition to the direct experimental data on water transport, also the internal deformations occurring in temperature-controlled bentonite samples were obtained using non-intrusive X-ray tomographic technique. The data thereby obtained includes spatial and temporal evolution of the internal deformation and water content fields in the bentonite samples during the saturation phase.

All experiments were performed using small scale cylindrical samples with two sizes and target dry densities and a simple Olkiluoto ground water simulant was used in the experiments. The saturation process took place in confined conditions in the X-ray transparent sample cell.

7.1.1 Material

The basic material is Wyoming Na-bentonite (with tradename BARA-KADE) powder as provided by the manufacturer.

7.1.2 Research plan

The original plan was to conduct 18 wetting experiments at elevated uniform temperature by using two sample heights: 21 and 42 mm, dry densities of bentonite: 1.40 and 1.65 g/cm^3, and three temperature values: room temperature, 50, 90 °C. The diameter of the cylindrical sample was 42 mm in each case. During the project, the research plan was updated and the experiments at 130 °C were included in the plan. The experiments above 100°C became possible after some updates in the experimental setup and were considered interesting by the project participants. According to the original plan the duration of the experiments was 1 month for experiments on 21 mm high samples and 4 months for experiments on 42 mm high samples. Including the experiments at 130 °C the total number of experiments were 22. The original plan contained also similar wetting experiments in the presence of temperature gradient. *Deviations from the original research plan*: we planned to perform experiments also in the presence of temperature gradient, however, to the date we haven't been able to build a stable cooling and heating system which could be applied to obtain reliable experimental data. Based on the testing, cooling and heating of the sample is required also during the tomographic scan and this is the main challenge at the moment. On the other hand, experiments above 100 °C were not in the original research. We planned also to increase the temperature to 120 °C at saturated steady state at the end of experiments, but this was not done because the process is essentially finished and the heating may cause problems in the analysis, i.e., problems in the calibration due to possible drying of the sample.

7.1.2.1 Material (BoM item): Bara-Kade (Na type), powder as delivered by manufacturer.
7.1.2.2 Material treatment (sample preparation for test and loading procedure): Compaction for the sample holder. Target dry densities 1.40 g/cm^3 and 1.65 g/cm^3. Initial water content is about 10 %. Wetting is done by using a Posiva Reference solution which is prepared by dissolving $CaCl_2$ and NaCl in an aqueous medium (distilled water) at a Ca^{2+}/Na^+ mass ratio of 1:2 to a total dissolved solids content = 10 g/l. Concentrations: c(NaCl) = 0,111 M; c($CaCl_2$) = 0,032 M.
7.1.2.3 Temperature (at which measurements/tests are carried out) Uniform elevated temperatures: room temperature (20-25°C), 50°C, 90°C, 130 °C
7.1.2.4 Tests carried out (name, description, sample preparation, procedure, results): Test 1.1 Uniform temperature 1. Small samples (JYU) X-ray tomography method was used to monitor wetting and swelling of temperature-controlled bentonite samples. Bentonite samples were held in a constant cylindrical volume while wetted from one end. The sample diameter *d* was 42 mm and height *h* was 21 mm. The sample, sample holder and water were held at constant uniform temperature. The sample holder was equipped with force sensors to monitor the swelling pressure during the wetting of bentonite. During the wetting process X-ray imaging and/or X-ray tomography method was used to monitor water transport and deformation in temperature-controlled bentonite samples. The duration of the experiments was 1 month for experiments below 100 °C. The experiments at 130 °C were shorter than other experiments, about one week, due to faster saturation. Measurements were done using two target overall dry densities and at four temperatures with a repetition for each case. In total, 16 wetting experiments were performed during the project. Test 1.2 Uniform temperature 2. Large samples (GTK) X-ray tomography method was used to monitor wetting and swelling of temperature-controlled bentonite samples. Experimental setup will be like the one in JYU (test 1.1). The essential difference was the larger height of the sample, *h* = 42 mm, whereby the estimated duration of one measurement run was much longer (estimated 4 months). The duration of the experiments at room temperature and 50 °C was four months as in the original plan. The experiments at 90 °C were finished after two months of wetting due to problems in the wetting system caused by the elevated temperature and salt build-up. However, the samples were essentially saturated after one month of wetting as the saturation speed increases with increasing temperature, allowing comparable observations as from samples with 4 months duration. The total number of measurements at GTK was smaller than in JYU due to the longer saturation time. Only one target dry density, 1.65 g/cm^3, was used and measurements was done at three temperatures: room temperature (20-25°C), 50°C, 90°C.
7.1.2.5 Schedule and expected date(s) of results delivery: Test 1.1 Preparatory work: M1-M12 Test 1.1 Experiments: M6-M50 Test 1.2 Preparatory work: M1-M12 Test 1.2 Experiments: M12-M48 Reporting and publications: M13-M18, M28-M33, M43-M60

Table 7.1 JYU+GTK – Water transport in compacted bentonite sample at elevated temperatures

7.2 Procedures

In both cases, tests 1.1 and 1.2 in **Erreur ! Source du renvoi introuvable.**, compacted cylindrical bentonite samples were held in a constant cylindrical volume while wetted from one end. Samples were prepared by using uniaxial compaction and the initial water content of the powder was approximately 10 % in all the experiments. The sample holder is described in Figure 7.1. The sample holder is equipped with two high-temperature force sensors to monitor the swelling pressure during the wetting of bentonite. To monitor the water transport and deformation processes by using the 4D X-ray tomographic method, 10 tomographic scans were performed during the saturation of the sample. The experiments on 21 mm sample height and below 100 °C were imaged according to the following schedule: 0 hours (initial state), 2 hours, 10 hours, 1 days, 2 days, 4 days, 8 days, 16 days, 24 days, and 32 days. The experiments on 42 mm sample height were imaged according to the following schedule: 0 hours (initial state), 6 hours, 2 days, 4 days, 8 days, 16 days, 32 days, 64 days, 96 days, and 128 days. The sample, sample holder and water were held in the heating chamber at constant uniform temperature and while performing the tomographic imaging, the sample holder was placed in the insulating box to minimize the cooling of the sample. The duration of one tomographic scan was about 20 minutes. The duration of the scan was optimized to minimize the cooling of the sample but still yield sufficient image quality which facilitates the 4D image analysis. At the end of the experiment, the sample was carefully removed from the sample holder and the average water content of the sample was measured gravimetrically. The end state information was utilized in the calibration of the 4D X-ray tomographic method. The aim of the measurements was to obtain detailed spatial information about water transport inside the clay using X-ray tomographic images. Good spatial resolution also facilitates the deformation measurement which is a vital part of the analysis. At the same time, the tomographic scan must be fast enough that one can assume stationary state of the sample during the scan. The optimisation of the duration of the tomographic scans and spatial resolution leads to the duration of 20 minutes per scan. In the images which were analysed the image voxel sizes (3D version of pixel) were 192 µm at JYU and 169 µm at GTK. The difference in voxels sizes between the laboratories is due to the slight differences in the geometry of the tomographic imaging setups.

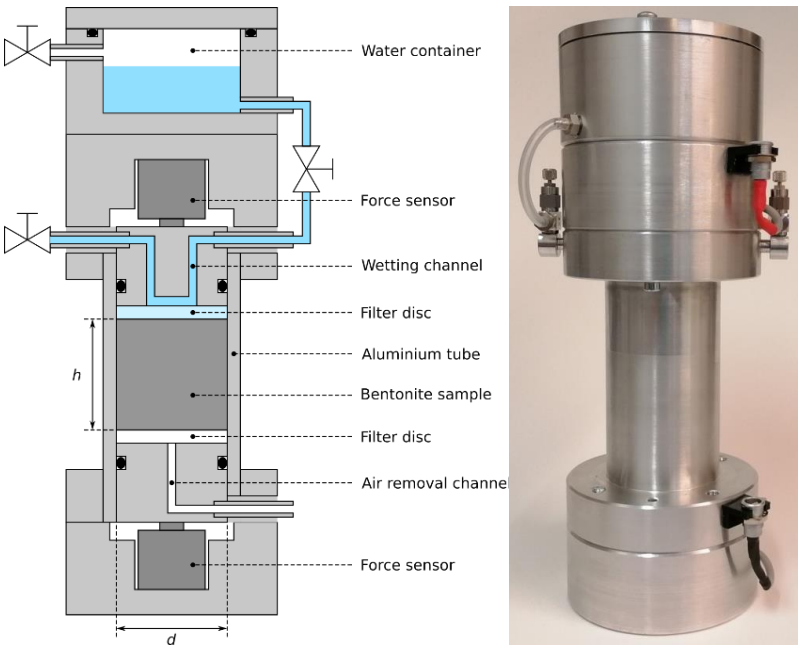

Figure 7.1 – Schematic illustration (left) and a photo (right) of the sample holder.

During the experiments below 100 °C the air removal channel, visible in bottom part of the sample holder in Figure 7.1, was open. Also, during the first tests at 130°C the air removal channel was open, but it was observed that sample will dry due to the evaporation of the water through that channel. In other

words, although water entered the sample from the top, the net water content decreased during the experiment. In order to saturate the sample, the air removal channel was sealed, and the air removal procedure was done occasionally using the valves in the top part of the sample holder. Thus, the boundary conditions are different in experiments below 100 °C and above 100 °C.

For µ-XRF, Tornado plus (with AMICS) instrument from Bruker at the Geological Survey of Finland (GTK) was used. The system has an Rh X-ray 30-Watt Rh anode target, two simultaneously operating 30mm^2 silicon drift detectors (SDDs) with an energy resolution of < 145 eV at 275 kcps (measured on MnKα) via beryllium windows and poly-capillary optics. Scanning and sample navigation is carried out via a motorized stage which moves the sample beneath the static X-ray beam. For analysis, cylindrical samples were cut in half and flat surfaces were scanned. The accelerating voltage was 50 kV with a beam current of 600 µA, using a fixed spot size of 20 µm under 4 mbar vacuum. The samples were mapped in separate runs: low resolution scan (n = 5) using a step size of 50-80 µm, depending on the sample, and a pixel dwell time of 10 ms and high-resolution scan (n = 2) using a step size of 20 µm and a pixel dwell time of 5 ms. The qualitative elemental maps and line scans were generated using the Bruker M4 software.

For CEC analysis of one test sample, Cu-trien method (Meier and Kahr 1999) was used (performed at University of Helsinki, Department of Radiochemistry).

7.3 Results

Saturation process of cylindrical compacted Wyoming sodium bentonite samples was monitored using X-ray tomography and 4D image analysis at elevated uniform temperatures of 20, 50, 90, and 130 °C. Based on the experimental results, water transport appears faster, the higher the temperature. This effect is significant already when temperature was increased from room temperature, approximately 20 °C, to 50 °C. Time evolution of the average degree of saturation of the selected samples is presented in Figure 7.2 which contains data from 12 experiments on 21 mm high samples: 2 target initial dry densities, three temperatures, and repetition in each case. From Figure 7.2 one can see that the saturation level is attained significantly faster when temperature is increased. The degree of saturation is based on the calculations done using the grain density value 2.78 g/cm^3 based on the information provided by Posiva Oy and the characterisations of essentially the same Wyoming sodium bentonite material ([5] Kiviranta & Kumpulainen (2011) and [6] Kiviranta et al. (2018)).

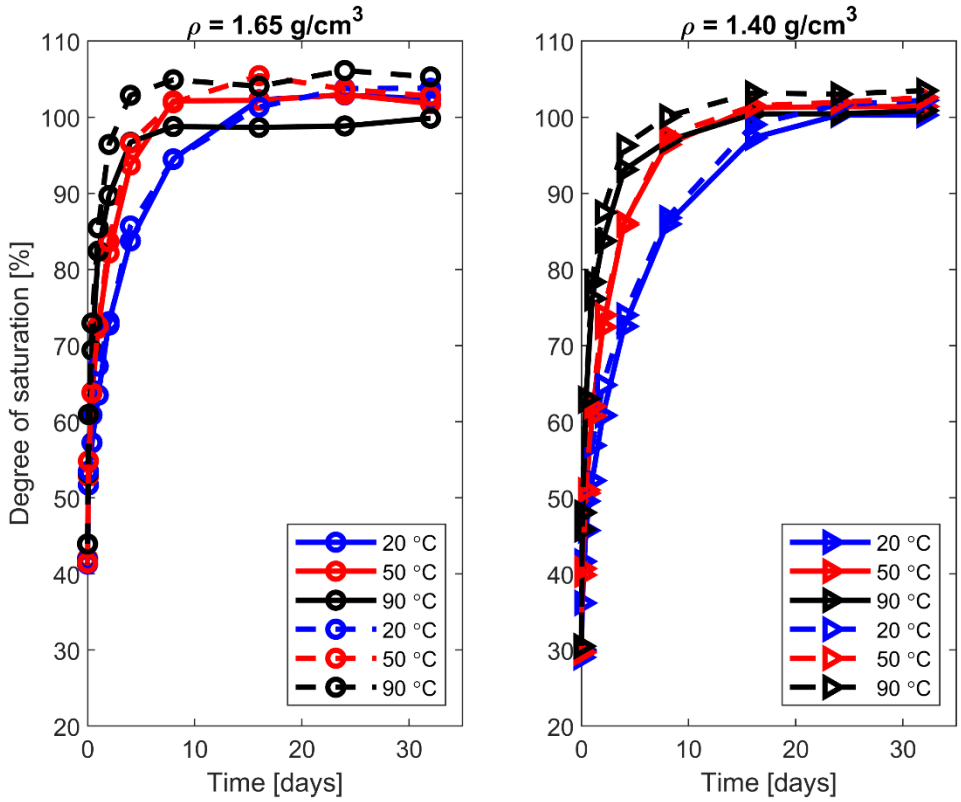

Figure 7.2 – Time evolution of the average degree of saturation

The average degree of saturation of the whole sample, Figure 7.2, contains no information concerning spatial distribution the water content. Therefore, in Figure 7.3, in addition to the time evolution also the 3D spatial distribution of the water content is visualised as an azimuthal average at four temperatures and three instances of time. Also, based on Figure 7.3, one can see qualitatively the increase in 'speed of saturation'. Whether the wavelike features in the spatial distributions in Figure 7.3, for example at 10 h and 24 h instants at 90°C, are a real phenomenon or artifacts of the analysis method remains unclear. The origin of this phenomenon requires further research.

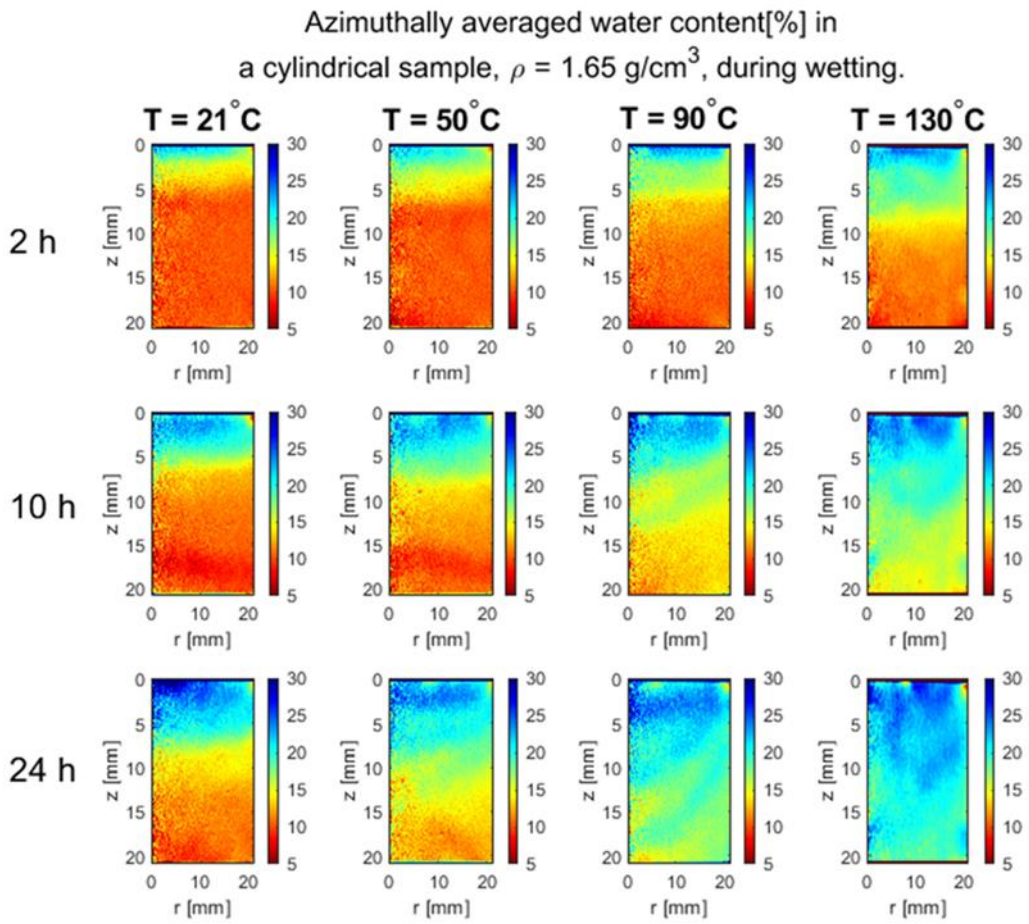

Figure 7.3 – Azimuthally averaged water content at four temperatures: 20°C, 50°C, 90°C, and 130°C. The row corresponds an instant of time after the wetting of the samples was initiated. These experiments are not fully comparable due to the sealing of the air removal channel during the experiments at 130°C. Without the sealing of the air removal channel, the net water content of the sample decreased during the wetting experiment.

Another approach to visualise the 4D information is presented in Figure 7.4, which contains depth profiles of the degree of saturation at selected instants of time at 90°C and 130°C. There is no clear waterfront visible in the profiles, suggesting that the diffusion may have a role in the transport process in addition to advection. Qualitatively, there is slight increase in the speed of the saturation when temperature is increased from 90°C to 130°C, although these experiments are not fully comparable due to the sealing of the air removal channel during the experiments at 130°C.

The X-ray tomographic method is based on the measurements of the changes in the local values of the linear X-ray attenuation coefficients. However, the simple point-wise comparison of the images will lead to errors in the analysis because the wetting of the sample will cause complex internal 3D deformations in the sample. A vital part of the analysis is the measurement of the internal displacements based on digital image correlations, more accurately this measurement is done using a blockmatching method which is based on phase correlation. In practise, the displacement field computations were done with the pi2 software (available at https://github.com/arttumiettinen/pi2).

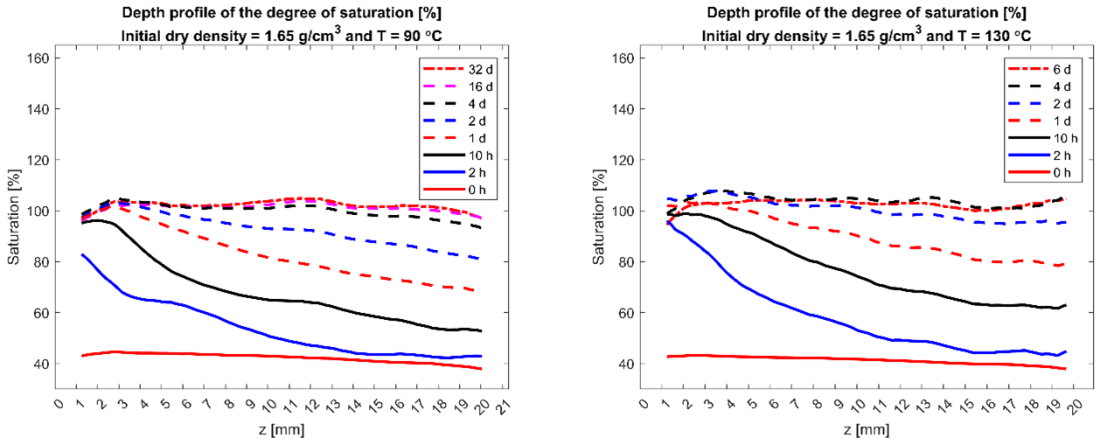

Figure 7.4 – Depth profiles of the degree of saturation at certain instants of time and at two temperatures: 90 °C (left) and 130 °C (right). These experiments are not fully comparable due to the sealing of the air removal channel during the experiments at 130 °C. Without the sealing of the air removal channel, the net water content of the sample decreased during the wetting experiment.

The measured displacements, examples in Figure 7.5, are utilized in two steps of the analysis: to pull-back the deformed image to match the initial image and calculations of the local partial density of dry bentonite. When the internal displacements of the clay sample are considered, the measurement of the difference in the local linear attenuation coefficient yields estimate for the change in the local water content. In order to determine an accurate quantitative estimate, a careful calibration procedure must be performed based on the known values for the initial and final average water contents of the samples. These initial and final average water contents are determined gravimetrically.

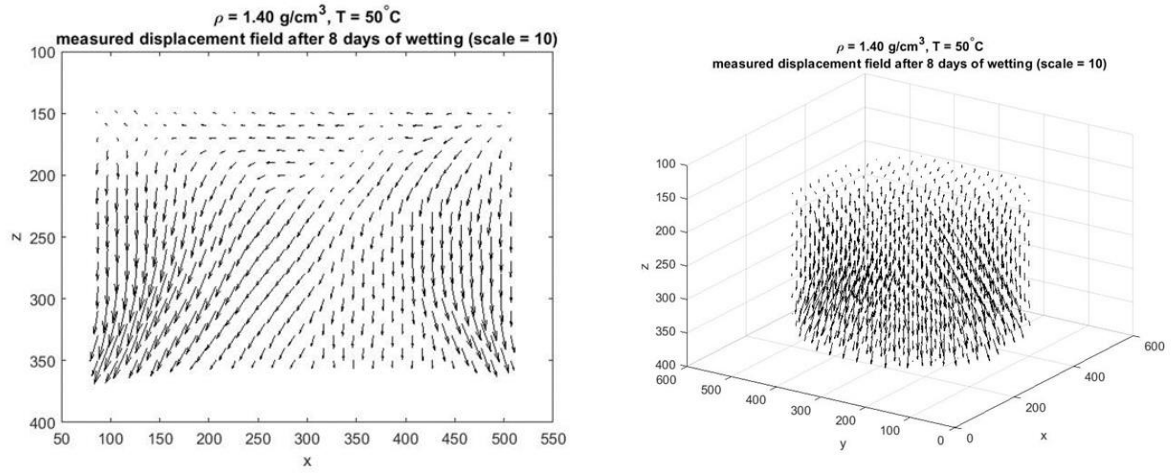

Figure 7.5 – Visualisations of the measured displacement fields in a cylindrical bentonite clay sample: 2D visualisation (left) and 3D visualisation (right).

The X-ray tomographic method has been validated by comparing the results of the analysis to the water content values determined based on post-mortem slicing of the sample and gravimetric measurements of the water content of the individual slices. The results of the validation experiment are presented in Figure 7.6. The black solid line in Figure 7.6 corresponds to the final state in which sample was sliced and the red asterisks are the values of the reference slicing method. Thickness of the slices varied, close to z=0, i.e., the end from which water entered the sample, thickness of the slices was approximately 0.5 mm and then thickness of the slices was increased to approximately 1 mm. Starting from z = 7 slice thickness was approximately 2 mm and the last slice was approximately 4 mm in thickness. In general, the results of the analysis are close to reference values except near the edges of the sample. Possible reasons for the difference are the fact that now, the displacements close to the edges can't be measured reliably and the local linear attenuation coefficient of two materials will mix

into each other near the interface of materials. Now the interface is between bentonite clay and the glass fibre filter disks. The mixing of attenuation coefficient in the vicinity of interface of materials is caused partially by scattering effects and the finite resolution of the X-ray cameras and the geometry of the imaging set-up. Since the results near the edges of the sample are unreliable, the volumes close to the ends of the sample, approximately 1 mm thick layers, will be rejected in the analysis.

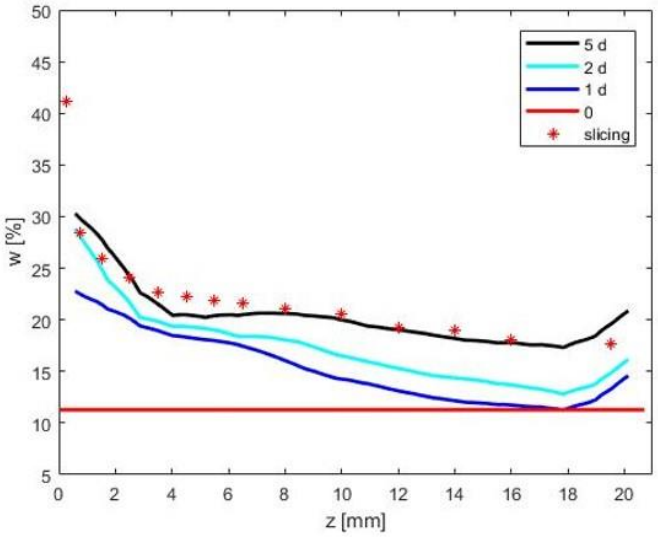

Figure 7.6 – Validation of the X-ray tomographic method based on the measurement of the depth profiles of the water content. The results of the analysis of the final water content (black solid line) are compared to the post-mortem slicing of the sample (red asterisks). In general, good agreement between two approaches are observed.

Based on the observations, one can see that the uptake of water is sensitive to elevated temperatures, examples are presented in Figure 7.2, Figure 7.3, and Figure 7.4. The "speed of the saturation'' as a function of temperature will be determined quantitatively based on the time evolution of the degree of saturation which is determined by fitting a simple 1D diffusion model to experimental data. Examples of the fitting results are presented in Figure 7.7 which contains experimentally determined time evolution of the average degree of saturation of the whole sample at three temperatures: room temperature, 90°C, and 130°C and the fits based on the diffusion model. Although the real water transport process is not described by this simplified model, the chosen fitting procedure serves as an objective approach to obtain numerical values describing the speed of the saturation process. This approach is more objective compared to, for example, visually estimating the moment when the saturation level is reached. Fitting of the model yields so called effective diffusion coefficient which depends on the properties of the sample, e.g., initial dry density of the clay, and wetting water, temperature in which the experiment is performed, and the practical implementation of the wetting experiment, i.e., boundary conditions. Effective diffusion coefficient depends also on the values of the local linear attenuation coefficient, thus all factors affecting the results of the tomographic reconstruction, also affects the values of the effective diffusion coefficient. The detailed results of the fitting procedures will be published in J. Yliharju, et.al. *Observation of water transport in swelling compacted bentonite sample at elevated temperatures using an X-ray tomographic method (in preparation).* Based on the fitting and the preliminary conclusions, the saturation of the sample at 50°C is roughly two times faster than at room temperature and the saturation at 90°C appears to be roughly four times faster than at room temperature. At 130°C the saturation process is approximately 1.5 times faster than at 90°C. Additional analysis is required to conclude whether all the observations can be explained by the changes in the water properties, e.g., the temperature dependency of the viscosity of water, as a function of temperature, or whether there were some changes in the bentonite itself. Also here, the experiments are not fully comparable due to the sealing of the air removal channel during the experiments at 130°C.

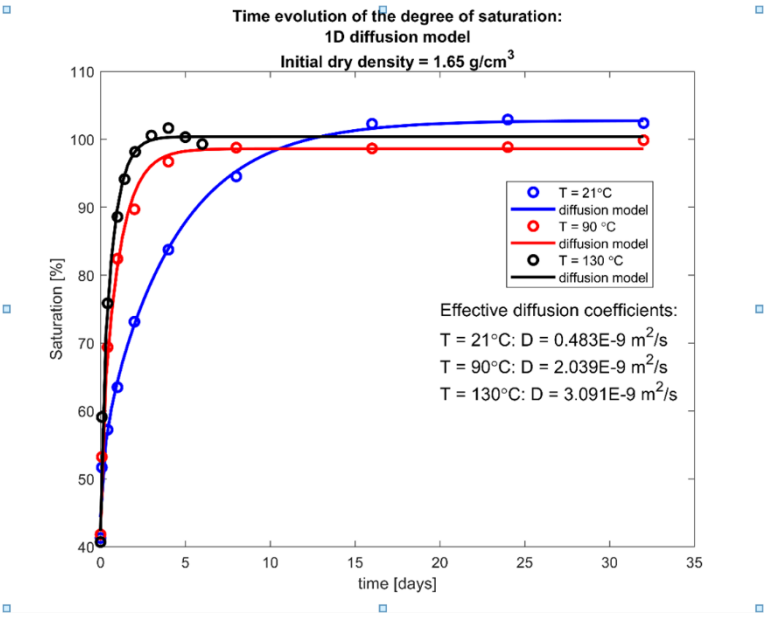

Figure 7.7 – Time evolution of the degree of saturation at three temperatures: 21°C, 90°C, and 130°C and simple 1D diffusion fitting. The obtained values of the fitting parameter, i.e., ''effective'' diffusion coefficient, are indicated in the text box.

When the effective diffusion coefficient is determined using the average degree of saturation, one can plot depth profiles of the degree of saturation at different points in time. Some example profiles are presented in Figure 7.8. When comparing the experimental results to the diffusion model, it becomes evident that the experimental results exhibit some resemblance to diffusion. However, the discrepancy between model and experiments is significant and increases when the saturation proceeds, thus, most likely the effective diffusion coefficient depends on the water content. So, it depends both on time and the location inside the partially saturated sample. Furthermore, the model is too simple because most likely the advection plays significant role in the water transport and diffusion of water vapour affects the spatial distribution of the water content, not only liquid water. One could also assume that when the temperature is increased the role of the diffusion of water vapour increases.

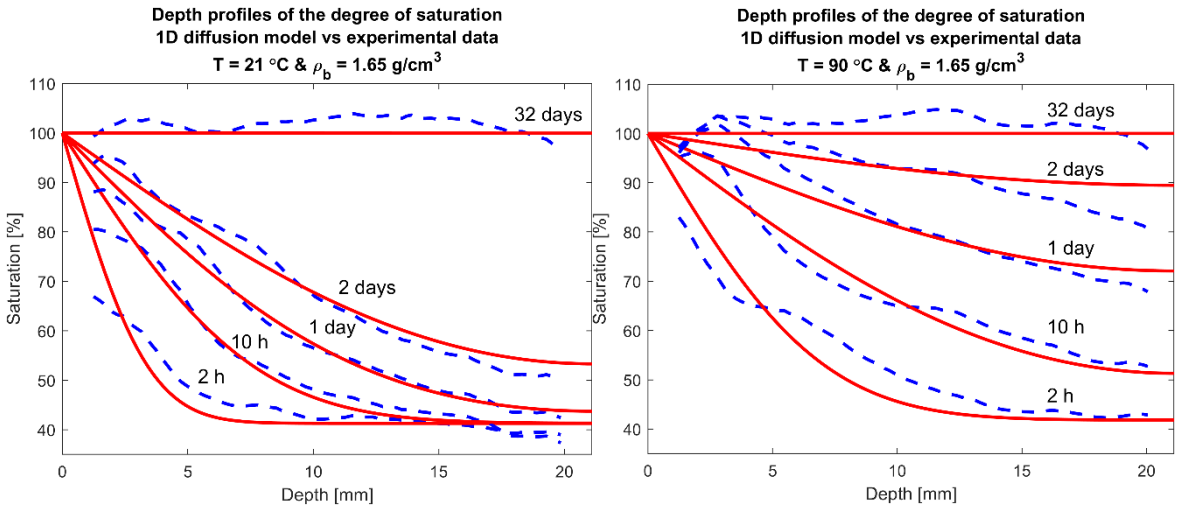

Figure 7.8 – Depth profiles of the degree of saturation at two temperatures: 21°C and 90°C. Figures contains both experimental data (blue dashed line) and theoretical profiles (red solid line) which are based on a simple 1D diffusion model and the fit in the time evolution of the degree of saturation (Figure 7.7).

Time evolution of the bentonite swelling pressure was also monitored during the experiments. Example results are presented in the Figure 7.9 and Figure 7.10. Each experiment yielded two graphs because two force sensors were employed in the sample holder: one at the top and one at the bottom. Ideally, the values from these sensors should be equal, but most likely due to the wall friction, there are often significant differences in the values they provide. In Figure 7.9, the time evolution of swelling pressure from experiments conducted at an initial target dry density of 1.40 g/cm^3 is presented at three temperatures: room temperature, 50°C, and 90°C. For each case, the results of the repetition experiment are also included. Similarly, Figure 7.10 contains results from experiments conducted at an initial target dry density of 1.60 g/cm^3. To facilitate comparison between the graphs, the estimated real densities of each sample are indicated in the legend box of the figures since the swelling pressure is sensitive to the real dry density of the sample. For clarity, the results from the two sensors are separated into two plots: one for the top sensor and one for the bottom sensor.

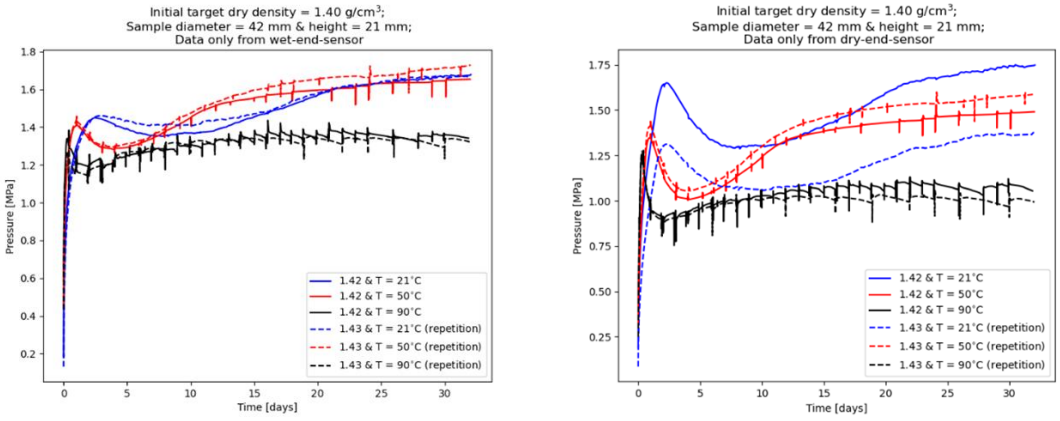

Figure 7.9 – Time evolution of the swelling pressure of the bentonite sample during the wetting experiments. Here, the initial target dry density has been 1.40 g/cm^3. The estimated real densities are indicated in the legend box. The left-hand side plot contains the data from the top sensor, i.e., wet end, and right-hand side plot contains the data from the bottom sensor, i.e., dry end.

Based on the measurements there are some indications that saturation pressure appears to be lower at higher temperatures, but uncertainties in the pressure measurement are significant. The decrease of the saturation pressure can be observed in the example graphs of Figure 7.9 and Figure 7.10. Furthermore, the decrease in saturation pressure seems to be more pronounced, approximately 1 MPa, in larger density samples with a dry density of 1.65 g/cm3 (Figure 7.10) compared to samples with a dry density of 1.40 g/cm3 (Figure 7.9), where the decrease in pressure was roughly 0.3 MPa. However, due to the discrepancies observed in repeated measurements at fixed temperatures, conducting additional repetitions is necessary to draw robust conclusions regarding the temperature dependence of the swelling pressure and the effect of dry density. The sudden drops in the pressure values are caused by the disturbances in the heating which are caused by the tomographic imaging and maintenance of the wetting system. For example, during the tomographic scan, the connection to the force sensors is removed.

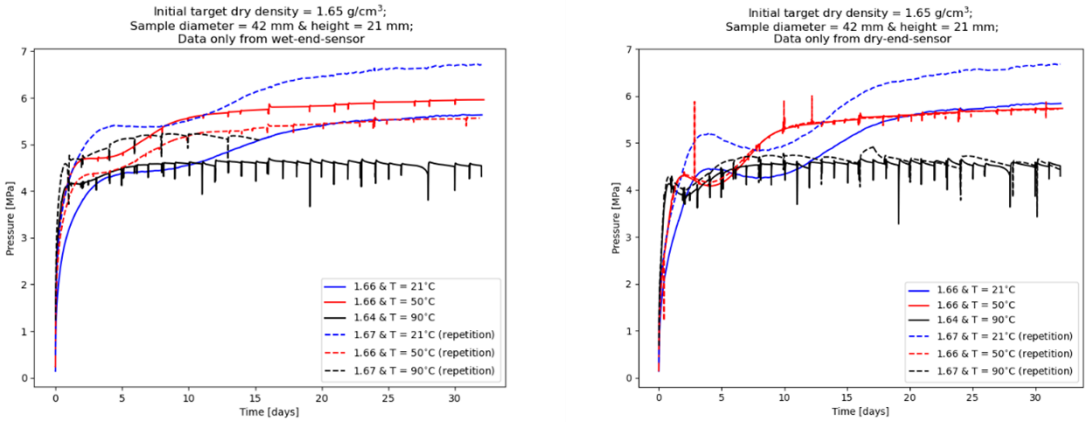

Figure 7.10 – Time evolution of the swelling pressure of the bentonite sample during the wetting experiments. Here, the initial target dry density has been 1.65 g/cm³. The estimated real densities are indicated in the legend box. The left-hand side plot contains the data from the top sensor, i.e., wet end, and right-hand side plot contains the data from the bottom sensor, i.e., dry end.

Preliminary chemical analysis (µXRF and CEC) of the system stability indicates some chemical gradients (ingress of Cl from the water used and potential dissolution of S bearing phase), although the overall chemistry remains stable, e.g., regarding Ca (Figure 7.11). Note that levels of counts are not directly related to absolute concentration (different levels in different samples). The data is suited to observe trends within individual sample. Despite overall chemical stability, it is likely that exchangeable cation composition of the clay is altered during experiments; preliminary cation exchange capacity analysis of one sample (EB07) showed lower values (from 73 to 80 mmol /100g) at 90°C compared to initial values (reported from the same material), but these were not analysed in this project in detail. Further CEC analyses and determination of composition of exchangeable cations before and after experiments would be of great value in further assessment of the observed changes in swelling pressure (Figure 7.9 and Figure 7.10). The source for sulphur dissolving is also unclear as gypsum is not reported for this material, although it could be present in bentonite. Additional mineralogical analysis would be recommended for each initial sample batch and after the analysis in future studies.

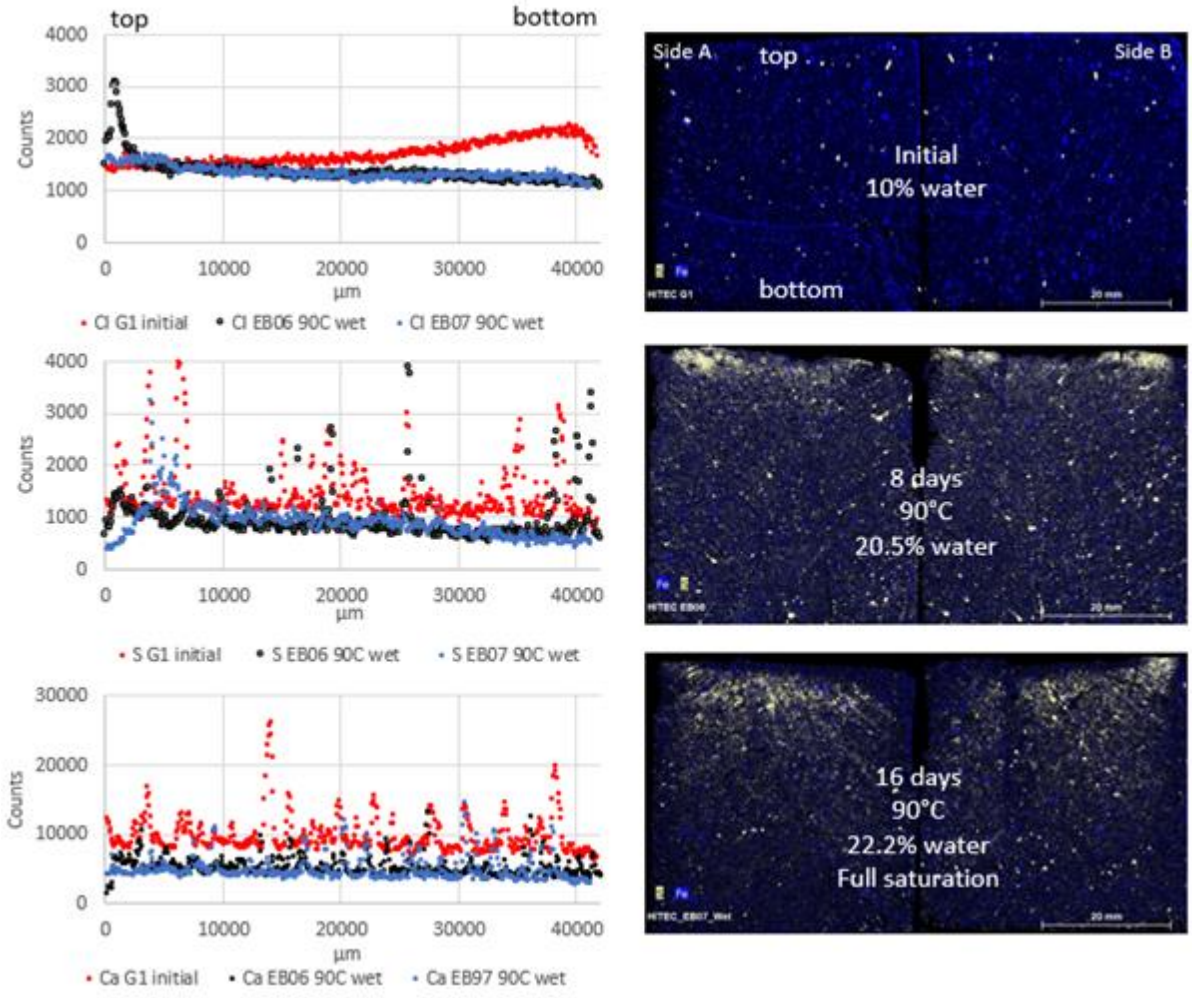

Figure 7.11 – Elemental composition of samples G1, EB06 and EB07 for Cl, S and Ca along samples profile (left) and for Fe and S elemental map examples (right).

7.4 Conclusion

Based on the validation conducted by comparing the water content measurement results of the X-ray tomographic method to post-mortem analysis of sliced, partially-saturated samples, the quantitative results of the method appear to be plausible, in general. This was the first time when the method developed at the University of Jyväskylä was applied to such a large sample size and sample holder. From the perspective of X-ray imaging, the anticipated increase in energy requirements was expected to pose challenges in the analysis. However, it now appears that the methodology is suitable for the larger sample size studied here in the EURAD program. Due to uncertainties in the displacement measurements near the edges of the sample, the results closest to the edges, approximately 1 mm layers, will be excluded from the analysis. Based on the experimental results, water transport appears faster, the higher the temperature. The 'speed of the saturation' as a function of temperature will be estimated based on the time evolution of the average degree of saturation of the sample which is determined by fitting a simple diffusion model to experimental data, and the detailed results will be published in J. Yliharju, et.al. *Observation of water transport in swelling compacted bentonite sample at elevated temperatures using an X-ray tomographic method (in preparation).* At 130°C, the saturation process is approximately 1.5 times faster than at 90°C. Additional analysis is required to conclude whether all the observations can be explained by the changes in the water properties, e.g., the temperature dependency of the viscosity of water, as a function of temperature, or whether there were some changes in the bentonite itself. Based on the measurements, there are some indications that saturation pressure appears to be lower at higher temperatures, but uncertainties in the pressure

measurement are significant. However, observations made regarding the temperature dependence of the speed of saturation is significant, and likely beneficial, regarding the repository safety. The faster the target degree of saturation is reached, the faster the safety functions of the clay are met.

Preliminary chemical analysis of the system stability indicates some chemical gradients, although the overall chemistry remains stable. It is likely that exchangeable cation composition of the clay was altered during experiments, preliminary cation exchange capacity analysis of one sample shows lower values at 90°C compared to the initial values, but these were not analysed in this project in detail. Further analyses would be required to assess the extent of the cation exchange.

8 KIPT (ChRDI)

8.1 Introduction

8.1.1 Material

The largest deposits of bentonite in Ukraine are located in the Cherkasy region in Dashukovka. This bentonite is under consideration as a buffer and backfill material in the system of geological disposal of spent nuclear fuel and high-level waste. Consequently the bentonite of the Dashukovka's deposit (Cherkasy region), is used in research carried out by the KIPT team within the framework of the HITEC project, and the material was named as PBC (**P**owder **B**entonite from **C**herkasy region of Ukraine). PBC contains Na-montmorillonite up to 60% and Ca, Mg - montmorillonite up to 20%. Natural bentonite of the Dashukovskoye deposit is polyphase minerals - along with the main phase of montmorillonite, there are α-quartz and calcite $CaCO_3$. Studies of the behavior of PBC bentonite at temperatures > 100°C are carried out for the first time in Ukraine.

8.1.2 Research plan

The main aim of research was to investigate the properties (permeability and swelling pressure) of Ukrainian bentonite at high temperatures (> 100°C).

Planned experimental procedure:

- development and manufacture of high-temperature measuring cell and all parts of experimental laboratory installation, assembly of all parts into a single whole, calibration and testing of all units.
- conducting trial experiments at temperatures > 100°C to saturate sand with water as a simulator of bentonite (sand will provide a faster saturation, which will facilitate the process of debugging the installation) and measurements of permeability and swelling pressure.

Planned investigation:

- measurements of PBC properties (permeability and swelling pressure) at temperatures > 100°C. They will be started after complete adjustment of the installation for measurements at high temperatures (planned for 25-30 M).

8.1.2.1 Material (BoM item): PBC bentonite (Ca-Mg type and sodium-fortified), powder as delivered by producer Joint stock company “Dashukovskiy bentonites” (Dashukovka, Cherkasy region of Ukraine).
8.1.2.2 Material treatment (sample preparation for test and loading procedure): Laboratory 150°C thermo-treated BPC powder from T3.1 will be used. Heat treated at 150°C, PBC powder will be placed and compacted directly in the measuring cell, then the cell will be sealed and water will be fed from below to saturate the bentonite.
8.1.2.3 Temperature (to which material was/will be exposed to) and exposure time Temperatures 120°C-130°C will be preferable.
8.1.2.4 Tests carried out (name, description, sample preparation, procedure, results): Permeability and swelling pressure will be measured in a constant volume cell (D = 32 mm, H = 15 mm). At first permeability was measured followed by swelling pressure determination. 8.1.2.5 Permeability - K [m/s] Permeability will be measured on a designed and manufactured laboratory installation (Figure 8.2) at a constant pressure gradient and automatically maintaining a constant sample volume. To heat the sample to a temperature of more than 100°C to prevent boiling of water, the installation is designed to maintain a water pressure of up to 5 bar. The samples are compacted directly in the measuring cell, then a water pressure gradient is applied, and during the impregnation process the total pressure development is measured at constant volume. Once a stable flow (and total pressure) is obtained, the permeability is calculated. The pressure gradient is then released and swelling pressure measurement begins. 8.1.2.6 Swelling pressure - σsw [MPa] The swelling pressure is determined on a fully saturated sample. The pressure gradient is no longer applied, and once the total pressure has stabilized, it becomes equal to the swelling pressure (no pore pressure in the sample).
8.1.2.7 Schedule and expected date(s) of results delivery: Start of measurements: M25 First results → M25-M30 Results for reporting → M36

Table 8.1 – KIPT - Permeability and swelling pressure in constant volume cell

8.2 Procedures

8.2.1 Laboratory set-ups, procedures and protocols

All parts of the experimental installation for measuring the permeability and swelling pressure of PBC bentonite at a temperatures > 100°C have been manufactured and assembled in one set. Of course, this setup allows performing accurate measurements of PBC bentonite characteristics from room temperature to 100°C. A schematic drawing and an external view of the manufactured installation are shown in Figure 8.1 and Figure 8.2 respectively.

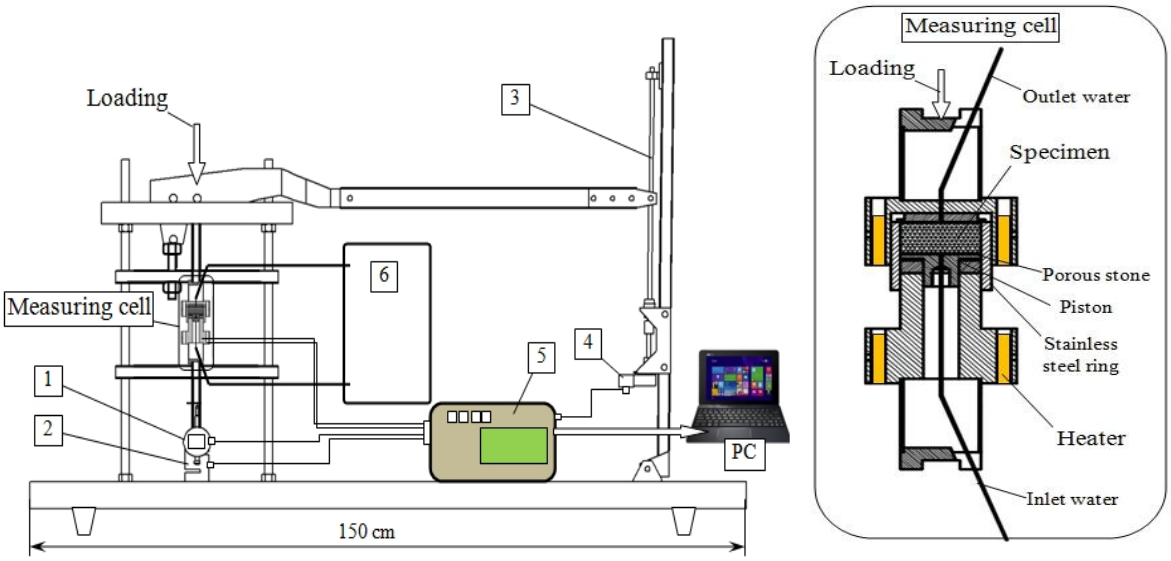

1 – digital displacement sensor, 2 - force sensor, 3 – screw, 4 - electric drive, 5 – controller and logger for data acquisition, 6 – water supply and volume measurement unit

Figure 8.1 – Schematic drawing of installation

Figure 8.2 – KIPT laboratory installation to measure the permeability and swelling pressure of PBC bentonite at a temperature > 100°C

The main parts of installation are presented below in Figure 8.3.

Measuring cell

Force sensor & digital displacement sensor

Controller and data acquisition

Electric drive

Figure 8.3 – External view of the main parts of the installation

8.2.2 Data and other results available

An electronic unit was manufactured for measuring the swelling pressure under controlling the density of a bentonite sample in a measuring cell. A block for maintaining the set temperature of the measuring cell has been manufactured and calibrated.

The software for the controller of the experimental setup has been developed and debugged.

8.3 Results

8.3.1 Investigation performed

The complete adjustment of the installation was finalized and measurements of the permeability and swelling pressure of PBC bentonite at high temperatures were started.

8.3.2 Results from investigation

Trial experiments were carried out using a sample in the form of sand as a simulator of the investigated porous material. This made it possible to check and debug all parts of the laboratory installation, namely:

- tightness of all connections;
- heating and temperature stabilization;
- creating and determining the axial force in the measuring cell;
- maintaining a constant height of the bentonite layer (hence the volume of the sample);

- indication of all measured parameters on the controller display and recording them in the permanent memory (logger).

Also, in the course of trial experiments, the flow rate of water through the sample under study was measured using a glass measuring capillary with a scale division of 0.002 cm^3.

A test measurement of the permeability of the sand was carried out with the help of the manufactured laboratory installation and the value of which was 10^{-8} m/s, and this result is in satisfactory agreement with the data of literature sources.

8.4 Conclusion

The main achievement in research activities over the past period is that an experimental laboratory complex has been created for high-temperature measurements of PBC bentonite properties, in particular:

- The modern laboratory installation for high-temperature measurements of permeability and swelling pressure was designed;
- The high temperature measuring cell was designed and manufactured;
- All necessary parts are manufactured and assembled into a single unit;
- The software for the controller of the laboratory installation has been developed and debugged for various operation modes;
- Full optimization of the installation operation was performed ;
- The installation allows to explore the properties (permeability and swelling pressure) of PBC bentonite at a temperature of (120-150)°C.

Tests and validation of the laboratory installation were carried out and measurements started. Unfortunately, in February 2022, research was interrupted due to military aggression from Russia.

9 VTT

9.1 Introduction

9.1.1 Objectives

The main objective of VTT's research is to characterize the effect of high and medium temperatures (up to 100°C) on mechanical elastoplastic properties of bentonite, more specifically on compressibility (isotropic compression tests) and on shear behaviour (isochoric shear tests.).

The aim of the isotropic compression tests is to obtain data on the volumetric elastoplastic behaviour of bentonite at elevated temperatures. To separate the plastic and elastic deformations, the tests are conducted cyclically such that the pressure is increased in steps and the pressure is relaxed to zero between the steps.

The aim of the shear tests is to obtain data on the (isochoric) shear elastoplastic behaviour of bentonite at elevated temperatures. To separate the plastic and elastic deformations, the shear stress is increased cyclically stepwise such that the shear stress is relaxed to zero between the steps.

9.1.2 Material

The basic material is Wyoming Na-bentonite (with tradename BARA-KADE) powder as provided by the manufacturer.

9.2 Procedures

As with the experiments on heat-treated bentonite (EURAD HITEC D7.7), the procedure for experiments at high temperature (Figure 9.1) is planned such that

- the material history is known in detail,
- mechanical and chemical disturbances are minimized,
- the structure of the samples is isotropic,
- the elastic and plastic volumetric and isochoric deformations can be separated from the obtained data, and
- the obtained data can be straight-forwardly utilized in model development.

The test cycles are performed relatively fast (time scale is minutes) to avoid adsorbed water diffusion within the samples.

9.2.1 Sample preparation procedure

The sample preparation procedure includes the following steps (see also flow chart in Figure 9.1):

1. Saturation of bentonite powder to desired water content by
    a. Water vapour equilibrium: The powder is saturated to a desired water content by placing it to Sicco Star-Vitrum desiccator cabinet with controlled relative humidity for suitably long period of time
        i. The method is used to
            1. minimise dissolution of side minerals (to prevent possible cation exchange)
            2. minimise mechanical disturbances (no mixing needed)
            3. allow wetting of larger batches at a time.
    b. Mixing: The powder is mechanically mixed with salt solution to reach a wanted water content
        i. The method allows much faster wetting of the material but the batch volume is limited and the control of mechanical disturbances is poorer than with water vapour equilibrium technique.

2. Compaction of pre-samples with isotropic pressure in with the volumetric compaction device or with the triaxial cell (Figure 9.2).
    a. The powder is first de-aired with a vacuum pump.
    b. Volume deformation is measured while compaction.
    c. Cyclic compression to be able to differentiate between elastic and plastic deformations.
        i. The pressure steps are for example 0-2-0-4-0-8-0-16-0-32 MPa, but the exact steps vary by water content and desired dry density.
3. Machining the pre-samples
    a. Machining the samples to correct shape and size for the elevated temperature cyclic volumetric deformation and isochoric shearing experiments.
    b. Sample size: cylinder with 50 mm diameter and 100 mm height.

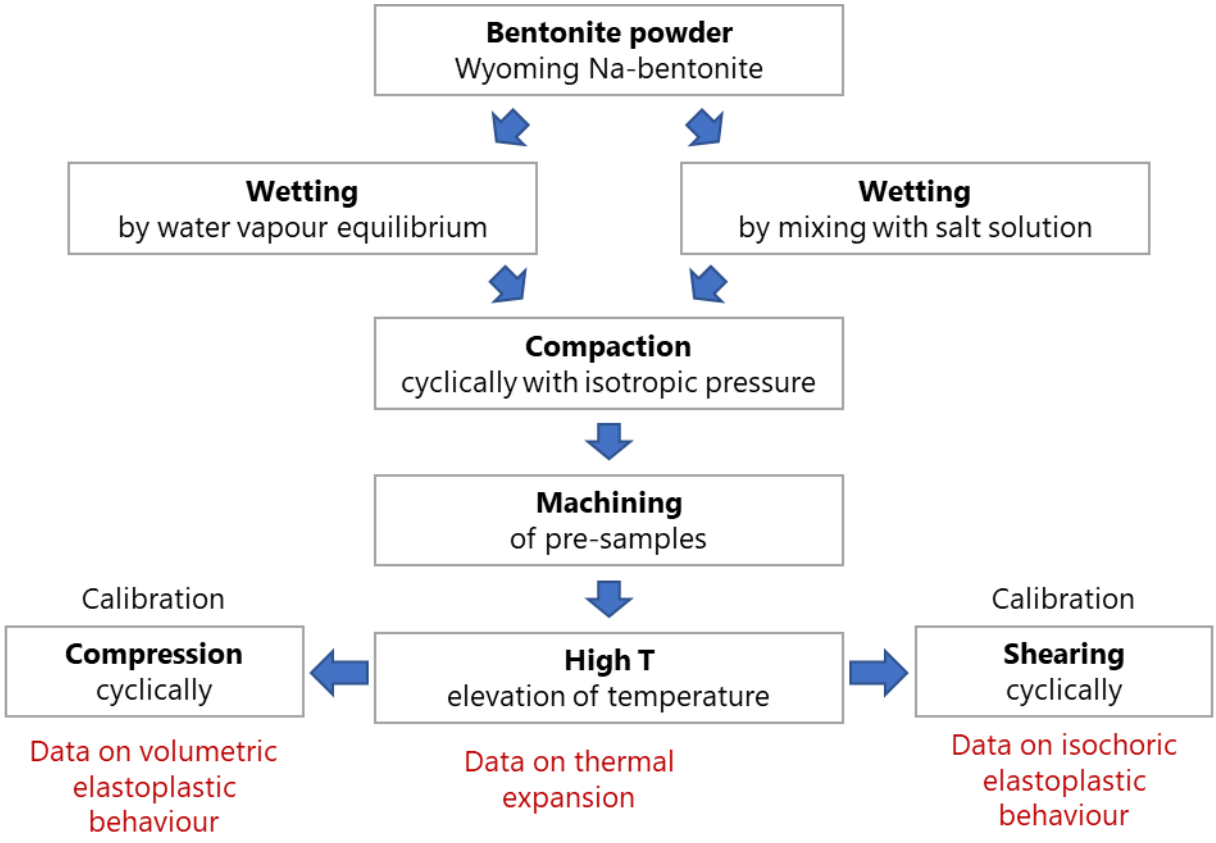

Figure 9.1 – Process for sample preparation and experiments at high temperature.

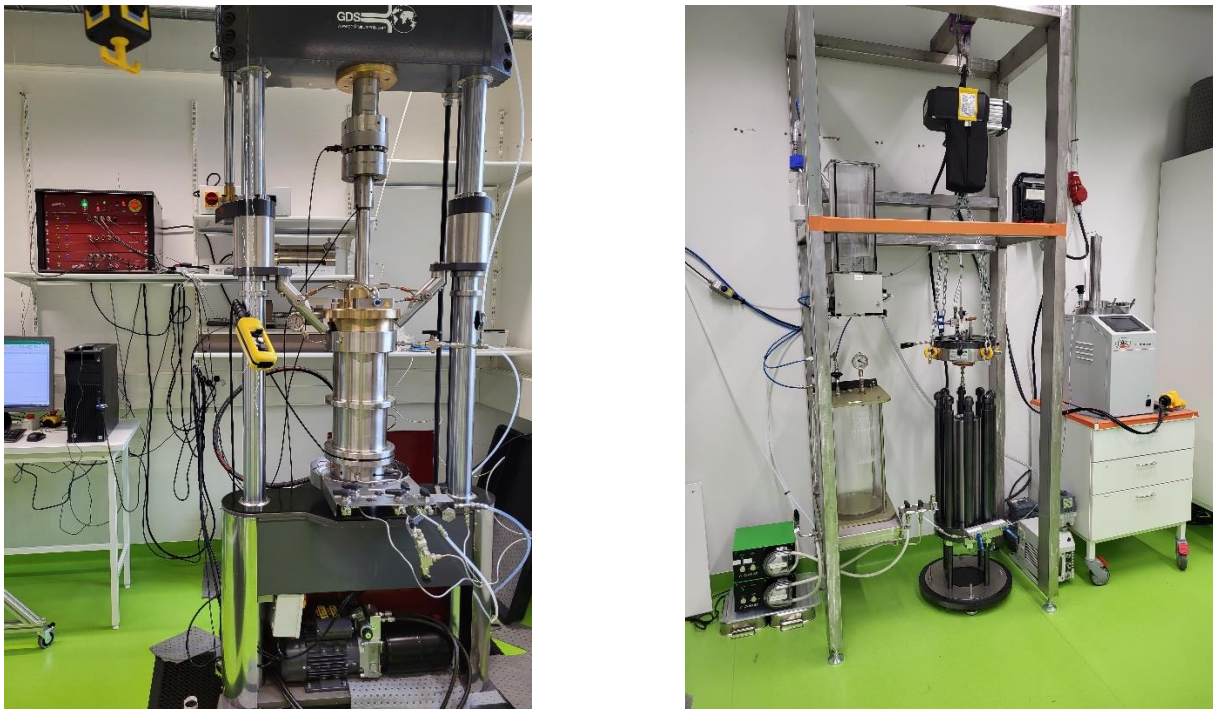

Figure 9.2 – The triaxial device (left) and the self-built alternative experimental system for isotropic compaction (right). The detailed description of the volumetric compaction device is in EURAD HITED Deliverable D7.7.

9.2.2 Triaxial compression and shear experiments at high temperatures

As a difference to the heat-treated experiments, the samples are compacted in room temperature, but both the volumetric compression and isochoric shearing experiments are carried out at elevated temperature (up to 100°C). The hydraulically actuated triaxial measurement system (GDS Instruments HLF 250 kN load frame with 32 MPa triaxial cell, Figure 9.2 and Figure 9.3) is used to perform the experiments. An insulating wbottom plate and an extended valve panel are added on the triaxial cell bottom closure under the sample holder and a top plate on top of the cell. Heating element mats, controlled by a heating pack, are wrapped around the cell. The insulation system is closed with an insulating shell that closes around the triaxial cell connecting the top and bottom plates. The low viscosity silicon oil (Julabo H10 Thermal fluid) as the cell fluid allows raising the temperature to 100°C for experiments. Sample behaviour during the temperature elevation can also be measured, but with limited accuracy.

Figure 9.3 - Triaxial cell temperature control system with heating elements, insulating covers and a heater pack.

9.3 Results

The experimental procedure for heat mechanical tests has been created, but the related laboratory equipment are still being set up and tested while writing this deliverable (October 2023). The original plan for conducting the experiments has been hindered by reliability issues combined to the worldwide supply chain disturbances followed from COVID-19 as well as by the simultaneous updating the triaxial system to enable high temperatures (also other updates), developing shear test procedures and producing volumetrically compacted samples. Especially the supply chain issues have delayed the development of the equipment for the experiments at elevated temperatures significantly. As a mitigation action of this realised risk and to ensure the finalisation of experiments for heat treated bentonite (EURAD HITEC D7.7), a separate volumetric compaction device has been successfully built from components with a tight schedule, but it has taken a portion of working time allocated for the experiments at high temperature. The device allows volumetrically compacting the samples with a separate device, while concentrating on the shear tests and tests at high temperatures with the triaxial cell.

10 General Conclusions

This report summarises work carried out as part of Task 3.2 of EURAD HITEC, which had a central objective to determine hydro-mechanical properties of bentonite for temperatures greater than 100°C. Bentonites under assessment included BCV, FEBEX, Kunipia, MX-80. In general, fully saturated bentonite is not expected to be exposed to temperatures exceeding 100°C in normal operation of a disposal facility. However, significant advantages would result if a design able to tolerate greater temperatures could be achieved (most notably, a reduced repository footprint). This is the primary rationale for examination of the impacts of higher temperatures within this task. In this report, the experimental approach and results are described for eight experimental programmes (Sections 2-9), which examined key behaviours including saturation/resaturation, water retention capacity, swelling pressure development and changes to permeability across a range of temperatures (predominantly 80-200° C).

A variety of techniques have been utilised within this subtask, the majority of which have required the construction or development of laboratory equipment, during a time of substantial disruption including the Covid-19 and global supply chain issues. As such, and despite this context, substantial methodological progress has been made, resulting in an enhancement in Europe wide capability on this topic. Particular novel developments include the development of a miniature oedometer cell, enabling imaging of bentonite microstructure and measurement of swelling pressure evolution during its hydration (Section 3) and an X-ray tomographic method to measure water content, which can be applied to relatively large samples (Section 7). In addition, despite the situation in Ukraine, a new laboratory for high-temperature measurements of permeability and swelling pressure has been completed and testing initiated (Section 8).

Findings from the experiments conducted in this subtask are outlined in detail in this report, but several primary conclusions can be drawn from across multiple project partners in this task and are outlined briefly here. Additionally, key impacts for repository design are highlighted, as supported for the temperatures, materials and conditions assessed in this subtask.

The rate of hydration/saturation of barrier materials is an important constraint on the assessment of repository evolution since this influences the time until the final target safety functions are achieved. The saturation process is expected to be impacted by higher temperatures and this has been examined through the determination of Water Retention Curves (WRC). This was found to be a non-trivial task in the low suction range (Section 4). However, where WRCs have been obtained, a sharper decrease of suction with water content was observed at higher temperatures (particularly above 60°C), confirming the expected influence of increasing temperature on the saturation behaviour of the barrier. As may be expected, differences in the water retention capacity of FEBEX (predominantly divalent) and MX-80 (predominantly sodic) bentonite were also observed under the conditions considered in this study. Observations from this task will, therefore, allow the incorporation of more representative WRC into numerical models simulating the saturation evolution of barriers at higher temperatures.

X-ray tomographic studies examining the resaturation of bentonite samples have provided additional insight into the hydration process. Observations indicate that the hydration process under isothermal conditions (in the absence of a thermal gradient), is accelerated at higher temperatures (between 50 and 130°C). Additional work will continue until the end of EURAD HITEC to assess the impact of the presence of a temperature gradient on these findings.

Impact: All observations confirm that saturation behaviour of the barrier is impacted by increasing temperature. However, additional work is required to assess the impact of boundary condition on this behaviour.

Several experimental programmes in T3.2 have examined the impact of higher temperatures on bentonite swelling pressure development. Relatively consistent observations are apparent across all

project partners, with the repeated finding that swelling pressure is seen to reduce with increasing temperature (Sections 2, 4, 5, 6 and 7). This change was not observed between 20 and 50°C (Section 7), but is apparent in test programmes between 50 and 200°C (Sections 2, 4, 5, 6 and 7) in all bentonites tested (BCV, FEBEX, Kunipia, MX-80) and was observed to become more pronounced with increasing temperature. In addition, where partners considered the influence of density, a similar consensus is apparent, with the magnitude of temperature-dependent swelling pressure reduction becoming more significant at higher dry densities (Sections 2, 4, 5, 6 and 7). This is perhaps particularly significant, since increasing dry density of bentonite is often used to elevate the swelling pressure achieved in repository designs. In one study, the temperature at which the total stress curve was seen to change slope was also found to depend on the bulk density (Section 5).

It should be noted that observations of swelling pressure reduction in response to heating were conducted under either constant volume or oedometric loading conditions, whilst a negligible effect of heating was reported in a swelling strain test (Section 6). However, additional testing is necessary to understand the influence of boundary conditions on these observations. Several test programmes also considered the permanency of swelling pressure changes, by cycling test temperatures and returning to initial values (Sections 2, 5 and 6). All findings presented in this report indicate that the reduction in swelling pressure can be substantial and is hysteric in nature; values are not recovered after cooling. Nevertheless, additional testing may be necessary to assess the permanency of these observations over longer timescales.

Impact: Swelling pressure of bentonite may be impacted by temperatures between 50 and 200°C and is more pronounced at higher temperatures and dry densities. Robust assessment of bentonite swelling pressures as a function of temperature will be necessary to design barrier materials for repositories intended to operate at elevated temperatures (>100°C).

A common finding in several test programmes was also the apparent temporal degradation in swelling pressure, when held at a constant temperature conditions over timescales of 10's of days (Sections 2, 5 and 6). This behaviour may be described as a form of thermally-induced creep, though further work is necessary to explore this hypothesis and explore the underlying mechanisms. Current numerical simulations do not account for this process. This behaviour was observed in samples which had a relatively high initial saturation or were fully saturated before being exposed to high temperatures. Further experiments examining the impact of saturation state (from partial to complete) at the time of heating would be beneficial for predicting the conditions where this behaviour may occur.

Impact: The impact of high temperatures on swelling pressure over longer timescales than those considered in this Task is unclear. Improved understanding of the longevity or transience of these findings over long timescales would, therefore, be beneficial. Additional robust assessment of the long-term swelling behaviour of bentonite will be necessary to inform numerical simulations, which may need modification to allow for time-dependent swelling at elevated temperatures. The use of blind prediction modelling trials may be particularly beneficial to validate understanding over long timescales.

Despite the observed effects on swelling pressure development, permeability has been found to be less sensitive to exposure to high temperatures (Sections 2 and 5). In one study, a systematic increase in hydraulic conductivity was observed in BCV bentonite (up to a temperature of 150°C), the magnitude of which was found to relate to the dry density of the sample (Sections 2). However, after conversion of values to a constant reference temperature, these changes are relative minor in nature and all remain within one order of magnitude. Similar conclusions were drawn from testing in MX-80 bentonite, where only minimal changes in permeability (after correction for water hydraulic property changes as a function of temperature) were found to occur with increasing temperature (100-200°C). These findings run counter to the observed sensitivity of swelling pressure to temperature and the reasons for this remain

unclear. Further expansion of this dataset would improve understanding and confidence in this finding, across a wider range of bentonites and dry densities.

Impact: Findings indicate that the hydraulic permeability of tested bentonites is not detrimentally affected by thermal loading up to temperatures of 200°C.

Finally, outputs from Task 3.2 form an extensive dataset, providing parameters and experimental validation data that can facilitate the development of future numerical model development handling the thermo-hydro-mechanical behaviour of bentonites at high temperature.

Several knowledge gaps are apparent after completion of this task. Despite experimental efforts, the shape of the WRC at high temperatures and low suctions has yet to be fully-defined. Further work considering the impact of thermal gradients on the saturation process would also be valuable (also dealt in Task 3.3). Moreover, an improved understanding of swelling pressure response would be beneficial for the development of robust repository designs intended for operation at high temperatures. Key uncertainties relate to:

- The mechanisms driving swelling pressure reduction
- The long-term evolution of swelling pressure degradation and the degree of persistence after longer periods of cooling
- The impact on a wider range of bentonite compositions (and bentonite-sand mixtures)
- The impact of boundary conditions on this behaviour

Further work assessing the influence of elevated temperatures on barrier performance is therefore recommended to further facilitate repository design. This would require additional experimentation to address target aspects of the gaps described above. For example, long-term testing would be key to assess the controls on thermal creep and relaxation, as well as the permanency of swelling pressure after long-term cooling. Expansion of the experimental dataset across a wider range of dry densities may also prove beneficial in determining scoping bentonites to tolerate higher temperatures without detrimental effects to the swelling pressure safety function. Whilst the impacts on permeability were not found to be substantial, parallel assessment of this safety function would also improve confidence in this finding across a wider range of dry densities. Finally, it is recommended that consideration of the implications for numerical prediction are fully assessed. This could include modification of numerical codes to incorporate observed behaviours (such as inclusion of visco-plastic behaviour to simulate thermally-induced creep) and examine the impact on repository performance. Experiments conducted in Task 3.2 of EURAD HITEC, and presented in this report, provide a suite of validation data for these efforts to begin.

References

Cekerevac, C., Laloui, L. (2004). Experimental study of thermal effects on the mechanical behaviour of a clay. International Journal for Numerical and Analytical Methods in Geomechanics, 28: 209–228.

Červinka, R., P. Večerník, V. Kašpar and R. Vasicek (2018). Kompletní charakterizace bentonitu BCV 2017. Prague, SÚRAO.

ENRESA (2006). FEBEX Full-scale Engineered Barriers Experiment, Updated Final Report 1994-2004. Madrid, ENRESA.

Hausmannová, L., I. Hanusová and M. Dohnálková (2018). Summary of the research of Czech bentonites for use in the deep geological repository – up to 2018. Prague, SÚRAO.

Jacinto, A. C., M. V. Villar and A. Ledesma (2012). "Influence of water density on the water-retention curve of expansive clays." Géotechnique **62**(8): 657-667.

Kiviranta, L. and S. Kumpulainen (2011). Quality control and characterization of bentonite materials. Posiva Working Report Olkiluoto, Posiva. **2011-84:** 154.

Kiviranta, L., S. Kumpulainen, X. Pintado, P. Karttunen and T. Schatz (2018). Characterization of bentonite and clay materials 2012-2015. Posiva Working Report Olkiluoto. **2016-05:** 154.

Lloret, A. and M. V. Villar (2007). "Advances on the knowledge of the thermo-hydro-mechanical behaviour of heavily compacted "FEBEX" bentonite." Physics and Chemistry of the Earth **32**(8-14): 701-715.

Massat, L., O. Cuisinier, I. Bihannic, F. Claret, M. Pelletier, F. Masrouri and S. Gaboreau (2016). "Swelling pressure development and inter-aggregate porosity evolution upon hydration of a compacted swelling clay." Applied Clay Science **124–125**: 197-210.

Meier, L. P. and G. Kahr (1999). "Determination of the Cation Exchange Capacity (CEC) of Clay Minerals Using the Complexes of Copper(II) Ion with Triethylenetetramine and Tetraethylenepentamine." Clays and Clay Minerals **47**(3): 386-388.

Svoboda, J. V. and e. al. (2019). Interakční experiment – přípravné a podpůrné práce [Kniha]. Prague, SÚRAO.

Uchaipchat, A., Khalili, N. (2009). Experimental investigation of thermo-hydro-mechanical behaviour of an unsaturated silt. Géotechnique 59(4): 339–353.

Villar, M. V. (2005). MX-80 bentonite. Thermo-hydro-mechanical characterisation performed at CIEMAT in the context of the Prototype Project. Informes Técnicos CIEMAT. Madrid, CIEMAT. **1053:** 39.

Villar, M. V. (2013). Long-term THM tests reports: Isothermal infiltration tests with materials from the HE-E. PEBS Deliverable 2.2-7.2. CIEMAT Technical Report Madrid, CIEMAT. **CIEMAT/DMA/2G210/07/2013:** 32.

Villar, M. V. and R. Gómez-Espina (2009). Report on thermo-hydro-mechanical laboratory tests performed by CIEMAT on FEBEX bentonite 2004-2008. Informes Técnicos CIEMAT. Madrid, CIEMAT. **1178:** 67.

Villar, M. V., R. Gómez-Espina and A. Lloret (2010). "Experimental investigation into temperature effect on hydro-mechanical behaviours of bentonite." Journal of Rock Mechanics and Geotechnical Engineering **2**(1): 71-78.

Villar, M. V., R. Gómez-Espina and P. L. Martín (2006). Behaviour of MX-80 bentonite at unsaturated conditions and under thermo-hydraulic gradient. Work performed by CIEMAT in the context of the TBT project. Informes Técnicos CIEMAT Madrid, CIEMAT. **1081:** 45.

Villar, M. V., C. Gutiérrez-Álvarez and P. L. Martín (2020). Low-suction water retention capacity of bentonite at high temperature. 4th European Conference on Unsaturated Soils (E-UNSAT 2020). R. Cardoso, C. Jommi and E. Romero. Lisboa, E3S Web of Conferences **195:** 04010.

Villar, M. V. and A. Lloret (2004). "Influence of temperature on the hydro-mechanical behaviour of a compacted bentonite." Applied Clay Science **26**(1-4): 337-350.

Villar, M. V. and A. Lloret (2008). "Influence of dry density and water content on the swelling of a compacted bentonite." Applied Clay Science **39**(1-2): 38-49.

Zihms, S.G. and Harrington, J.F., 2015. Thermal cycling: impact on bentonite permeability. Mineralogical Magazine, **79**(6), pp.1543-1550.